NASA Contractor Report 3145

A Compilation and Analysis of Helicopter Handling Qualities Data

Volume Two: Data Analysis

Robert K. Heffley

CONTRACT NAS2-9344
AUGUST 1979

NASA

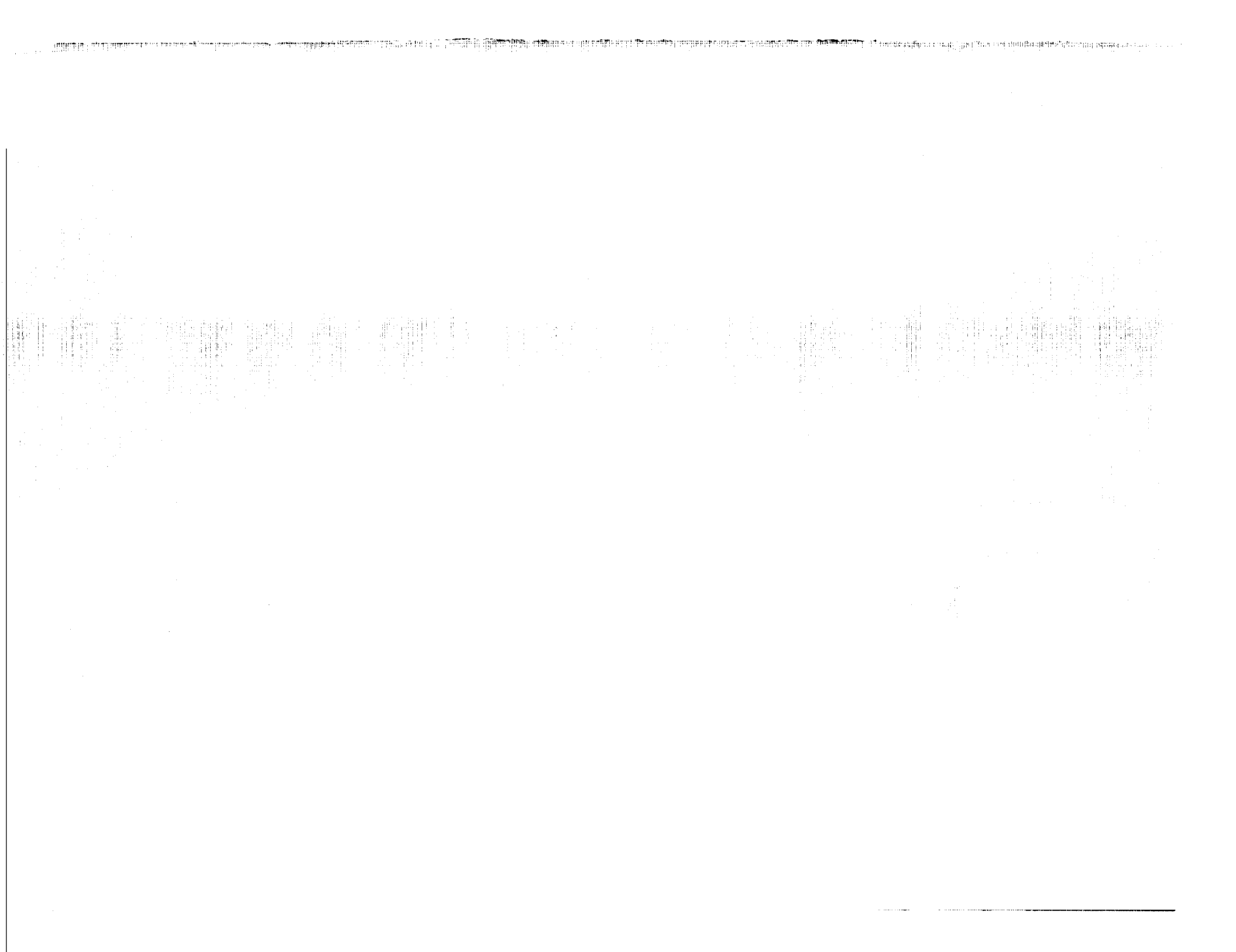

NASA Contractor Report 3145

A Compilation and Analysis of Helicopter Handling Qualities Data

Volume Two: Data Analysis

Robert K. Heffley
Systems Technology, Inc.
Mountain View, California

Prepared for
Ames Research Center
under Contract NAS2-9344

National Aeronautics
and Space Administration

Scientific and Technical
Information Branch

1979

FOREWORD

The preparation of this report was performed under NASA Contract NAS2-9344 with the joint sponsorship of the Aeromechanics Laboratory of the U. S. Army Research and Technology Laboratories (AVRADCOM) and NASA Ames Research Center. The Contract Technical Monitor was David L. Key, and the Systems Technology, Inc., Project Engineer was Robert K. Heffley. Work on this project was accomplished during the period from September 1976 to February 1978.

The author wishes to thank the following individuals for their contributions and help in preparing this volume: John M. Davis of the Aeromechanics Laboratory of the U. S. Army Research and Technology Laboratories, Warren F. Clement, Duane T. McRuer, John M. Lehman, Richard A. Van Winkle, Sharon A. Duerksen, and Irene M. Zielke of Systems Technology, Inc.

ABSTRACT

A compilation and an analysis of helicopter handling qualities data are presented. Volume One contains a collection of basic descriptive data, stability derivatives, and transfer functions for a six-degrees-of-freedom, quasi-static model. This, the second volume, analyzes those data using multi-loop manual control methods. A general compensatory loop structure is applied to coupled longitudinal-lateral-directional equations in such a way that key handling qualities features can be examined directly. But the overall mathematical complexity is reduced from that of the basic vehicle model. Extensive use is made of constrained state variable relationships and approximate factors in order to gain physical insight.

TABLE OF CONTENTS

TABLE OF CONTENTS (Concluded)

LIST OF TABLES

LIST OF TABLES (Concluded)

LIST OF FIGURES

LIST OF FIGURES (Concluded)

LIST OF ABBREVIATIONS

A	Pole or zero associated with stability or control augmentation system
HD	Pole or zero associated with dominant heave mode, heave damping
LD	Pole or zero associated with dominant sway (lateral) response, sway damping
NOE	Nap-of-the-earth
P	Pole or zero complex pair associated with longitudinal phugoid
PD	Pole or zero associated with pitch damping
PL	Pole or zero complex pair associated with lateral phugoid
rpm	Revolutions per minute
R	Pole or zero associated with dominant roll mode, roll damping
s	Laplace operator
SAS	Stability augmentation system (CH-53D)
SCAS	Stability and control augmentation system (AH-1G)
SD	Pole or zero associated with dominant surge (fore and aft) mode, surge damping
SP	Pole or zero complex pair associated with longitudinal short period mode
VTOL	Vertical takeoff and landing aircraft
YD	Pole or zero associated with dominant yaw mode, yaw damping

LIST OF SYMBOLS

A_{1_s}	Lateral cyclic swashplate deflection
A_θ	High frequency gain in θ/δ_B transfer function
A_φ	High frequency gain in φ/δ_A transfer function
A_ψ	High frequency gain in ψ/δ_p transfer function
B_{1_s}	Longitudinal cyclic swashplate deflection
c	Longitudinal tip path plane deflection of stabilizer bar (UH-1H)
d	Lateral tip path plane deflection of stabilizer bar (UH-1H)
g	Gravity constant
h	Altitude, $-z$
$\dot{h}$	Altitude rate, $-\dot{z}$
I_x	Moment of inertia about x-axis
I_{xz}	Moment of inertia cross product
I_y	Moment of inertia about y-axis
I_z	Moment of inertia about z-axis
$j\omega$	Imaginery component of s
K	General representation of a pure gain
K_p	Pilot gain
L	Rolling moment
$L_{(\ )}$	Dimensional rolling moment derivative, $(1/I_x)[\partial L/\partial(\ )]$
$L'_{(\ )}$	$[L_{(\ )} + (I_{xz}/I_x)N_{(\ )}]/[1 - (I_{xz}^2/I_xI_z)]$
m	Vehicle mass
M	Pitching moment
$M_{(\ )}$	Dimensional pitching moment derivative, $(1/I_y)[\partial M/\partial(\ )]$

N	Yawing moment
$N_{(\ )}$	Dimensional yawing moment derivative, $(1/I_z)[\partial N/\partial(\ )]$
$N'_{(\ )}$	$[N_{(\ )} + (I_{xz}/I_z)L_{(\ )}]/[1 - (I_{xz}^2/I_xI_z)]$
$N_b^a(s)$	Transfer function numerator for perturbation of motion quantity, a due to control or gust input, b
p	Angular rate
p_g	Rotary gust about earth fixed x-axis
q_g	Rotary gust about earth fixed y-axis
r_g	Rotary gust about earth fixed z-axis
t	Time
T_{sp}	High frequency time constant in predominant hover pitching mode
$1/T_{\theta_1}$	Low frequency root in θ/δ_B (associated with surge damping)
$1/T_{\theta_2}$	High frequency root in θ/δ_B numerator (associated with heave damping)
u	Perturbation velocity component in body fixed x-axis
u_g	Translational gust along earth fixed x-axis
v	Perturbation velocity component in body fixed y-axis
v_g	Translational gust along earth fixed y-axis
V	True airspeed
w	Perturbation velocity component in body fixed z-axis
w_g	Translational gust along earth fixed z-axis
x	Translation along earth fixed x-axis
X	x-force
$X_{(\ )}$	Dimensional x-force derivative $(1/m)[\partial X/\partial(\ )]$

y	Translation along earth fixed y-axis
Y	y-force
$Y_{(\ )}$	Dimensional y-force derivative, $(1/m)[\partial Y/\partial(\ )]$
Y_c	Controlled element transfer function
Y_p	Pilot element transfer function
z	Translation along earth fixed z-axis, $-h$
Z	z-force
$Z_{(\ )}$	Dimensional z-force derivative, $(1/m)[\partial Z/\partial(\ )]$
α_b	Perturbation angle of stabilizer bar with respect to mast in mast-fixed axis system
α_m	Perturbation angle of mast with respect to inertial reference frame in mast fixed axis system
β	Angle of sideslip
γ	Lock Number
δ_A	Lateral cyclic stick deflection
δ_B	Longitudinal cyclic stick deflection
δ_c	Collective stick deflection
δ_p	Rudder pedal deflection
δ_3	Rotor blade pitch-flap coupling
Δ	Determinant of open-loop characteristic equation
Δ'	Determinant of closed-loop characteristic equation
ϵ	Rotor hinge offset ratio
ζ	Damping ratio
θ	Pitch Euler angle
ρ	Air density
σ	Real component of s

τ_c	Effective control lag
τ_e	Effective pilot delay
φ	Roll Euler angle
φ_M	Phase margin
ψ	Yaw Euler angle
ω	Natural frequency
ω_c	Crossover frequency
Ω	Rotor system angular velocity
$\angle$	Phase angle

Subscripts

c	Controlled element, also command
CF	Crossfeed
d	Dutch roll
g	Gust
m	Rotor mast axis system
p	Pilot element, also phugoid
r	Roll
s	Spiral
sp	Short period
x	x-axis regulation
y	y-axis regulation
z	z-axis regulation
θ	Pitch axis regulation
φ	Roll axis regulation
ψ	Yaw axis regulation

SECTION I

INTRODUCTION

This volume presents a collection of closed-loop pilot-vehicle analyses based on the compiled helicopter handling qualities data presented in Volume One. The main purpose of this volume, in fact, is to serve as a guide to one use of the compiled data.

The approach taken utilizes elements of multiloop manual control theory with examples of representative helicopter vehicle dynamics to address important handling qualities aspects. In order to focus our efforts on a relevant application we are addressing handling qualities in the context of low-level, low-speed Army helicopter missions, especially in the nap-of-the-earth (NOE) environment.

The emphasis is distinctly on the method of analysis rather than on the specific numerical results obtained. While the basic data were obtained from each respective airframe manufacturer and therefore are presumably the best data available, certain inherent modeling limitations, nevertheless, are recognized. For example, all the data are based on a six-degrees-of-freedom set of equations of motion with quasi-static representation of the rotor tip path plane. While revealing some important cross coupling features, this form neglects short term control lag effects connected with the rotor degrees of freedom*. Where possible, flight test data have been used to qualify certain analytical results obtained. The general analytical approach, however, is not tied to a given level of mathematical complexity and could be used with higher-order models.

Use of a closed-loop pilot-vehicle analysis technique has allowed us to go considerably beyond the behavior of the strictly open-loop system which is demonstrated by the conventional bare airframe response modes.

---

* Short term control lag effects associated with the rotor degrees of freedom can be included, to some extent, in the effective time delay which will be introduced subsequently in connection with the crossover model.

Our has been to look at handling characteristics in terms of what the pilot perceives when manually controlling the helicopter. In doing so, we conclude that including the pilot-in-the-loop does not necessarily introduce complication but in some ways its inclusion tends to simplify the system analyses, especially where multiple loops are involved.

For the most part the analysis methods used are not new. They have been borrowed from various applications to other vehicles and operating conditions. Also, most of the features of helicopter flight dynamics identified here have been well known for some time. The material presented is a systematic description of multiloop analysis applied to several examples of cross-coupled helicopter vehicle dynamics. As a result a number of conclusions can be drawn regarding handling qualities metrics and simulator modeling.

The methods for performing multiloop analysis and the format used to describe vehicle dynamics are described in detail in Ref. 1. Manual control theory ideas which served as a guide are summarized in Ref. 2. The reader may wish to consult these two sources for a general background.

In preparing this volume only a small portion of the compiled data in Volume One was used. In most cases only hover and 60 kt nominal loading flight conditions were analyzed. At the same time, an effort was made to search for interesting and significant features. Some of the items found include an analytically pathological roll response tendency at high rates of climb and a point of maximum sensitivity to horizontal wind shear in the low-speed range.

The report is organized in a manner which divides handling qualities aspects into well-defined groups. Following a general discussion of pilot loop structure topics (Section II), the handling qualities features are addressed according to inner-loop (attitude regulation) features (Section III), outer-loop (position/velocity regulation) features (Section IV), and gust disturbance effects (Section V). Vehicle stability and control augmentation effects are discussed in Section VI. The report ends with a summary of conclusions and recommendations (Section VII). An appendix is provided which summarizes transfer functions appropriate for viewing specific handling features.

SECTION II

GENERAL PILOT-VEHICLE LOOP STRUCTURE

In the following pages we shall discuss the features of the pilot-vehicle loop structure to be used in the subsequent handling qualities analyses. In formulating this structure, we shall utilize results from the investigation of multiloop manual control theory in order to choose a pilot model of minimal complexity but at the same time to reveal important closed-loop handling features.

We begin by defining certain piloting objectives which help us to formulate an assumed piloting technique. Then we discuss features of the pilot model itself and especially its numerical definition. Other concepts useful in subsequent sections are also discussed including the use of constrained variables as a device for simplifying the multiloop system and identification and labeling of response modes.

A. PILOTING OBJECTIVES

In this study the piloting objectives are expressed so as to be relevant to low-level flight while at the same time recognizing the limitations of the helicopter mathematical model involved. In particular, we address nap-of-the-earth (NOE) operation which is defined in Ref. 3 as "flight as close to the earth's surface as vegetation or obstacles will permit, and generally following the contours of the earth." According to Ref. 4, much of the time in a typical NOE mission is spent in very slow flight or hover with occasional accelerations to higher speeds when dashing across open areas. When flying in close proximity to the ground, the pilot must be constantly aware of rotor clearance to obstacles and must be able to judge whether to go around, between, or over obstacles. While operations can take place during night and day conditions, essentially all visual information available to the pilot is from outside reference. Aural or vibrational

cues, such as rotor rpm, may be used, but head-down cockpit reference is not involved.

Working within the context described above, our pilot-vehicle analyses involve only those state variables corresponding to outside visual reference, that is, attitudes defined in terms of body Euler angle rotations and translational components in terms of an earth-fixed reference system. The effects of varying airspeed are addressed, in general, by considering flight conditions at hover and 60 kt.

Pilot-vehicle analyses are applied in the context of short- to medium-term maneuvering and regulating operations of the helicopter. We exclude the long-term trimming or configuration change effects. Also, because of model limitations, we must limit the pilot's actions to use of basic flight controls and assume that the pilot is taking appropriate measures to regulate rotor rpm effectively (in the model, rotor rpm is constant). In this context, the function of the pilot's basic flight control loop structure is to (1) stabilize and regulate attitudes and (2) regulate position (or velocity).

The attitude loop structure consists of roll, pitch, and, where applicable, yaw regulation. Such regulation can range from being highly precise to the point of merely staying right-side-up. We make certain assumptions regarding precision of the attitude regulation depending upon the piloting task and the degree of simplification required. The loop structure connected with regulation of yaw depends upon whether we are considering a hover or forward flight condition. In hover, yaw must be regulated actively; while in higher speed forward flight, yaw regulation is unnecessary if directional (sideslip) stability is adequate. The aspects of inner loop regulation will be fully discussed in Section III.

Regulation of position or velocity constitutes the outer loop structure and must be addressed subsequent to applying appropriate inner loop regulation. The distinction between position and velocity regulation is crucial in terms of the degree of pilot compensation required. Naturally, position regulation refers most directly to near-hover conditions while velocity regulation is more appropriate to forward flight conditions. Outer loop regulation will be the subject of Section IV.

B. ASSUMED PILOTING TECHNIQUE

In general, a normal helicopter piloting technique will be assumed, i.e.,:

- Pitch attitude controlled by longitudinal cyclic stick
- Roll attitude controlled by lateral cyclic stick
- Yaw controlled by rudder pedals (at low speeds)
- Longitudinal position or velocity controlled by commanded pitch attitude
- Lateral position or velocity controlled by commanded roll attitude
- Altitude or flight path angle controlled by collective stick.

This structure is depicted in block diagram form in Fig. II-1. It will be shown by analysis that the determining feature in closed-loop pilot-vehicle dynamics is the implicit loop structure itself rather than the explicit pilot gains and compensation. In other words, under certain conditions it is sufficient to recognize only the fact of active pilot regulation rather than the numerical value of a gain representing that regulation. This is not to say that specific features of the overall pilot loop structure will be neglected. We will, in fact, look at pilot compensation requirements and note where manual control difficulties could be expected. For the most part, though, pilot model complexities will be minimized in order to concentrate on airframe-related characteristics.

C. ASPECTS OF MULTILOOP MANUAL CONTROL THEORY

Our objective in applying manual control theory to helicopter vehicle dynamics is to reveal handling quality features in as realistic a way as possible. A secondary objective is to focus on individual aspects of handling qualities so as to separate potential handling qualities problems. One approach to this is to consider the pilot-vehicle system as a

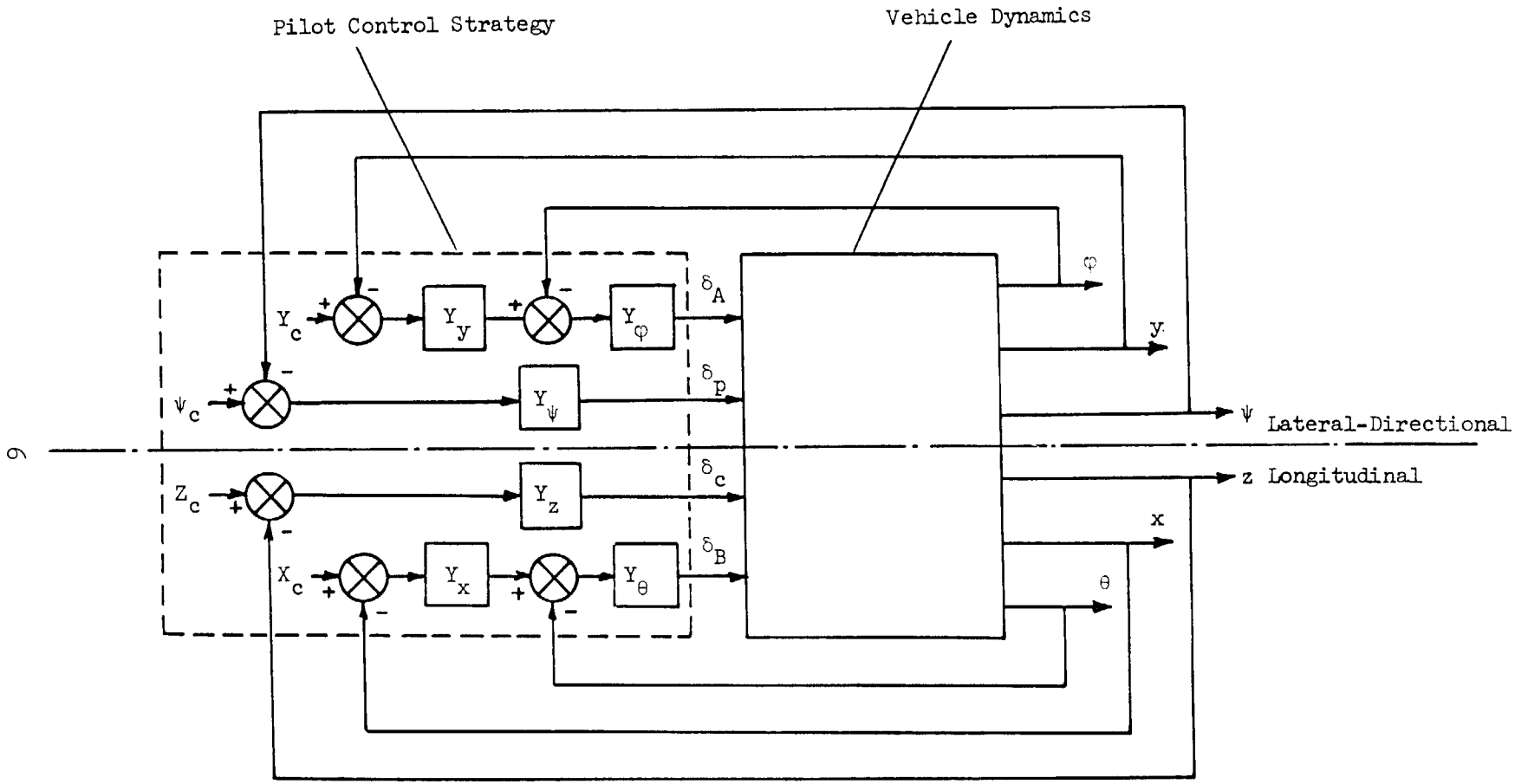

Figure II-1. Assumed Pilot-Vehicle Loop Structure for Low Speed Flight

compensatory* control situation and to apply the "crossover model"† or extended crossover model in a multiloop sense.

The crossover model, as described in Ref. 5, is a guide to setting numerical values for closed-loop control system compensation, where the pilot is assumed to be the essential element of that compensation. We shall review the details of the crossover model shortly.

The successful extension of the crossover model to multiloop control situations is described in Ref. 2. In fact, we utilize direct experimental results from pertinent multiloop manual control experiments in order to set numerical values for pilot-in-the-loop features in the analyses to follow. These experimental data consist of the investigations reported in Refs. 6 through 10.

D. APPLICATION OF THE CROSSOVER MODEL

It will be useful to review briefly the application of the crossover model to the manual control situation. The crossover model is described in detail in Ref. 11, but we can summarize the main points as follows. First, consider the pilot-vehicle combination expressed in vector block diagram form according to Fig. II-2. The controlled element, Y_c, is specified in terms of the helicopter mathematical model. Our task is to establish an appropriate pilot strategy, Y_p; to do so we can utilize the so-called primary rule of thumb from Ref. 5:

> "At frequencies just within and beyond the input bandwidth, seek or create (by equalization) a fair stretch of - 20 dB/decade slope for the amplitude ratio and adjust the loop gain so as to put the unity-amplitude crossover frequency near the higher edge of this region, while maintaining adequate stability margins."

---

* Control action depends only on perceived errors in states — precognitive actions and pursuit tracking (e.g., control crossfeeding) are not involved.

† The name "crossover" refers to the frequency range of validity where the model's open-loop amplitude ratio "crosses over" unity.

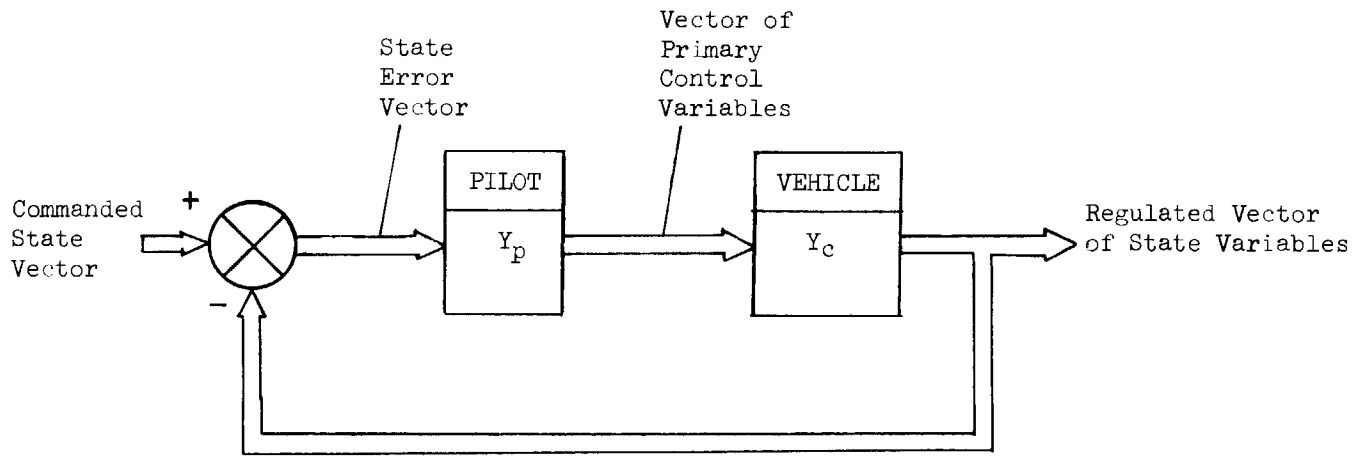

Figure II-2. Closed-Loop Pilot-Vehicle System

In applying the primary rule of thumb it is convenient to have an established value for the desired crossover frequency, ω_c. As mentioned previously we shall rely heavily on observed crossover frequencies from the experimentally derived data previously referred to. For inner loop control we shall regard a reasonable level of regulation as having a crossover frequency range between 1 and 2 rad/sec. For outer loops (position, velocity) we shall consider 0.2 to 0.5 rad/sec as an appropriate crossover frequency range. Any more preciseness in specifying loop tightness, fortunately, will be unnecessary.

We should add that the choice of crossover frequency cannot be completely arbitrary. If ω_c is too low then the closed-loop response of the regulated state variable is sluggish and the disturbance error suppression ineffective. On the other hand, if ω_c is too high, precision suffers from pilot-induced noise or remnant and, in the limit, system instability results. Even if remnant is low, then the system stability is limited by effective delays in the pilot and controlled elements. Methods for rationally determining ω_c are available as exemplified in Ref. 12, but this degree of sophistication is considered unnecessary for our purposes. Hence, we make use of experimentally determined ω_c's.

In addition to requiring a choice of crossover frequency, the crossover model also calls for an effective time delay, τ_e, which is normally on the order of 0.3 sec for a purely visual compensatory task not requiring low-frequency lead compensation.* Based on the following sketch from Ref. 2, we can see that τ_e increases with increasing pilot lead, i.e., an increase in slope of Y_p versus ω at the crossover frequency.

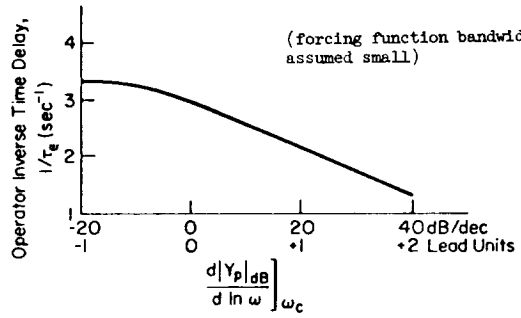

* The forcing function bandwidth is assumed to be much less than 1 rad/sec.

In the interest of maximizing mathematical simplicity we shall selectively include the effects of τ_e only where it is significant. Use of a six-degree-of-freedom quasi-static model, of course, automatically sets a limit on the validity of our analyses in the high frequency range because rotor system lags are neglected.

Let us conclude our review of the crossover model by considering an example. Suppose that roll response due to lateral control is given by:

$$Y_c \triangleq \frac{\varphi}{\delta_A} = \frac{1.2}{(s - 0.07)(s + 1.5)} \quad \text{(rad/in)} \qquad \text{(II-1)}$$

Spiral Mode / Roll Mode

In order to achieve $\omega_{c_\varphi} = 2$ rad/sec, Y_p would require first-order lead compensation at 1.5 rad/sec because of the presence of the roll mode so as to make:

$$Y_p Y_c \doteq \frac{\omega_{c_\varphi} e^{-\tau_e s}}{s} \; * \qquad \text{(II-2)}$$

This implies that

$$Y_p \doteq K_p (s + 1.5) e^{-\tau_e s} \qquad \text{(II-3)}$$

and

$$\left.\frac{d|Y_p|\,\text{db}}{d\,\ell n(\omega)}\right]_{\omega_{c_\varphi}} \doteq +10 \qquad \text{(II-4)}$$

---

* The crossover model here is written in terms of the Laplace operator, s, to emphasize that it is valid for a broad class of inputs; however, Y_p in the crossover model is strictly valid only in the frequency domain when it is based on describing function measurements.

Thus from the above sketch,

$$\tau_e \doteq 0.4 \text{ sec} \tag{II-5}$$

and

$$K_p = \frac{\omega_{c_\varphi}}{1.2} = 1.67 \frac{\text{in.}}{\text{rad}} \tag{II-6}$$

The open-loop Bode plot of Y_pY_c is shown in Fig. II-3 and two varieties of root locus plots (Bode root locus and conventional root locus) are shown in Figs. II-4 and II-5, respectively. We would expect this to be an example of a good loop closure since (i) a generous amount of phase margin (approximately 45 deg) exists at the assumed crossover frequency, and (ii) a large amplitude ratio is present at low frequencies (nearly 30 db). The most direct impact on pilot opinion would probably be associated with the anticipation involved in the lead compensation, although the lead in this situation would have only a slight adverse effect according to the results presented in the following sketch from Ref. 2 for pilot rating decrement versus order of lead equalization.

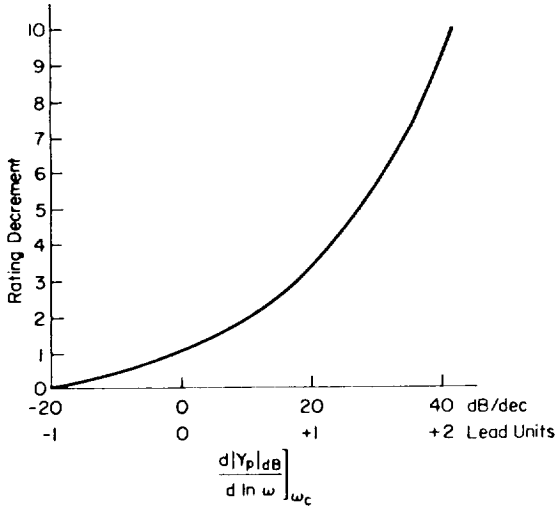

E. USE OF A PURE GAIN PILOT MODEL

The form of pilot compensation is a fundamental aspect of the closed-loop pilot-vehicle analysis described in this report. It is desirable to introduce the pilot in a way that will minimize added system complexity.

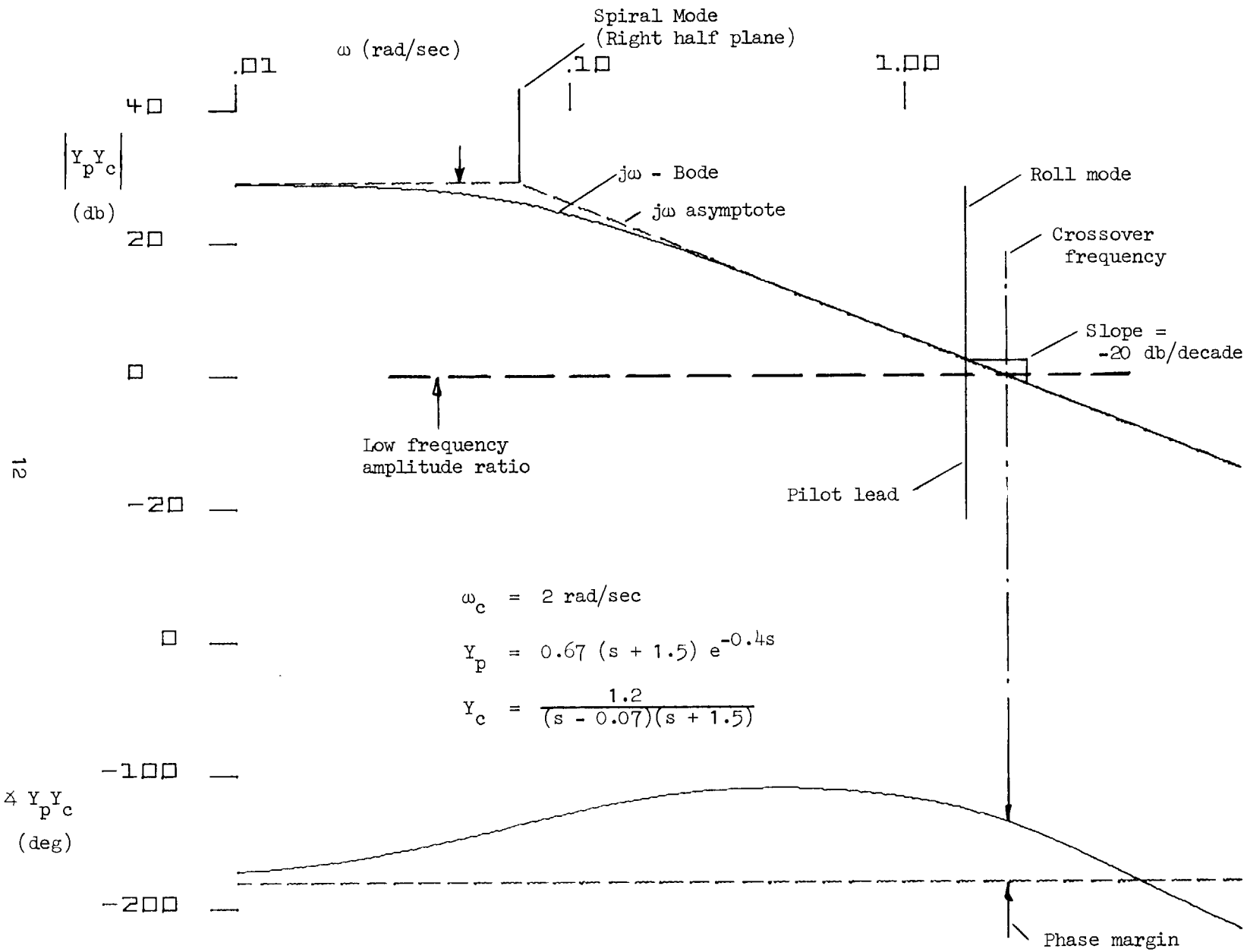

Figure II-3. Conventional Bode Plot Illustration of Crossover Model Example

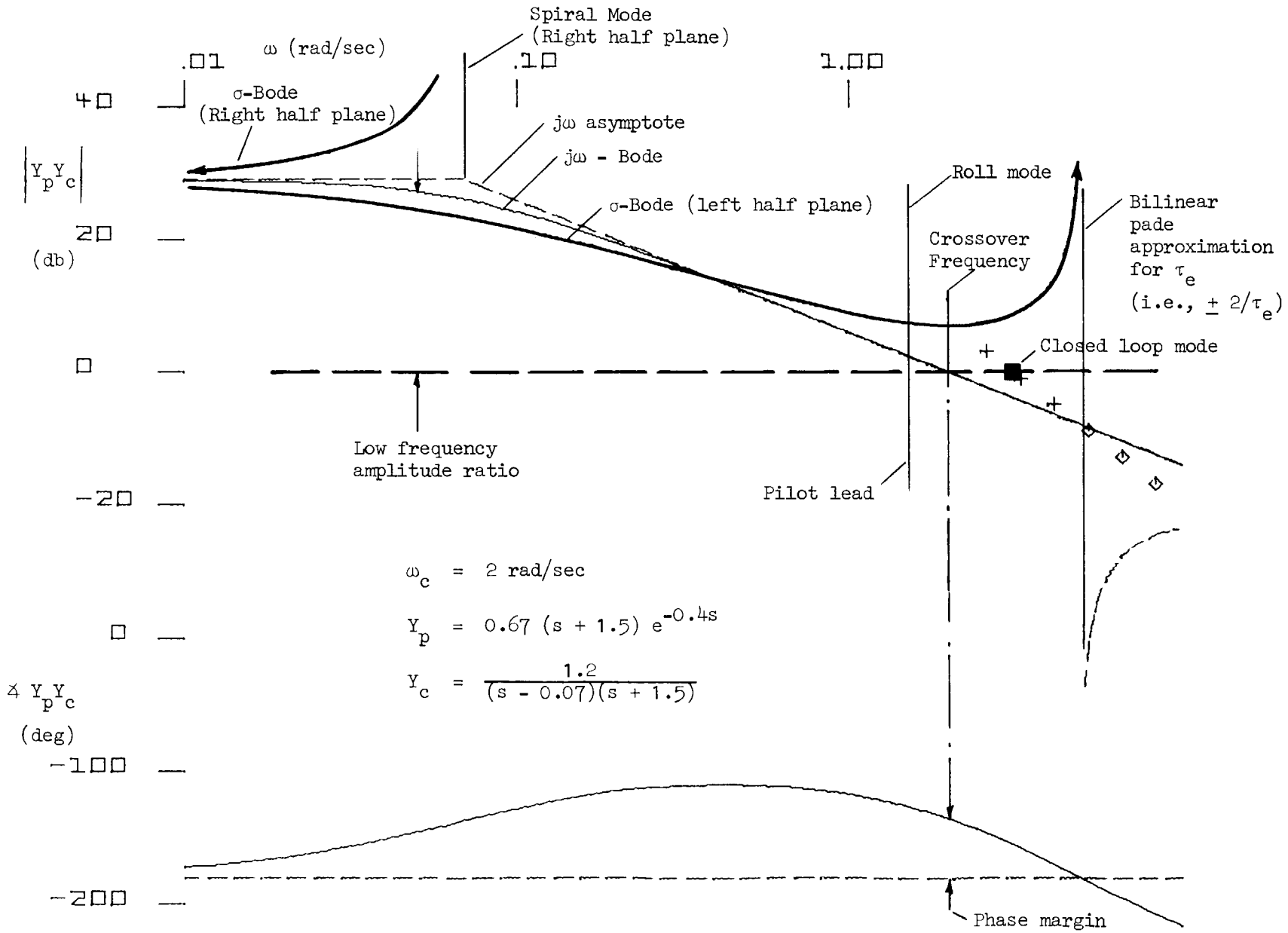

Figure II-4. Bode Root Locus Illustration of Crossover Model Example

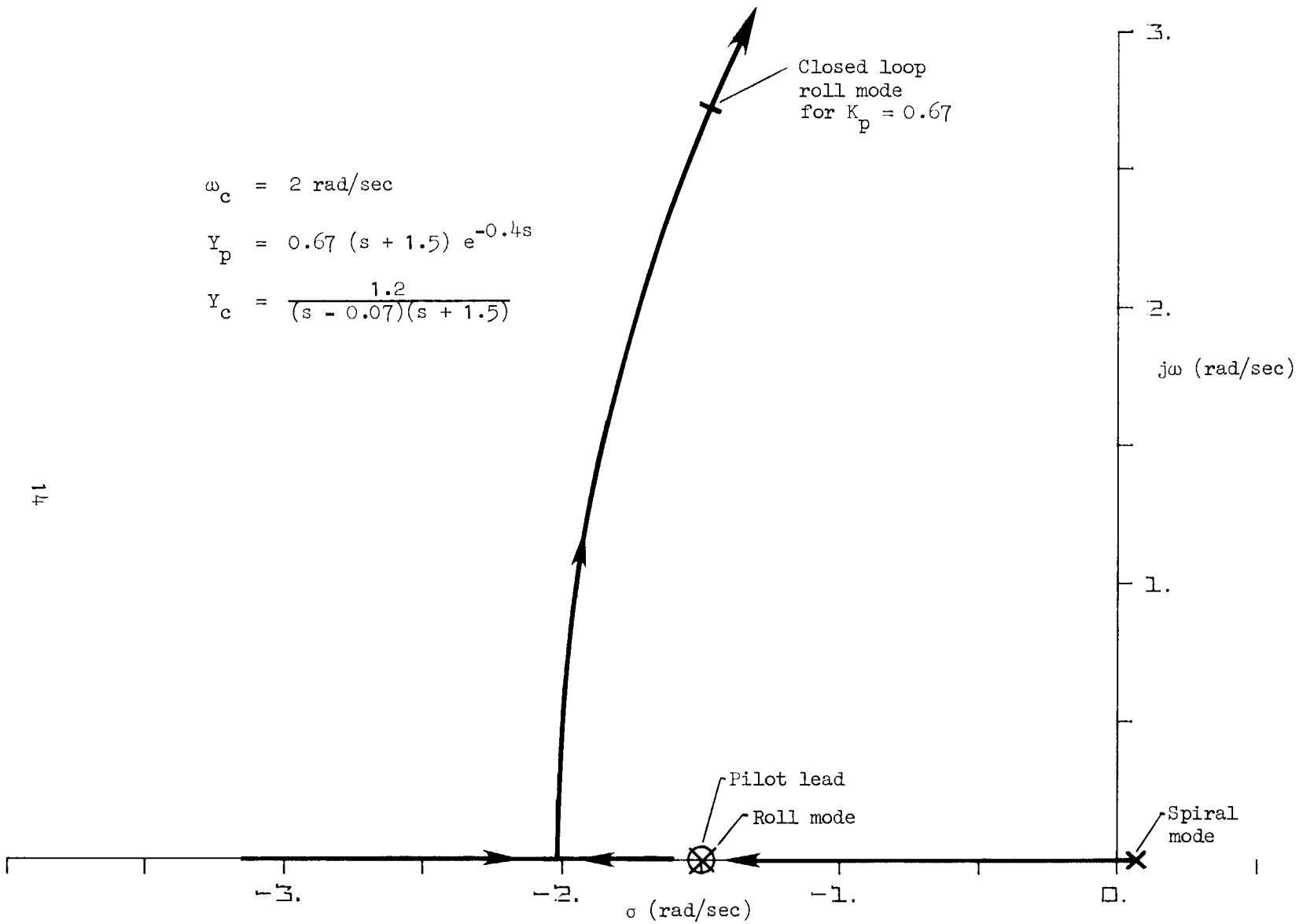

Figure II-5. Conventional Root Locus of Crossover Model Example

Strict use of the crossover model, however, forces consideration of a variety of pilot compensation possibilities in each loop thereby increasing system order and adding new variables.

We can avoid this increased complexity, though, by making use of a corollary of the crossover model which can be stated as follows. First, it has been experimentally determined that all human operator loop closures lead to crossover-model-like characteristics, i.e., Y_p is adjusted to make $|Y_pY_c|$ like $|K/s|$. Second, the lowest pilot workload seems to be imposed when $Y_c = K/s$.* These two ideas taken together imply that the pilot desires to function with only pure gain compensation. Further, if a pure gain pilot compensation cannot produce suitable closed-loop dynamics then a handling problem is indicated.

Hence, we shall use a pure gain pilot to explore various handling qualities features. If good closures cannot be produced using pure gain compensation then we can assume the pilot would have to adjust his strategy with the penalty of correspondingly higher workload. Most importantly, vehicle features which would force a departure from a pure gain can therefore be considered as significant handling qualities features.

F. USE OF CONSTRAINED VARIABLES

Our approach to analyzing handling qualities relies heavily on the use of ideally constrained (i.e., perfectly regulated) variables for a number of reasons. The main advantage is that it greatly simplifies the mathematical relationships while at the same time it retains important aspects of the full six-degree-of-freedom quasi-static vehicle model used here. Further, it enables us to dwell on the airframe features rather than to introduce an unnecessary number of pilot-related parameters.

The process of artificially constraining variables is an idealization of the pilot's role in each of the loops. For example, by constraining pitch attitude we mean to represent the essential results of a pilot (or autopilot) regulating pitch attitude. Historically, this technique was

---

* A "rate command" controlled element.

applied in the analysis of aircraft dynamics at an early stage (Refs. 13 and 14) and is equally useful in the application considered here.

Prior to using constrained variable relationships we need to consider their limitations. This can be done in a general way, but we will only illustrate the general approach using heuristic examples. These examples will be adequate to show the nature of any limitations involved but will not detract from the main objectives of Section III and IV — to analyze aspects of inner loop and outer loop regulation in helicopters.

Three kinds of constrained variable relationships which are of interest include:

- Direct commanded response
- Off-axis cross coupling
- Direct control response with off-axis regulation.

These are exemplified by (i) θ/θ_c with $\theta \longrightarrow \delta_B$*, (ii) φ/θ_c with $\theta \longrightarrow \delta_B$, and (iii) θ/δ_B with $\varphi \longrightarrow \delta_A$, respectively. Figure II-6 shows corresponding block diagrams, and Table II-1 indicates how well each is characterized by numerator ratios. The key to showing conditions of validity for constrained variable relationships is assumption of cross-over-model-like behavior in the pilot-vehicle, e.g., for $\theta \longrightarrow \delta_B$ regulation in the region of crossover:

$$\frac{Y_\theta N_{\delta_B}^{\theta}}{\Delta} \doteq \frac{\omega_{c_\theta}}{s} e^{-\tau_e s} \doteq \frac{\omega_{c_\theta}\left(1 - \frac{\tau_e s}{2}\right)}{s\left(1 + \frac{\tau_e s}{2}\right)} \qquad \text{(II-7)}$$

The implications of Table II-1 are significant. First, in cases where we desire a reasonable approximation to commanded attitude response we can express it in terms of crossover model parameters, i.e., crossover frequency and effective delay. For example, assume $\omega_{c_\theta} = 1.5$ rad/sec and $\tau = 0.3$ sec.

---

* $\theta \longrightarrow \delta_B$ signifies pitch attitude, θ, controlled by longitudinal cyclic, δ_B.

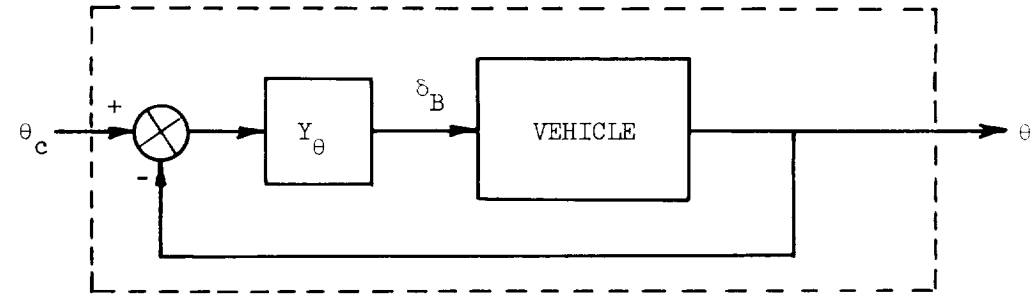

a. Direct Commanded Response

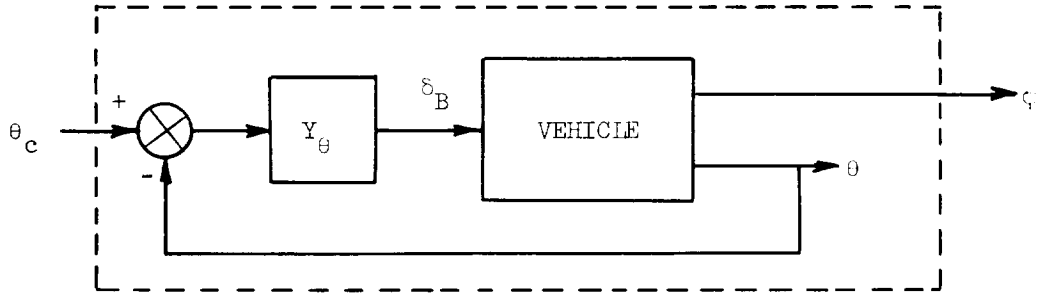

b. Off-Axis Cross-Coupling

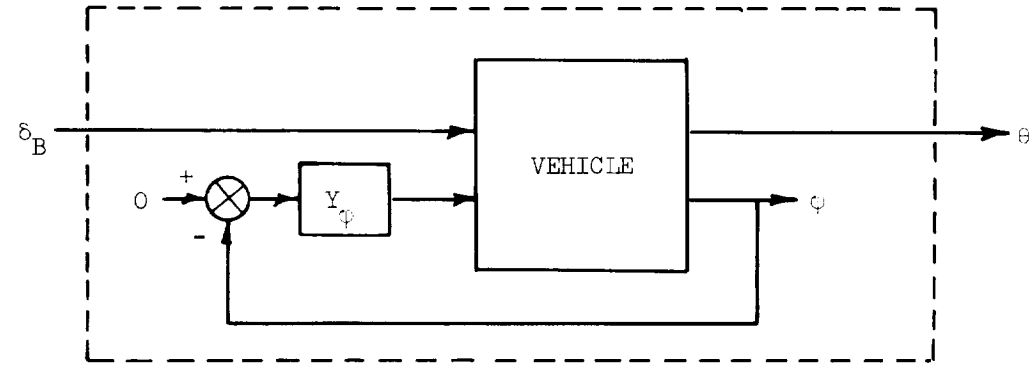

c. Direct Control Response with Off-Axis Regulation

Figure II-6. Examples of Closed-Loop Relationships (Block Diagrams)

TABLE II-1

EXAMPLES OF CLOSED LOOP RELATIONSHIPS

(Simplified Expressions)

	DIRECT COMMANDED RESPONSE	OFF-AXIS CROSS COUPLING	DIRECT CONTROL RESPONSE WITH OFF-AXIS REGULATION
CLOSED-LOOP QUANTITY	$\frac{\theta}{\theta_c}$ with $\theta \rightarrow \delta_B$	$\frac{\zeta}{\theta_c}$ with $\theta \rightarrow \delta_B$	$\frac{\zeta}{\delta_B}$ with $\zeta \rightarrow \delta_A$
EXACT RELATIONSHIP	$\frac{\theta}{\theta_c} = \frac{Y_\theta N^\theta_{\delta_B}}{\Delta + Y_\theta N^\theta_{\delta_B}}$	$\frac{\zeta}{\theta_c} = \frac{Y_\theta N^\zeta_{\delta_B}}{\Delta + Y_\theta N^\theta_{\delta_B}}$	$\frac{\theta}{\delta_B} = \frac{N^\theta_{\delta_B} + Y_\zeta N^\zeta_{\delta_A} N^\theta_{\delta_B}}{\Delta + Y_\zeta N^\zeta_{\delta_A}}$
REARRANGED EXPRESSION	$\frac{\frac{Y_\theta N^\theta_{\delta_B}}{\Delta}}{1 + \frac{Y_\theta N^\theta_{\delta_B}}{\Delta}}$	$\frac{N^\zeta_{\delta_B}}{N^\theta_{\delta_B}} \frac{\frac{Y_\theta N^\theta_{\delta_B}}{\Delta}}{\left(1 + \frac{Y_\theta N^\theta_{\delta_B}}{\Delta}\right)}$	$\frac{N^\zeta_{\delta_A} N^\theta_{\delta_B}}{N^\zeta_{\delta_A}} \frac{\left[\frac{Y_\zeta N^\zeta_{\delta_A}}{\Delta} + \frac{1}{1 - \frac{N^\zeta_{\delta_B} N^\theta_{\delta_A}}{N^\theta_{\delta_B} N^\zeta_{\delta_A}}}\right]}{\left[\frac{Y_\zeta N^\zeta_{\delta_A}}{\Delta} + 1\right]}$
VALUE IN REGION OF CROSSOVER USING CROSSOVER MODEL SUBSTITUTION*	$\frac{1 - \frac{\tau_e}{2}s}{\frac{\tau_e}{2\omega_{c_\theta}} s^2 + \left(\frac{1}{\omega_{c_\theta}} - \frac{\tau_e}{2}\right)s + 1}$	$\frac{N^\zeta_{\delta_B}}{N^\theta_{\delta_B}} \frac{\left(1 - \frac{\tau_e}{2}s\right)}{\left[\frac{\tau_e}{2\omega_{c_\theta}} s^2 + \left(\frac{1}{\omega_{c_\theta}} - \frac{\tau_e}{2}\right)s + 1\right]}$	$\frac{N^\zeta_{\delta_A} N^\theta_{\delta_B}}{N^\zeta_{\delta_A}} \frac{\left[\frac{\omega_{c_\theta}}{s}\frac{\left(1 - \frac{\tau_e}{2}s\right)}{\left(1 + \frac{\tau_e}{2}s\right)} + \frac{1}{1 - \frac{N^\zeta_{\delta_B} N^\theta_{\delta_A}}{N^\theta_{\delta_B} N^\zeta_{\delta_A}}}\right]}{\left[\frac{\omega_{c_\theta}}{s}\frac{\left(1 - \frac{\tau_e}{2}s\right)}{\left(1 + \frac{\tau_e}{2}s\right)} + 1\right]}$
LOW FREQUENCY VALUE	1	$\frac{N^\zeta_{\delta_B}}{N^\theta_{\delta_B}}$	$\frac{N^\zeta_{\delta_A} N^\theta_{\delta_B}}{N^\zeta_{\delta_A}}$
ESSENTIAL FEATURES	• Time delay τ_e • Undamped natural frequency $\omega_n = \sqrt{\frac{2\omega_{c_\theta}}{\tau_e}}$ • Damping ratio $\zeta = \frac{1}{2}\left(\frac{1}{\omega_{c_\theta}} - \frac{\tau_e}{2}\right)\omega_n$	• Magnitude and shape of ζ/θ_c response given by numerator ratio • Delay and response same as for θ/θ_c	• Overall character given by numerator ratio except where mutual cross coupling product is significant, i.e., $N^\zeta_{\delta_B} N^\theta_{\delta_A}$ • Crossover model parameters are higher order effects

* According to the crossover model:

$$\frac{Y_\theta N^\theta_{\delta_B}}{\Delta} = \frac{\omega_{c_\theta}}{s} e^{-\tau_e s} \doteq \frac{\omega_{c_\theta}}{s}\frac{\left(1 - \frac{\tau_e}{2}s\right)}{\left(1 + \frac{\tau_e}{2}s\right)}$$

and $$\frac{Y_\zeta N^\zeta_{\delta_A}}{\Delta} = \frac{\omega_{c_\zeta}}{s} e^{-\tau_e s} \doteq \frac{\omega_{c_\zeta}}{s}\frac{\left(1 - \frac{\tau_e}{2}s\right)}{\left(1 + \frac{\tau_e}{2}s\right)}$$

then,

$$\frac{\theta}{\theta_c} \doteq \frac{1 - 0.15\ s}{0.1\ s^2 + 0.52\ s + 1} \qquad \text{(II-8)}$$

i.e., $\omega_n = 3.2$ rad/sec, $\zeta = 0.82$. Next, for cross-coupling characteristics we can use a simple numerator ratio in combination with the direct commanded response, or

$$\frac{\varphi}{\theta_c} \doteq \frac{N^{\varphi}_{\delta_B}}{N^{\theta}_{\delta_B}} \cdot \frac{\theta}{\theta_c} \qquad \text{(II-9)}$$

Finally, off-axis regulation can be included in a direct control response transfer function such as θ/δ_B by simply using the appropriate coupling numerator ratio. Thus to include the effects of roll regulation in the basic pitch response,

$$\frac{\theta}{\delta_B} \doteq \frac{N^{\varphi}_{\delta_A} N^{\theta}_{\delta_B}}{N^{\varphi}_{\delta_A}} \qquad \text{(II-10)}$$

Hence, the off-axis control numerator becomes the transfer function denominator.

G. IDENTIFICATION AND LABELING OF RESPONSE MODES

It is frequently convenient to assign labels to dominant modes. Normally, there is little difficulty in doing so if longitudinal equations of motion are decoupled from lateral-directional ones. In the case of six degrees of freedom (or more) we must consider a more rigorous procedure for determining dominant modes. The following approach serves our purposes.

The method we shall use to identify response modes is based on the assumption of a conventional transfer function form for a closely related state variable-cockpit control combination, e.g., θ, and δ_B. As long as the longitudinal-lateral-directional coupling is not too extreme, we know that the numerator-denominator combination should have an effective minimal degree of freedom form although it involves a number of approximately cancelling dipole factors. As an example, consider the OH-6A in hover:

$$\frac{\theta}{\delta_B} = \frac{\overbrace{-.74(0.02)^*}^{\text{Effective minimal degree of freedom form}} \overbrace{[-.03;0.5](0.24)(0.9)(5.0)}^{\text{Approximately cancelling dipole factors}}}{[0;0.4](2.0)\ [-.03;0.5](0.23)(0.8)(4.9)} \qquad \text{(II-11)}$$

The effective minimal degree of freedom form can be easily related to normal dominant modes. In the case above, the second order roots are clearly the phugoid, and the first order is pitch damping. All other denominator (poles) roots are nearly cancelled by respective numerator roots (zeros). These other roots must be identified by considering appropriate transfer functions. For example, to identify roll damping we would use the φ/δ_A transfer function.

---

* The following shorthand will be used to express polynomial factors:

$$(a) \triangleq (s + a) \quad \text{and} \quad [\zeta,\omega] \triangleq [s^2 + 2\zeta\omega s + \omega^2] \qquad \text{(II-12)}$$

Mode label formulation is summarized in Table II-2. In addition to considering basic open-loop denominator modes we also assign labels to certain numerator roots which ultimately become response modes in a closed-loop sense, e.g., surge (or speed) damping does become a response mode when pitch attitude is regulated. Also, we take the liberty of applying conventional labels in other than purely open-loop transfer functions. For example, phugoid and pitch damping labels are used for denominator factors in the θ/δ_B transfer function where roll and yaw are constrained. This is convenient for keeping track of important response modes as loops in other axes are variously closed.

A note of caution — this procedure cannot be considered as exact nor does it always apply. In many cases response modes cannot be identified such as when the response deviates too far from the norm, when two modes are very close in numerical value, or when augmentation significantly changes the complexion of the pole-zero form.

TABLE II-2. MODE LABEL FORMULATION

	GENERAL FORM	EXAMPLE: OH-6A, OPEN-LOOP	EXAMPLE: OH-6A, OFF-AXES CONSTRAINED
Longitudinal Hover:	$\frac{\theta}{\delta_B} = \frac{A_\theta(^{SD}) \{\ \}}{[_P\ ](_{PD})\{\ \}}$	$\frac{N^{\theta}_{\delta_B}}{\Delta} = \frac{-.74\ (.02)\{[-.03,.5](.24)(.9)(5.0)\}}{[0,.4](2.0)\{[-.03,.5](.23)(.8)(4.9)\}}$ (SD; P, PD)	$\frac{N^{\theta\ \varphi\ \psi}_{\delta_B\delta_A\delta_p}}{N^{\varphi\ \psi}_{\delta_A\delta_p}} = \frac{-.75\ (.01)\{(.02)(.34)\}}{[-.1,.47](1.9)\{(.02)(.36)\}}$ (SD; P, PD)
Forward Flight:	$= \frac{A_\theta(^{SD})(^{HD})\{\ \}}{[_P\ ][_{SP}]\{\ \}}$	$\frac{N^{\theta}_{\delta_B}}{\Delta} = \frac{-.74\ (.02)(.73)\ \{(.06)(5.7)[.2,2.7]\}}{[.04,.3][.98,1.7]\{(.06)(5.7)[.2,2.6]\}}$ (SD, HD; P, SP)	$\frac{N^{\varphi\ \varphi}_{\delta_B\delta_A}}{N^{\varphi}_{\delta_A}} = \frac{-.75\ (.02)(.74)\{[.27,2.7]\}}{[.05,.30](1.4)(1.9)\{[.27,2.6]\}}$ (SD, HD; P, SP)
Lateral Hover:	$\frac{\varphi}{\delta_A} = \frac{A_\theta(^{LD})\ \{\ \}}{[_{PL}](_R)\{\ \}}$	$\frac{N^{\varphi}_{\delta_A}}{\Delta} = \frac{1.28\ (.02)\{[-.0,.4](.2)(.8)(1.9)\}}{[-.03,.5](4.9)\{[.0,.4](.2)(.8)(2.0)\}}$ (LD; PL, R)	$\frac{N^{\varphi\ \theta\ \psi}_{\delta_A\delta_B\delta_p}}{N^{\theta\ \psi}_{\delta_B\delta_p}} = \frac{1.28\ (.02)\{(.01)(.34)\}}{[-.0,.56](4.9)\{(.01)(.34)\}}$ (LD; PL, R)
Forward Flight:	$= \frac{A_\varphi\ \{\ \}}{(_S)(_R)\{\ \}}$	$\frac{N^{\varphi}_{\delta_A}}{\Delta} = \frac{1.3\ \{[.05,.3](1.4)(1.9)[.3,2.6]\}}{(.06)(5.7)\{[.04,.3][.98,1.7]\ [.2,2.6]\}}$ (S, R)	$\frac{N^{\varphi\ \theta}_{\delta_A\delta_B}}{N^{\theta}_{\delta_B}} = \frac{1.27\ \{(.02)(.74)[.27,2.7]\}}{(.06)(5.7)\{(.02)(.73)[.22,2.7]\}}$ (S, R)
Directional Hover:	$\frac{\psi}{\delta_p} = \frac{A_\psi\ \{\ \}}{(0)(_{YD})\{\ \}}$	$\frac{N^{\psi}_{\delta_p}}{\Delta} = \frac{-2.6\ \{[-.2,.5]\ [.05,.5](.4)\ (2)\ (4.8)\}}{(0)(.8)\{\ [0,.4][-.08,.5](.2)(2.0)(4.9)\}}$ (YD)	$\frac{N^{\psi\ \theta\ \varphi}_{\delta_p\delta_B\delta_A}}{N^{\theta\ \varphi}_{\delta_B\delta_A}} = \frac{-2.55\{(.01)(.02)(.34)\}}{(0)(.9)\{(.01)(.02)(.25)\}}$ (YD)
Forward Flight:	$= \frac{A_\psi\ [\ ]\{\ \}}{(0)(_S)[_D\ ]\{\ \}}$	$\frac{N^{\psi}_{\delta_p}}{\Delta} = \frac{-2.7\ [.4,.5]\ \{(5.5)(.9)(2.2)[-.35,.4]\}}{(0)(.06)[.2,2.6]\{(5.7)[.98,1.7][.04,.3]\}}$ (S, D)	$\frac{N^{\psi\ \theta\ \varphi}_{\delta_p\delta_B\delta_A}}{N^{\theta\ \varphi}_{\delta_B\delta_A}} = \frac{-2.7\ (.01)\ \{(.02)(.73)\}}{(0)[.27,2.7]\{(.02)(.74)\}}$ (D)

( ) first order factor, [ ] second order factors, {( )...[ ]} approximately cancelling dipole factors.

( ) / X } mode label according to the following key: P - phugoid, PL - lateral phugoid, PD - pitch damping, R - roll damping, YD - yaw damping, SP - short period, D - dutch roll, S - spiral, SD - surge damping, LD - sway damping, HD - heave damping

SECTION III

INNER LOOP REGULATION

A. BACKGROUND

In this section we discuss how helicopter handling qualities related to inner loop regulation (roll, pitch, and yaw regulation) can be put in the context of the overall pilot-vehicle. To do so we treat inner loop aspects in terms of (1) primary control response and (2) cross coupling effects.

We shall show that primary control response features for a coupled longitudinal-lateral-directional system are, in fact, essentially similar to the more conventional two- and three-degree-of-freedom descriptions (e.g., as variously described in Refs. 1, 15, 16, 17, and 18). Our main task will be to reduce the apparent complexity of high order transfer functions coupled with multi-axis manual loop closures. One point of interest will be the effect of off-axis regulation on each primary response mode, for example, the effect of roll attitude regulation on pitch attitude response.

In dealing more directly with cross-coupling effects, we exercise the six-degrees-of-freedom helicopter model combined with the pilot-in-the-loop. One aspect demonstrated is the variety of potential cross-coupling effects, and we propose a method for defining each in terms of an overall closed-loop metric which is devoid of an explicit numerical pilot description.

B. PRIMARY CONTROL RESPONSE

Primary control response for the inner loops refers specifically to:

- Roll due to lateral cyclic stick, δ_A
- Pitch due to longitudinal cyclic stick, δ_B
- Yaw due to rotary rudder pedal, δ_p.

Each of these responses is expressed in terms of an Euler angle* and respective cockpit controller deflection.

In viewing any particular primary control response it will be important to deal effectively with the other two axes. That is to say, the primary response in one axis should be considered in the context of realistic regulation of the other axes. There are two compelling reasons for this:

(i) There may be off-axis dominant modes which are lightly damped or even unstable which would unnecessarily complicate analysis of the primary axis.

(ii) Regulation of off-axis variables may alter the transfer function of the axis in question — its gain, poles, and zeros.

Among the following examples which exemplify the effects of off-axis regulation on primary pitch control response, we shall assume perfect regulation of roll attitude and yaw. This assumption permits the use of coupling numerator ratios to represent limiting values of the transfer function in Eq. III-1, i.e.:

$$\left.\frac{\theta}{\delta_B}\right|_{\substack{\varphi \to \delta_A \\ \psi \to \delta_p}} = \frac{N^{\theta}_{\delta_B} + Y_{\varphi}N^{\theta\ \varphi}_{\delta_B\ \delta_A} + Y_{\psi}N^{\theta\ \psi}_{\delta_B\ \delta_p} + Y_{\varphi}Y_{\psi}N^{\theta\ \varphi\ \psi}_{\delta_B\ \delta_A\ \delta_p}}{\Delta + Y_{\varphi}N^{\varphi}_{\delta_A} + Y_{\psi}N^{\psi}_{\delta_p} + Y_{\varphi}Y_{\psi}N^{\varphi\ \psi}_{\delta_A\ \delta_p}} \qquad \text{(III-1)}$$

with regulation of roll attitude and yaw defined by transfer functions Y_{φ} and Y_{ψ}, respectively. Note that pitch response is simply

$$\frac{\theta}{\delta_B} = \frac{N^{\theta}_{\delta_B}}{\Delta} \qquad \text{(III-2)}$$

without regulation of roll attitude and yaw ($Y_{\varphi} = Y_{\psi} = 0$).

---

*The standard aircraft Euler angle set as described in Volume One.

Also,

$$\left.\frac{\theta}{\delta_B}\right|_{\varphi} \doteq \frac{N^{\theta\ \varphi}_{\delta_B \delta_A}}{N^{\varphi}_{\delta_A}} \qquad \text{(III-3)}$$

with perfect roll attitude regulation but without yaw regulation ($Y_\psi = 0$)

Finally,

$$\left.\frac{\theta}{\delta_B}\right|_{\varphi,\psi} \doteq \frac{N^{\theta\ \varphi\ \psi}_{\delta_B \delta_A \delta_p}}{N^{\varphi\ \psi}_{\delta_A \delta_p}} \qquad \text{(III-4)}$$

with perfect roll attitude and yaw regulation where Y_φ and Y_ψ are the pilot's compensatory control actions in regulating roll and yaw. According to Table II-1, the assumption of perfect roll axis regulation is valid if $1 - (N^{\varphi}_{\delta_B} N^{\theta}_{\delta_A} / N^{\theta}_{\delta_B} N^{\varphi}_{\delta_A})$ is small in the frequency range of interest (say, approximately 1 rad/sec). Similarly, perfect yaw regulation is valid if $1 - (N^{\psi}_{\delta_B} N^{\theta}_{\delta_p} / N^{\theta}_{\delta_B} N^{\psi}_{\delta_p})$ is small. We can give an indication, by example, of how good are the perfect regulation assumptions.

As an example of the above let us consider the pitch attitude response of the OH-6A in hover. For a six-degrees-of-freedom quasi-static model the completely open loop pitch attitude-to-longitudinal cyclic control transfer function is:

$$\frac{\theta}{\delta_B} = \frac{N^{\theta}_{\delta_B}}{\Delta} = \underbrace{\frac{-.737(0.0164)}{[0.001;0.408](2.01)}}_{\text{Dominant Pitch Response}} \underbrace{\frac{\{(0.249)(0.892)(4.96)[-.034;0.554]\}}{\{(0.229)(0.821)(4.93)[-.028;0.512]\}}}_{\text{Approximately Cancelling Dipoles}} \qquad \text{(III-5)}$$

P PD HD YD R PL

The various response modes have been identified and are labeled according to the procedure outlined previously. Note that the lateral phugoid mode is unstable and would remain so even with pitch attitude perfectly regulated.

(The pair of zeros corresponding to the lateral phugoid is also in the right half plane.) This lateral instability would not exist, however, with normal manual regulation of roll. Therefore, it is important to provide some degree of roll attitude regulation when describing pitch response.

If perfect roll attitude regulation be implemented, then pitch response to longitudinal cyclic becomes:

$$\left.\frac{\theta}{\delta_B}\right|_{\varphi} = \frac{N^{\theta\ \varphi}_{\delta_B \delta_A}}{N^{\varphi}_{\delta_A}} = \frac{-.747(0.0161)\quad \{(0.253)(0.892)(0.0216)\}}{[-.008;0.395](1.87)\{(0.232)(0.812)(0.0216)\}} \qquad \text{(III-6)}$$

P PD HD YD LD

Dominant Pitch Response — Approximately Cancelling Dipoles

The lateral phugoid complex dipole pair disappears and a low frequency sway damping dipole emerges. But, more important to the pitch loop, the longitudinal phugiod is destabilized by the roll loop!

If we also consider yaw regulation, the pitch response to longitudinal cyclic is further altered. This is shown in the limiting case of perfect roll attitude and yaw regulation, i.e.,

$$\left.\frac{\theta}{\delta_B}\right|_{\varphi,\psi} = \frac{N^{\theta\ \varphi\ \psi}_{\delta_B \delta_A \delta_p}}{N^{\varphi\ \psi}_{\delta_A \delta_p}} = \frac{-.746(0.0148)\quad \{(0.340)(0.0218)\}}{[-.125;0.471](1.85)\{(0.358)(0.0216)\}} \qquad \text{(III-7)}$$

P PD HD LD

Dominant Pitch Response — Approximately Cancelling Dipoles

Two things occur, the yaw damping mode disappears and the phugoid becomes even more unstable.

For the same case as was used in the previous examples, if Y_φ and Y_ψ are defined as a pure gain corresponding to 1 rad/sec crossover frequency for roll and yaw, then:

$$\frac{\theta}{\delta_B} = \frac{-.737(0.016)\quad\{(0.333)(0.478)(6.28)(17.3)[0.203;1.11]\}}{[-.196;0.462](1.82)\{(0.368)(0.464)(6.28)(12.3)[0.202;1.12]\}} \qquad \text{(III-8)}$$

P PD HD

Dominant Pitch Response

Approximately Cancelling Dipoles

Compare the dominant pitch response in Eq. III-8 with that in Eq. III-7. The same closed-loop features appear in the dominant pitch response as when perfect roll attitude and yaw regulation are assumed. The phugoid damping is destabilized and the pitch damping is reduced slightly.

To summarize, we have used an example of the pitch attitude response of the OH-6A in hover to illustrate that:

- Primary (pitch attitude) control response does vary with off-axis regulation.
- The nature of variation in primary control response due to normal off-axis regulation can be indicated by assuming perfect off-axis regulation.
- Assumption of perfect off-axis regulation, in fact, simplifies the primary control response transfer function by reducing transfer function order (effectively, stabilizing lightly damped or unstable off-axis dominant modes).

These results are motivation for looking at primary inner loop control response in the context of realistic manual off-axis regulation. Further, in creating this context, we have demonstrated that there is considerable advantage to assuming perfect off-axis regulation. Hence, these ideas are central to the analysis of primary control response for each of the three inner loop functions: pitch and roll attitude and yaw regulation.

In the following pages we do not dwell on handling qualities aspects related to the dominant response features. This is done in a comprehensive way in Ref. 16 for VTOL aircraft in general, and specifically for helicopters in Refs. 15 and 19. The latter source contains a detailed discussion of the long standing helicopter handling qualities military specification (MIL-H-8501A, Ref. 20) in the context of the closed-loop pilot-vehicle. We do point out, however, those features of the five helicopters included in Volume One which are important to primary control response.

1. Pitch Axis

The predominant features of pitch axis control for an unaugmented helicopter can be summarized in terms of the general form of the transfer function given in Section II, i.e., for hover,

$$\frac{\theta}{\delta_B} = \frac{A_\theta \left(\quad\right)^{SD} \left\{\left(\quad\right)^{HD} \right\} e^{-\tau_c s^*}}{\left[\quad\right]_P \left(\quad\right)_{PD} \left\{\left(\quad\right)_{HD}\right\}} \qquad \text{(III-9)}$$

Approximately cancelling dipole factors

for forward flight,

$$\frac{\theta}{\delta_B} = \frac{A_\theta \left(\quad\right)^{SD} \left(\quad\right)^{HD} \left\{ \right\} e^{-\tau_c s^*}}{\left[\quad\right]_P \left[\quad\right]_{SP} \left\{ \right\}} \qquad \text{(III-10)}$$

Approximately cancelling dipole factors

---

*A transport delay function has been added to the above expressions to indicate the existence of some effective lag associated with rotor system tip path plane dynamics and control system dynamics which are, of course, absent in the six-degrees-of-freedom quasi-static form employed here. A similar effect is involved in the other control transfer functions. For simplicity, however, we shall omit this effective lag notation and absorb it in the pilot's effective delay, τ_e.

The above form is meant primarily as a guide to arranging the transfer function factors which are cataloged in Volume One and, if possible, assigning labels to those factors which are especially relevant to the pitch axis response. Although a separate form is shown for hover and forward flight, there is really a continuity between the two forms, because the pitch damping and heave damping modes, usually two first-order roots in hover, do couple to form a classical short period mode as forward velocity is increased. We shall consider the bridge between hover and forward flight more thoroughly in Section VII.

a. Hovering Flight

A survey of pitch axis response in hover for various helicopter examples with varying degrees of off-axis regulation is shown in Table III-1. This survey, as well as those to follow regarding other features, is meant primarily as an illustration of how the basic handling qualities data presented in Volume One can be viewed, and is some indication of how the handling qualities features are likely to vary among several vehicles. In this table dominant transfer function factors are labeled where possible. In the cases of the AH-1G and UH-1H, the normal classification of the factors does not apply well because of low levels of pitch damping and substantial cross-coupling effects with other axes. In the case of the CH-53D there is an example of the inability to discriminate between two modes which are nearly equal in value, i.e., yaw damping and heave damping. We shall see that the ability to apply classical mode labels to transfer function factors is sometimes a problem in other axes as well.

One aspect shown in Table III-1 is the effect of off-axis regulation, i.e., roll and yaw regulation, on the primary pitch response. Except for the BO-105 there is consistently a degradation of phugoid damping as roll and yaw loops are closed. For the OH-6A the largest source of degradation appears to be the yaw loop regulation; however, in the other three examples it is the roll loop which destabilizes the phugoid. Knowledge of how the off-axis regulation affects primary control response (in this case pitch)

TABLE III-1. SURVEY OF APPROXIMATE* PITCH AXIS RESPONSE TRANSFER FUNCTIONS (HOVER)

	OH-6A	BO-105	AH-1G (SCAS OFF)	UH-1H (WITHOUT STABILIZER BAR)	CH-53D (SAS OFF)
Open Loop: $\frac{N^{\theta}_{\delta_B}}{\Delta}$ =	$\frac{\overset{SD}{-.24}(.016)\overset{HD}{(.25)}}{\underset{P}{[.001,.41]}(.43)\underset{HD}{(.43)}(2.0)\underset{PD}{}}$	$\frac{\overset{SD}{-.97}(0)\overset{HD}{(.35)}}{\underset{P}{[-.05,.42]}(.35)\underset{HD}{(3.8)}\underset{PD}{}}$	$\frac{\overset{SD}{-.15}(.016)[.98,.47]}{\underset{P}{[-.29,.36]}[.84,.71](.44)}$	$\frac{\overset{SD}{-.17}(-.01)[.96,.41]}{\underset{P}{[-.37,.46]}(.47)[.80,.83]}$	$\frac{\overset{SD}{-.18}(.04)(.28)(.33)}{\underset{P}{[-.04,.67]}\underbrace{(.29)(.32)}_{\text{YD OR HD?}}(.59)\underset{PD}{}}$
Roll Perfectly Regulated: $\frac{N^{\theta}_{\delta_E}\xi_A}{N^{\theta}_{\xi_A}}$ =	$\frac{\overset{A_{ss}}{-.73}\overset{SD}{(.016)}\overset{HD}{(.25)}}{\underset{P}{[-.01,.40]}(.23)\underset{HD}{(1.9)}\underset{PD}{}}$	$\frac{\overset{SD}{-1.00}(0)\overset{HD}{(.39)}}{\underset{P}{[-.04,.45]}(.39)\underset{HD}{(3.6)}\underset{PD}{}}$	$\frac{\overset{SD}{-.15}(-.001)[.99,.45]}{\underset{P}{[-.43,.28]}[.88,.48](.52)}$	$\frac{\overset{SD}{-.17}(-.01)(.44)}{\underset{P}{[-.45,.38]}[.90,.51]}$	$\frac{\overset{SD}{-.18}(.04)(.28)(.33)}{\underset{P}{[-.24,.48]}\underbrace{(.30)(.32)}_{\text{YD OR HD?}}(.83)\underset{PD}{}}$
Roll and Yaw Perfectly Regulated: $\frac{N^{\theta}_{\delta_E}\xi_A\xi_p}{N^{\theta}_{\xi_A}\xi_p}$ =	$\frac{\overset{SD}{-.75}(.011)(.54)}{\underset{P}{[-.15,.47]}(.54)\underset{HD}{(1.9)}\underset{PD}{}}$	$\frac{\overset{SD}{-1.01}\overset{HD}{(0)(.35)}}{\underset{P}{[-.05,.43]}(.35)\underset{HD}{(3.6)}\underset{PD}{}}$	$\frac{\overset{SD}{-.15}\overset{HD}{(-.001)(.39)}}{\underset{P}{[-.45,.28]}[.90,.47]\underset{SP}{}}$	$\frac{\overset{SD}{-.17}\overset{HD}{(-.01)(.39)}}{\underset{P}{[-.44,.52]}[.92,.49]\underset{SP}{}}$	$\frac{\overset{SD}{-.18}\overset{HD}{(.04)(.30)}}{\underset{P}{[-.23,.47]}(.50)\underset{HD}{(.8)}\underset{PD}{}}$
Remarks:	•Decrease in ζ_p with $\varphi \rightarrow \delta_A$, $\psi \rightarrow \delta_p$. •Increase in heave damping with $\psi \rightarrow \delta_p$.	•Essentially no effect due to $\varphi \rightarrow \delta_A$, $\psi \rightarrow \delta_p$.	•Modes difficult to label. •Substantial loss of ζ_p with $\varphi \rightarrow \delta_A$. •Substantial coupling of off-axis modes, especially open loop.	•Large unstable ζ_p. •Similarities to AH-1G.	•Phugoid damping and pitch damping loss due $\varphi \rightarrow \delta_A$. •Can't discriminate between yaw damping and heave damping modes.

*Approximately cancelling dipole factors are omitted from 6 DOF quasi-static transfer function expressions shown.

( ) first order factor, [ ] second order factors, $\{( ) \ldots [ ]\}$ approximately cancelling dipole factors.

$\{{}^{(\ )}_{X}\}$ mode label according to the following key: P - phugoid, PL - lateral phugoid, PD - pitch damping, R - roll damping, YD - yaw damping, SP - short period, D - dutch roll, S - spiral, SD - surge damping, LD - sway damping, HD - heave damping,

is a direct benefit of the six-degrees-of-freedom model, i.e., coupled longitudinal-lateral-directional equations of motion. It is believed that additional information concerning such indirect cross-coupling effects would accrue from use of higher order equations of motion which included rotor flapping degrees of freedom, although the effects would likely be limited to the very short term effective control lag features. Data was not available to verify this, however.

Closed-loop pitch attitude control has been analyzed in a number of earlier efforts (e.g., Refs. 15, 16, and 19). The cases considered here indicate that the classical form is still a valid way of viewing direct pitch response although there are effects from off-axis regulation. For the purposes of this report it is nevertheless useful to consider briefly pitch axis regulation in a closed-loop context. This can be done relatively easily if we rely on a pilot model consisting of a pure gain feedback of pitch attitude to longitudinal cyclic control. The essential features of pitch attitude loop control in hover are summarized in Table III-2 which shows that the important stability derivatives in the pitch loop are simply M_q and M_u (and to a minor extent, X_u).

Note that the open-loop pitch response, without control lags, is approximately:

$$\frac{\theta}{\delta_B} \doteq \frac{M_{\delta_B}\, s}{\underbrace{\left[s^2 - \frac{gM_u}{M_q}\right]}_{P} \underbrace{(s - M_q)}_{PD}} \qquad \text{(III-11)}$$

The accuracy of this approximation for the vehicles in Volume One is shown in Table III-3, i.e.:

- The phugoid frequency, ω_p, is compared to $\sqrt{gM_u/-M_q}$
- The pitch damping mode, $1/T_{sp_2}$, is compared to $-M_q$

Where there is a fair level of pitch damping (e.g., OH-6A and BO-105) the separation of modes is wide, and the approximations are good.

TABLE III-2

ESSENTIAL FEATURES OF PITCH ATTITUDE CONTROL
IN HOVERING FLIGHT

TRANSFER FUNCTION:

$$\frac{\theta}{\delta_B} \doteq \frac{A_\theta\left(\frac{1}{T_{\theta_1}}\right)}{\underset{P}{[\zeta_p;\omega_p]}\underset{PD}{\left(\frac{1}{T_{sp_2}}\right)}}$$

APPROXIMATE FACTORS:

$$\frac{1}{T_{sp_2}} \doteq \frac{-3M_q}{4} + \sqrt{\frac{M_q^{\,2}}{16} - \frac{g}{2}\frac{M_u}{M_q}} \doteq -M_q$$

$$\omega_p^{\,2} \doteq \frac{gM_u}{1/T_{sp_2}} \doteq \frac{-gM_u}{M_q}$$

$$2\zeta_p\omega_p \doteq -X_u - M_q - \frac{1}{T_{sp_2}} \doteq 0$$

$$\frac{1}{T_{\theta_1}} \doteq -X_u + \frac{X_{\delta_B}}{M_{\delta_B}} M_u \doteq 0$$

$$A_\theta = M_{\delta_B}$$

TABLE III-3

CORRESPONDENCE OF PITCH RESPONSE MODES TO DOMINANT STABILITY DERIVATIVES
(HOVER)

	OH-6A	BO-105	AH-1G (SCAS Off)	UH-1H (Without Stabilizer Bar)	CH-53D (SAS Off)
$\sqrt{\frac{gM_u}{-M_q}}$ $(\frac{1}{sec})$	0.48	0.44	0.29	0.56	0.62
ω_p* $(\frac{rad}{sec})$ (phugoid natural frequency)	0.47	0.43	0.28	0.38	0.47
$-M_q$ $(\frac{1}{sec})$	1.8	3.4	0.23	0.19	0.50
$\frac{1}{T_{sp_2}}$* $(\frac{rad}{sec})$ (pitch damping)	1.9	3.6	$\doteq$ 0.5	$\doteq$ 0.5	0.82

* Taken from θ/δ_B response with φ and ψ constrained, i.e., from $N^{\varphi\ \psi}_{\delta_A \delta_p}$ coupling numerator

For the helicopter examples considered, the phugoid frequency at hover falls within the range between 0.3 and 0.5 rad/sec. Thus, for the θ/δ_B transfer function to be like K/s, the pitch damping mode (hence $-M_q$) should be at least as large or somewhat greater than the desired crossover frequency, ω_{c_θ}. This condition is met by the OH-6A and BO-105 examples. In the remaining three cases the pitch damping is low, and it is not surprising that stability augmentation is employed by each.

A way of viewing the quality of the θ/δ_B response is to consider the phase margin in the region of crossover. According to experimental measurements, a phase margin of about 30 deg is usually present in the open-loop pilot-vehicle transfer function. Since the phugoid normally involves low damping, its phase contribution at 1 to 2 rad/sec is small. Thus, the approximate phase margin for a pure gain pilot is:

$$\varphi_{M_\theta} \doteq \tan^{-1} \frac{-M_q}{\omega_{c_\theta}} \qquad \text{(III-12)}$$

If we use 30 deg phase margin as a rule of thumb for a minimum required level, then the required pitch damping must be:

$$-M_q \geq 0.58\, \omega_{c_\theta} \qquad \text{(III-13)}$$

The combined effect of pilot delay and control lag can be added by assuming an effective delay, τ_e:

$$\varphi_{M_\theta} \doteq \tan^{-1} \frac{-M_q}{\omega_{c_\theta}} - \tau_e \omega_{c_\theta} \qquad \text{(III-14)}$$

This function is plotted in Fig. III-1 for a phase margin of 30 deg to show the approximate relative importance of pitch damping and combined delay.

The Ref. 20 requirement for pitch damping as shown in Fig. III-2 contrasts with the level of pitch damping required to allow the pilot to operate with pure gain compensation with $1 < \omega_{c_\theta} < 2$ rad/sec and $\varphi_m > 30$ deg. The requirement is a function of pitch moment of inertia. While it may be adequate for

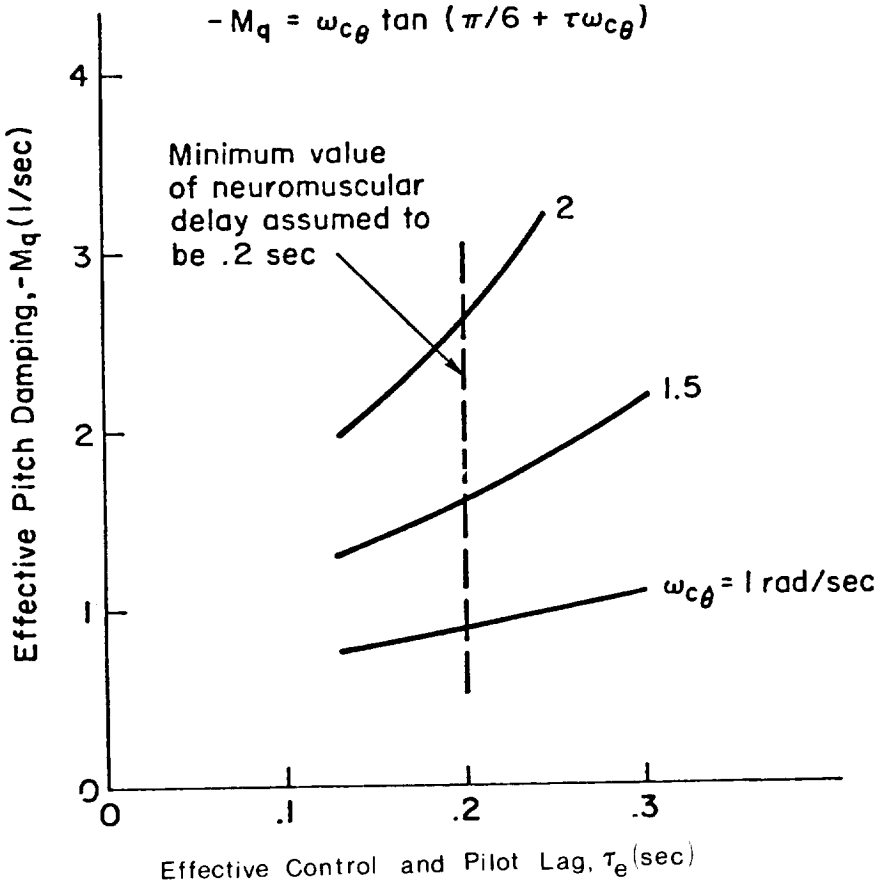

Figure III-1. Required Pitch Damping to Provide 30 deg Effective Phase Margin for a Given Control and Pilot Lag

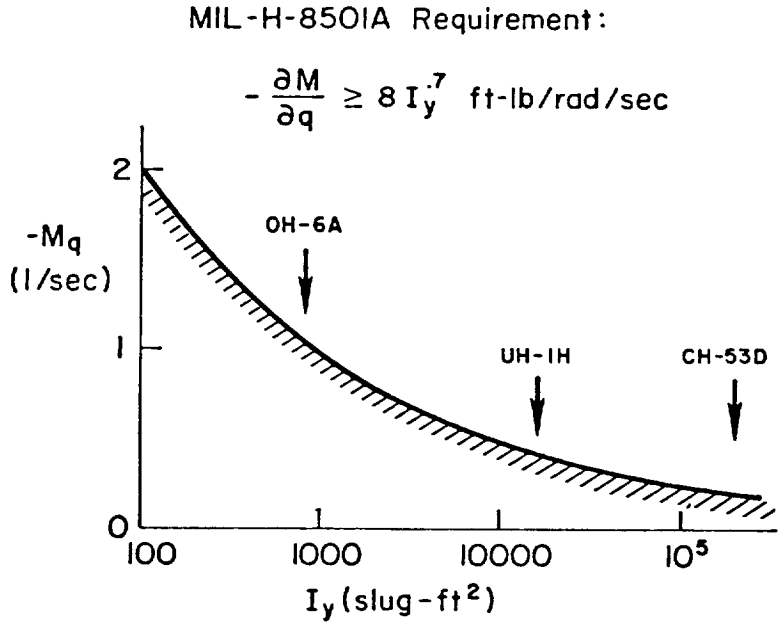

Figure III-2. Existing Pitch Damping Requirement

small vehicles (e.g., OH-6A), it is clearly inadequate for larger ones. The level suggested in Ref. 21, i.e., $-M_q > 2.5$/sec, is more realistic; however, an important implication of Fig. III-1 is that the level of pitch damping required is tied to the amount of effective control lag present.

In view of the importance of pitch damping, it is worthwhile to recall briefly the key factors which produce it, especially in connection with the vehicle examples considered here.

Reference 22 illustrates that, for those helicopters included in Volume One, the key rotor system parameters affecting rotary damping are flapping hinge offset, ϵ, and blade Lock No., γ. Figure III-3 shows a sketch of the relationships. Shaded areas indicate approximately where various rotor hub types are situated. In view of the parameters shown in Table III-4, this qualitatively explains the large difference in M_q between the hingeless BO-105 and teetering AH-1G and UH-1H. The difference between the articulated examples, OH-6A and CH-53D, can be traced to a combination of Lock No. and vehicle size (inertia).

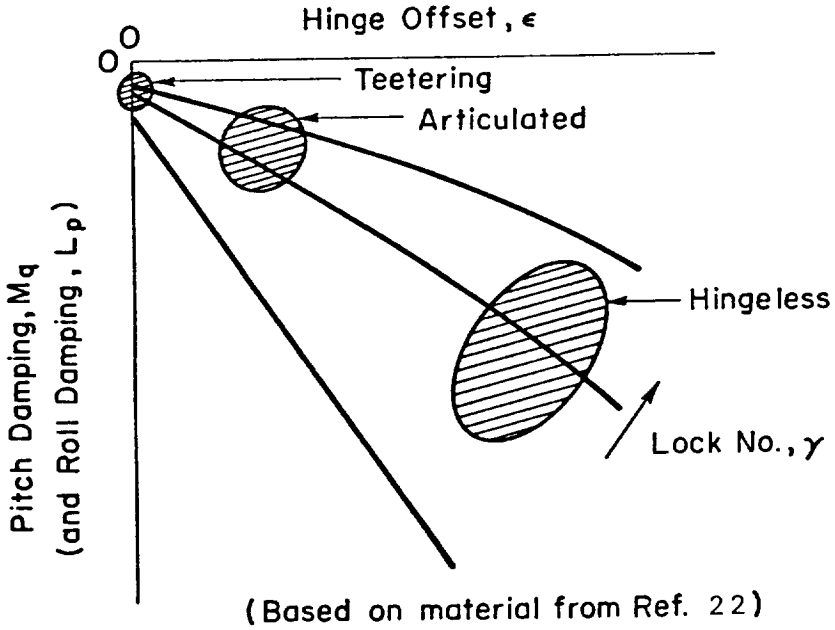

Figure III-3. Pitch Damping as a Function of Rotor Hinge Offset and Lock Number

TABLE III-4

SURVEY OF KEY ROTOR SYSTEM PROPERTIES

	OH-6A	BO-105	AH-1G	UH-1H	CH-53D
Main Rotor Type	Articulated	Hingeless	Teetering	Teetering	Articulated
Hinge Offset Ratio, ϵ	0.035	approx. 0.15*	Zero	Zero	0.055
Lock No., γ	5.8	7.9**	5.2	6.6	9.4
Flapping Hinge Restraint	No	Yes	No	No	No
Pitch-Flap Coupling, δ_3	Zero	Zero	Zero	Zero	Zero

* Ref. 23

** Referred to the virtual flapping hinge (Ref. 24)

Given the background regarding the pitch control response and closed-loop pilot-vehicle aspects, we shall consider two hovering examples which span a fairly wide range of characteristics:

- BO-105
- AH-1G, SCAS off

A Bode root locus is shown for each in Figs. III-4 and III-5. The most prominent difference is in the phase margin in the region of pitch attitude regulation which is primarily due to the disparity in pitch damping.

The phugoid is a prominent feature in both cases cited above. Note that as long as ω_p is well below the region of crossover the phugoid is subject to being effectively damped by closure of the pitch loop. This implies that a direct upper limit might be placed on phugoid frequency to insure effective damping with reasonable regulation of pitch attitude.

b. Forward Flight

As forward velocity is increased the pitch attitude dynamics transition to those of a conventional airplane so long as the sign of M_w is negative. According to Ref. 1 the main features of the pitch response in forward flight have the following dependency on airspeed:

$$\omega_{sp}^2 \doteq M_q Z_w - V \cdot M_w \qquad \text{(III-15)}$$

$$2\zeta_{sp}\omega_{sp} \doteq - Z_w - M_q \qquad \text{(III-16)}$$

$$\omega_p^2 \doteq \frac{g M_u}{-M_q + V \frac{M_w}{Z_w}} \qquad \text{(III-17)}$$

$$2\zeta_p\omega_p \doteq - X_u + \frac{M_u g}{\omega_{sp}^2} \qquad \text{(III-18)}$$

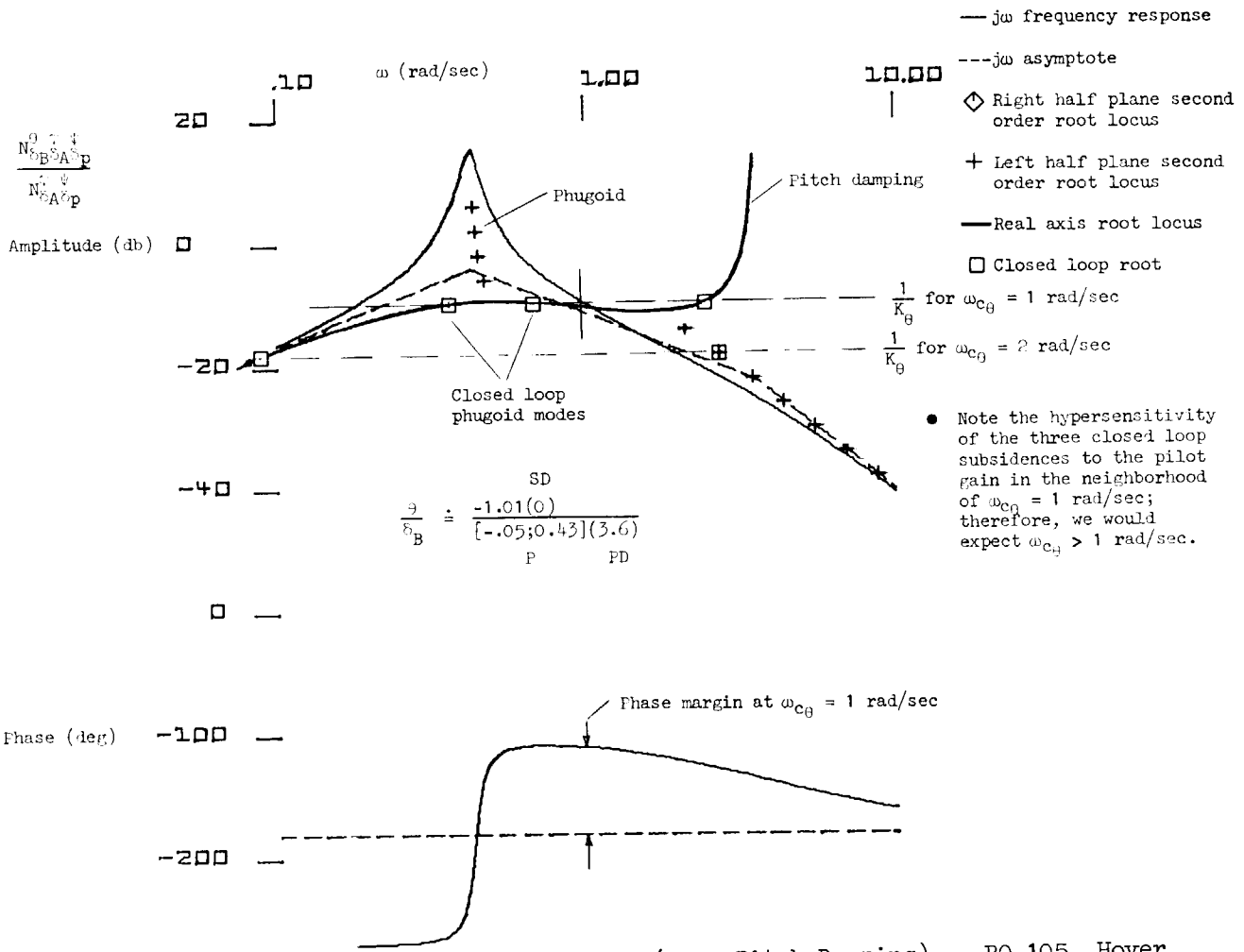

Figure III-4. Sample Pitch Loop Bode Root Locus (High Pitch Damping) — BO-105, Hover

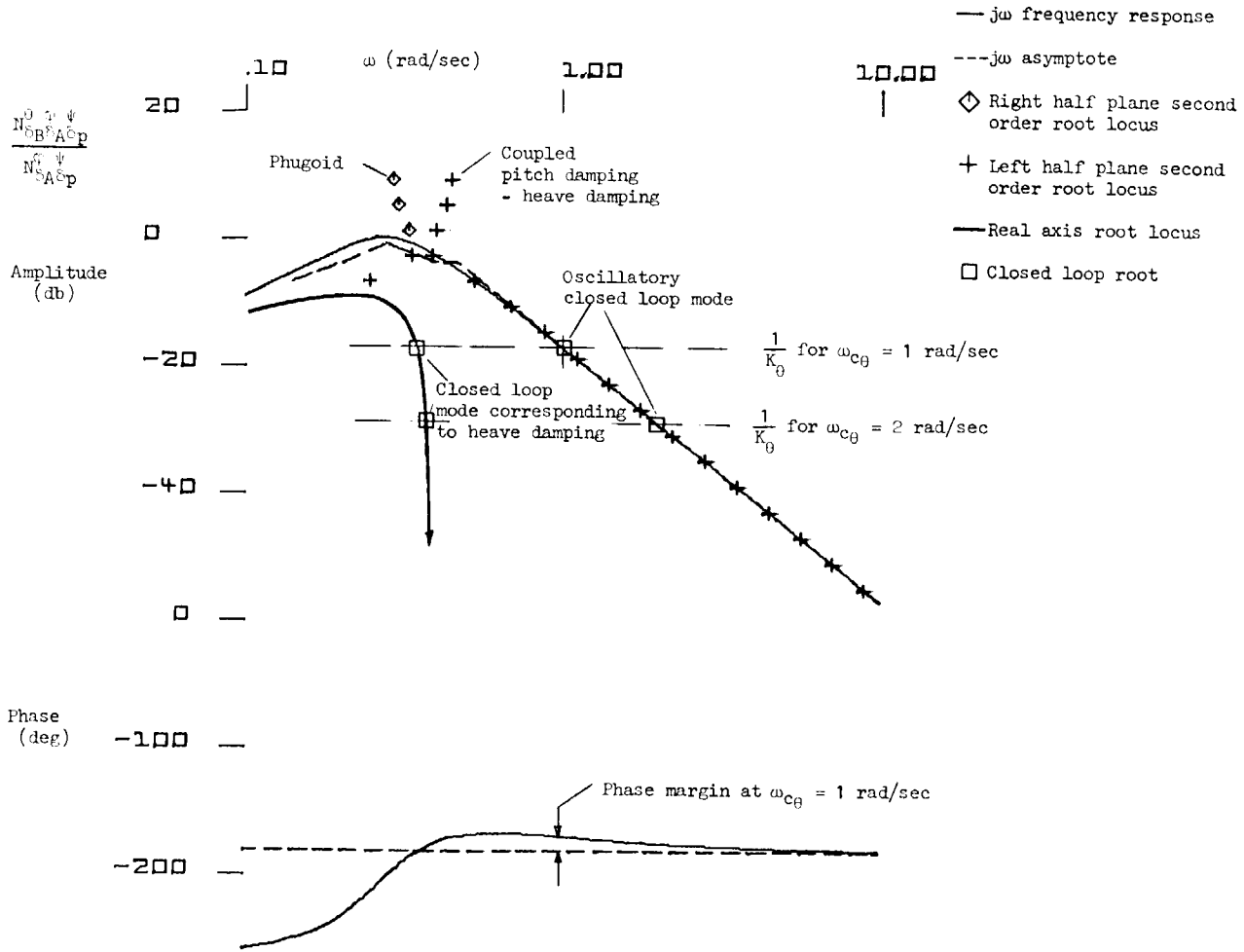

Figure III-5. Sample Pitch Loop Bode Root Locus (Low Pitch Damping) — AH-1G, Hover

$$\frac{1}{T_{\theta_1}} \doteq -X_u \qquad \text{(III-19)}$$

$$\frac{1}{T_{\theta_2}} \doteq -Z_w \qquad \text{(III-20)}$$

Thus, in forward flight we should expect to see:

- Pitch damping and heave damping combining to form an overdamped short period
- Increased phugoid frequency
- Increased phugoid damping.

As shown in Table III-5, the 60 kt pitch dynamics are characterized by a phugoid mode, not much different from that in hover, and a highly damped short period mode. As with the hover condition, the transfer function is composed of two parts — one with dominant response poles and zeros, the other with approximately cancelling dipole factors (only the former is shown in Table III-5).

In forward flight it is reasonable to assume only pitch and roll loops. Yaw regulation is largely unnecessary as we shall discuss shortly. For the reasons stated previously, perfect roll regulation is a valid assumption when considering the pitch response transfer function. (Again, the conditions for validity are stated in Table II-1.) For the 60 kt examples shown in Table III-5 there are various effects of roll regulation. The most prevalent are increases in short period damping and decreases in phugoid damping.

The most important feature in each of the 60 kt pitch response transfer functions shown is that, compared to hover, there is a net increase in phase margin in the expected vicinity of crossover (1 to 2 rad/sec). This can be deduced by inspection from the shift in the pole-zero combination involving short period and heave damping. The significance is that pitch attitude response in forward flight should be correspondingly less critical than in hover.

TABLE III-5. SURVEY OF APPROXIMATE* PITCH AXIS RESPONSE TRANSFER FUNCTIONS (60 KT FORWARD FLIGHT)

	OH-6A	BO-105	AH-1G (SCAS OFF)	UH-1H (WITHOUT STABILIZER BAR)	CH-53D (SAS OFF)
Open Loop: $\frac{N^{\dot{w}}_{\delta_B}}{\Delta}$ =	$\frac{-.74(.022)(.73)}{[.04,.29](.99,1.66]}$ (SD, HD; P, SP)	$\frac{-.99(.026)(.76)}{[-.20,.46](.51)(4.5)}$ (SD, HD; P, SP, SP)	$\frac{-.16(.004)(.92)}{[-.06,.26][.71,.82]}$ (SD, HD; P, SP)	$\frac{-.17(.006)(1.0)}{[-.006,.28][.64,.92]}$ (SD, HD; P, SP)	$\frac{-.17(.014)(.65)}{[-.24,.31][.99,.67]}$ (SD, HD; P, SP)
Roll Perfectly Regulated: $\frac{N^{\dot{\theta}\,\varphi}_{\delta_B\delta_A}}{N^{\varphi}_{\delta_A}}$ =	$\frac{-.75(.022)(.74)}{[.05,.30](1.39)(1.86)}$ (SD, HD; P, SP)	$\frac{-1.03(.022)(.76)}{[-.19,.45](.53)(4.2)}$ (SD, HD; P, SP)	$\frac{-.16(.007)(.91)}{[-.15,.32][.84,.79]}$ (SD, HD; P, SP)	$\frac{-.17(.005)(.92)}{[-.14,.35][.88,.87]}$ (SD, HD; P, SP)	$\frac{-.17(.015)(.65)}{[-.25,.33](.51)(.80)}$ (SD, HD; P, SP)
Remarks:	•Slight increase in short period damping due to $\varphi \rightarrow \delta_A$.	•Negligible effect of $\varphi \rightarrow \delta_A$.	•Slight loss in phugoid damping and gain in short period damping	•Same as AH-1G. •Also, slight loss in heave damping due to $\varphi \rightarrow \delta_A$.	•Slight increase in short period damping due to $\varphi \rightarrow \delta_A$ (same as OH-6A).

*Approximately cancelling dipole factors are omitted from 6 DOF quasi-static transfer function expressions shown.

( ) first order factor, [ ] second order factors, {( )...[ ]} approximately cancelling dipole factors.

( )
X } mode label according to the following key: P - phugoid, PL - lateral phugoid, PD - pitch damping, R - roll damping, YD - yaw damping, SP - short period, D - dutch roll, S - spiral, SD surge damping, LD - sway damping, HD - heave damping.

According to the approximate factor relationships, pitch damping shows up as the prime differentiating feature in pitch response dynamics at the hover and 60 kt conditions considered. Figure III-6 shows that for a given vehicle the magnitude of pitch damping, M_q, does not vary significantly over the entire range of low speed flight conditions. Inspection of the data in Volume One also shows that M_q does not vary with vertical velocity or altitude.

c. Summary

Prior to considering roll regulation, let us summarize the important features of the direct control response of the pitch axis with regard to the five helicopter examples:

- The essential θ/δ_B controlled element features can be factored from a high order transfer function
- The essential features can be identified in conventional terms (e.g., phugoid, pitch damping, short period, etc.)
- Approximate numerator ratios can be used to imbed off-axis regulation in the direct control response and, at the same time, to simplify the transfer function, i.e.,

$$\frac{\theta}{\delta_B} \doteq \frac{N^{\theta}_{\delta_B} N^{\varphi}_{\delta_A} N^{\psi}_{\delta_p}}{N^{\varphi}_{\delta_A} N^{\psi}_{\delta_p}} \quad \text{in hover}$$

$$\text{and} \qquad \doteq \frac{N^{\theta}_{\delta_B} N^{\varphi}_{\delta_A}}{N^{\varphi}_{\delta_A}} \quad \text{in forward flight} \qquad \text{(III-21)}$$

- Sequentially constraining off-axes can produce second-order effects in primary control response features, e.g., for the AH-1G in hover, SCAS off,

$$\frac{N^{\theta}_{\delta_B}}{\Delta} \quad \text{vs} \quad \frac{N^{\theta}_{\delta_B} N^{\varphi}_{\delta_A}}{N^{\varphi}_{\delta_A}} \qquad \text{(III-22)}$$

shows that roll regulation destabilizes the phugoid.

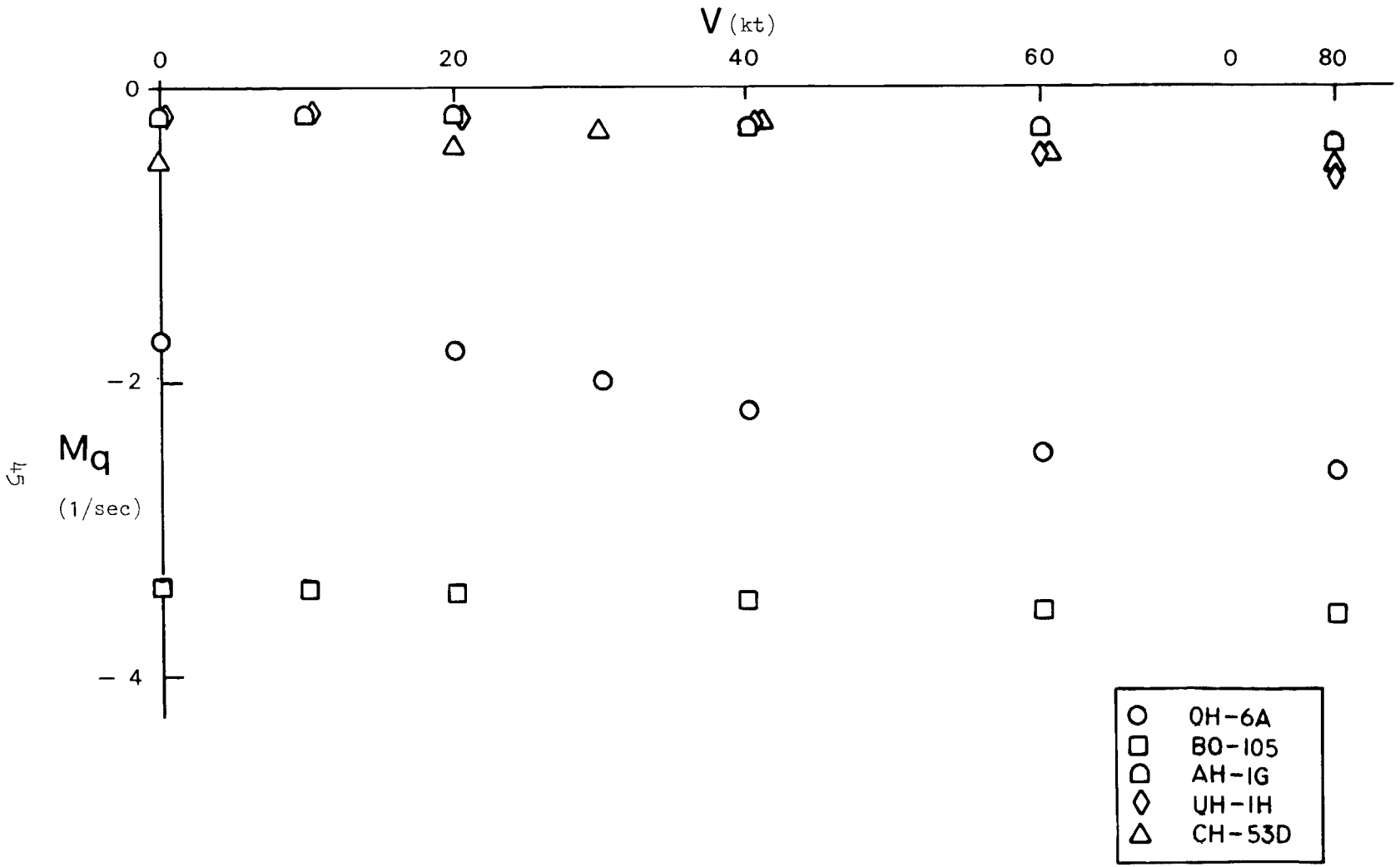

Figure III-6. Variation of M_q with Airspeed

- In those examples considered, the prime differentiating feature in pitch control is pitch damping, i.e., $-M_q$.

2. Roll Axis

The predominant features of the roll axis, just as in the pitch axis, can be summarized in terms of the general form of transfer function as given in Section II, i.e., for hover:

$$\frac{\varphi}{\delta_A} = \frac{A_\varphi (\quad) \left\{ \quad \right\} e^{-\tau_c s}}{\underset{PL}{[\quad]} \underset{R}{(\quad)} \left\{ \quad \right\}} \qquad \text{(III-23)}$$

(Approximately Cancelling Dipoles)

for forward flight,

$$\frac{\varphi}{\delta_A} = \frac{A_\varphi \left\{ \quad \right\} e^{-\tau_c s}}{\underset{S}{(\quad)} \underset{R}{(\quad)} \left\{ \quad \right\}} \qquad \text{(III-24)}$$

(Approximately Cancelling Dipoles)

a. Hovering Flight

For hover, the form shown for roll response is the same as for pitch response. The primary factor differentiating roll and pitch derivatives in hover is the ratio of roll inertia to pitch inertia, I_x/I_y. Hence,

$$L'_p \doteq \frac{M_q}{I_x/I_y} \qquad \text{(III-25)}$$

$$L'_v \doteq \frac{-M_u}{I_x/I_y} \qquad \text{(III-26)}$$

and

$$L'_{\delta_A} \doteq \frac{-M_{\delta_B}}{I_x/I_y} \qquad \text{(III-27)}$$

Therefore, there is a general increase in roll damping over pitch damping, little change in the phugoid, and the same angular rate sensitivity. If the roll response examples in Table III-6 are compared with those in Table III-1 (pitch response), the above generalities hold fairly well except that the lateral phugoid frequency and damping tend to be slightly higher. The effects of other inner loop closures (pitch and yaw) are not as large for the roll axis as for the pitch axis.

The numerical requirements on damping should apply in roll as in pitch if the control lags and desired crossover frequency and phase margin are the same (as they are in the experimental data of Ref. 7). Thus, the same plot in Fig. III-1 could be used to describe required roll damping, L'_p. However, Ref. 21 is in variance to this and suggests that a minimum level of roll damping be 4/sec vs 2.5/sec for pitch damping.

b. Forward Flight

In forward flight the roll damping time constant remains and the lateral phugoid disappears and is replaced by a spiral mode. So long as the spiral mode is well below the roll crossover frequency range and the roll mode is above, then the controlled element will appear like K/s and will permit easy regulation.

Table III-7 shows a survey of bare airframe roll dynamics at 60 kt for the five helicopters studied. The transfer functions themselves are all numerically similar to hover except for the disappearance of a lateral phugoid and emergence of a spiral mode.

Roll damping, the main determining factor in roll response is plotted as a function of airspeed in Fig. III-7. Like pitch damping, it does not vary significantly for a given vehicle. The same is not necessarily true for varying vertical velocity, however.

Where the basic value of roll damping is low (as in the teetering rotor examples which include the AH-1G and UH-1H), there is a significant variation of L'_p with vertical velocity. This is illustrated in Fig. III-8.

TABLE III-6. SURVEY OF APPROXIMATE* ROLL AXIS RESPONSE TRANSFER FUNCTION (HOVER)

	OH-6A	HO-10	AH-1G (SAS OFF)	UH-1H (WITHOUT STABILIZER BAR)	CH-47D (SAS OFF)
Open Loop: $\frac{\dot{\phi}}{\Delta}$	$\frac{\text{LD}}{1.9(.0\_)}$ $\frac{}{[-.0\_,.2\_](4.9)}$ PL R	$\frac{\text{LD}}{2.5(.004)}$ $\frac{}{[.03,.4\_](8.9)}$ PL R	$\frac{\text{LD}}{.4_1(.07)[.86,.4\_]}$ $\frac{}{[-.2\_,.5\_](.8\_)[.8\_,.7\_]}$ PL R SP	$\frac{\text{LD}}{.27(.0\_)}$ $\frac{}{[-.1\_,.5\_](.9\_)}$ PL R	$\frac{\text{LD}}{.\_(.0\_)}$ $\frac{}{[-.0\_,.6\_](\_.0)}$
Pitch Perfectly Regulated: $\frac{\dot{\phi}}{\Delta_{\delta_B}} = \frac{\dot{\phi}}{\delta_B}$	$\frac{\text{LD}}{1.\_0(.0\_\_)}$ $\frac{}{[-.0\_,.\_\_](\_.0)}$ PL R	$\frac{\text{LD}}{2.\_3(.00\_)}$ $\frac{}{[.01\_,.4\_](9.7)}$ PL R	$\frac{\text{LD}}{.\_7(.0\_)}$ $\frac{}{[-.\_1,.5\_](1.1\_)}$ PL R	$\frac{\text{LD}}{.\_7(.0\_)}$ $\frac{}{[-.1\_,.5\_](1.0\_)}$ PL R	$\frac{\text{LD}}{.\_\_(.0\_)}$ $\frac{}{[-.0\_,.\_7](\_.\_)}$
Pitch and Roll Perfectly Regulated: $\frac{\dot{\phi}}{\Delta_{\delta_A}\dot{\theta}_{\delta_B}\dot{\psi}_{\delta_p}} = \frac{\dot{\phi}}{\delta_B\delta_p}$	$\frac{\text{LD}}{1.\_9(.0\_\_)}$ $\frac{}{[-.0\_,.5\_](4.9)}$ PL	$\frac{\text{LD}}{2.74(.00\_)}$ $\frac{}{[-.01,.44](9.7)}$ PL R	$\frac{\text{LD}}{.\_9(-.001)(.39)}$ $\frac{}{[-.1\_,.40](.33)(1.13)}$ PL R	$\frac{\text{LD}}{.59(.00\_)}$ $\frac{}{[-.1\_,.41](.93)}$ PL R	$\frac{\text{LD}}{.\_4(.0\_)}$ $\frac{}{[.07,.65](2.3)}$
Remarks:	•No essential effect of off-axis regulation.	•Slight loss in lateral phugoid damping and increase in roll damping with pitch and roll loops closed.	•Pitch regulation increases roll damping. •Yaw regulation decreases lateral phugoid damping and sway damping.	•$\theta \rightarrow \delta_B$ increases roll damping, but $\psi - \delta_p$ reduces it. •Sway damping reduced by $\psi \rightarrow \delta_p$.	•Slight increase in roll damping with $\theta \rightarrow \delta_B$.

*Approximately cancelling dipole factors are omitted from 6 DOF quasi-static transfer function expressions shown.

( ) first order factor, [ ] second order factors, {( )...[ ]} approximately cancelling dipole factors.

( ) X } mode label according to the following key: P - phugoid, PL - lateral phugoid, PD - pitch damping, R - roll damping, YD - yaw damping, SP - short period, D - dutch roll, S - spiral, SD - surge damping, LD - sway damping, HD - heave damping.

TABLE III-7. SURVEY OF APPROXIMATE* ROLL AXIS RESPONSE TRANSFER FUNCTIONS (60 KT)

	OH-6A	BO-105	AH-1G (SCAS OFF)	UH-1H (WITHOUT STABILIZER BAR)	CH-53D (SAS OFF)
Open Loop: $\frac{N^{\varphi}_{\delta_A}}{\Delta}$	$\doteq \frac{1.26}{(0.064)(5.72)}$ S R	$\frac{2.62}{(0.048)(8.93)}$ S R	$\frac{0.49}{(0.073)(1.44)}$ S R	$\frac{0.56}{(0.063)(1.47)}$ S R	$\frac{0.49}{(0.121)(1.63)}$ S R
Pitch Perfectly Regulated: $\frac{N^{\varphi\ \theta}_{\delta_A \delta_B}}{N^{\theta}_{\delta_B}}$	$\doteq \frac{1.27}{(0.063)(5.70)}$ S R	$\frac{2.71}{(0.050)(9.86)}$ S R	$\frac{0.49}{(0.070)(1.34)}$ S R	$\frac{0.56}{(0.060)(1.11)}$ S R	$\frac{0.50}{(0.11)(1.82)}$ S R
Remarks:	●No essential effect of off-axis regulation.	●Slight increase in roll damping due to $\theta \rightarrow \delta_B$.	●Slight loss in roll damping due to $\theta \rightarrow \delta_B$.	●Loss in roll damping due to $\theta \rightarrow \delta_B$.	●Slight increase in roll damping due to $\theta \rightarrow \delta_B$.

* Approximately cancelling dipole factors omitted from 6 DOF quasi-static transfer function expressions shown.

( ) first order factor, [ ] second order factors, $\{( ) \ldots [ ]\}$ approximately cancelling dipole factors.

$\left.\begin{matrix}( ) \\ X\end{matrix}\right\}$ mode label according to the following key: P - phugoid, PL - lateral phugoid, PD - pitch damping, R - roll dampin, YD - yaw damping, SP - short period, D - dutch roll, S - spiral, SD surge damping, LD - sway damping, HD - heave damping

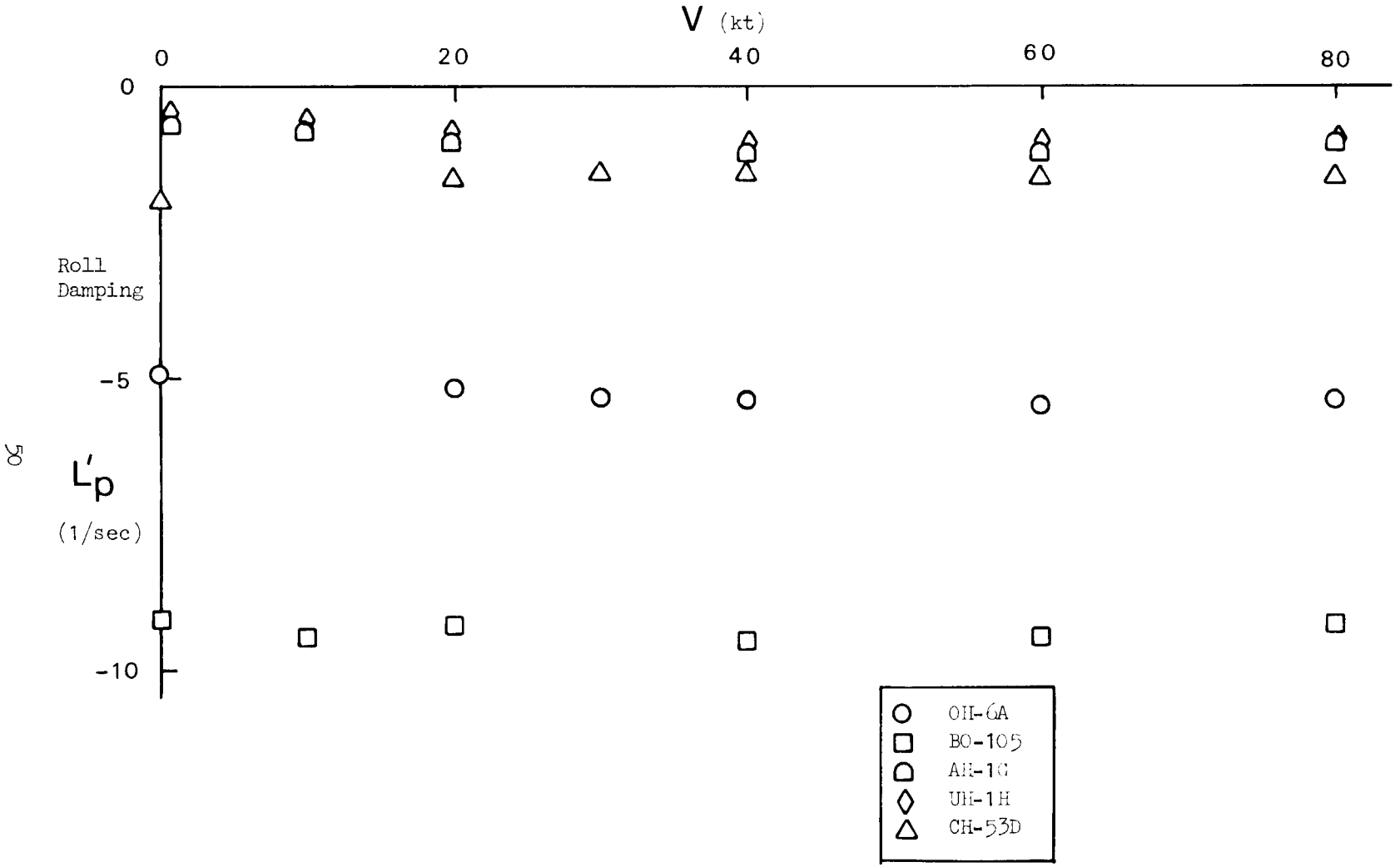

Figure III-7. Variation in Roll Damping with Airspeed

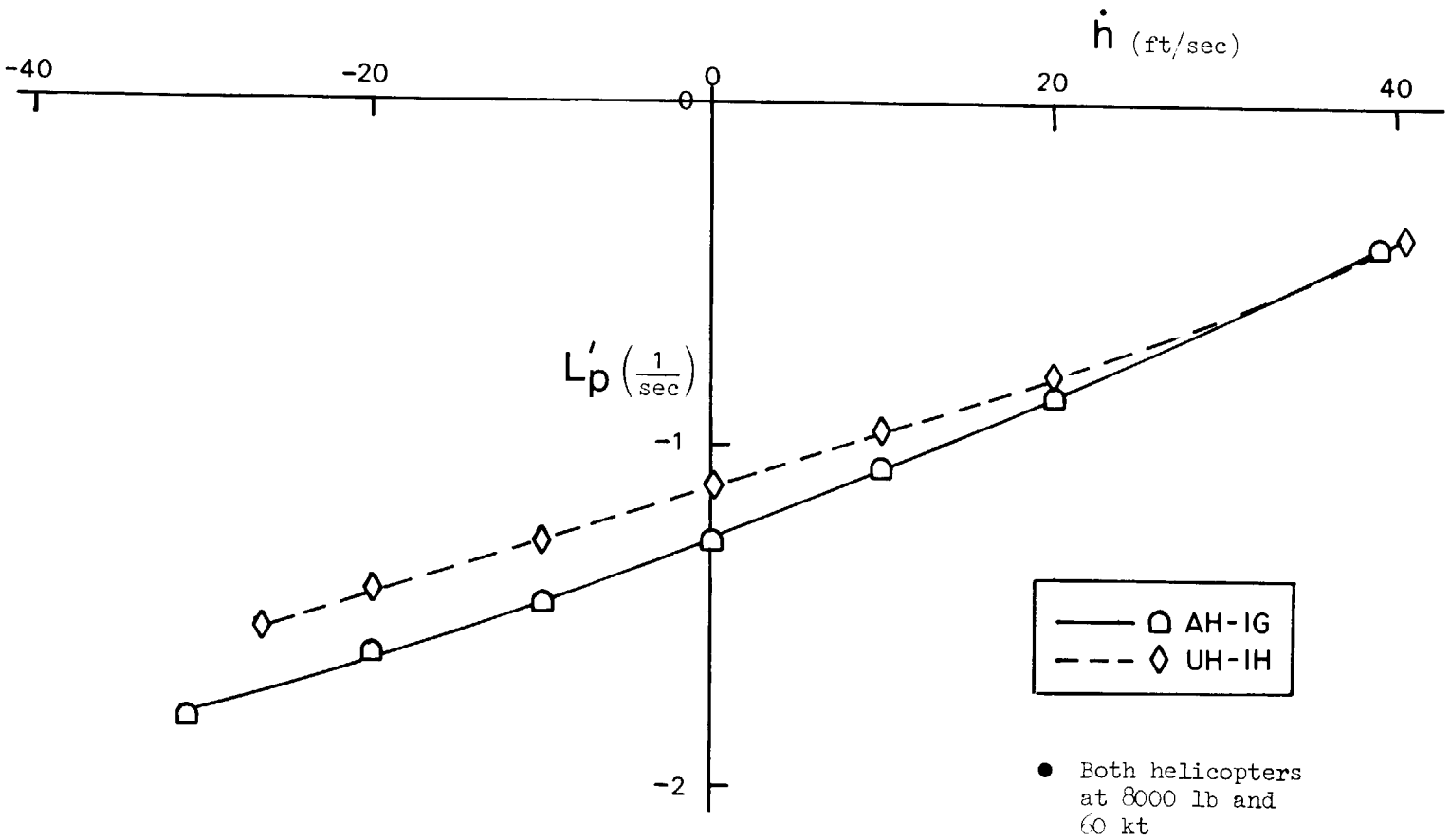

Figure III-8. Variation of Roll Damping with Vertical Velocity

At some light weight conditions the roll damping stability derivative, L'_p, even becomes positive. This is most apparent in the UH-1H and AH-1G data but the trend is apparent also in the OH-6A and BO-105 (all CH-53D flight conditions are level flight).

Roll response for varying vertical velocity was analyzed by considering the φ/δ_A transfer function, first completely open loop, then with pitch attitude regulated. Three flight conditions were compared ranging from autorotation to level flight to maximum power climb, all at 60 kt, for the AH-1G aircraft with SCAS off. Table III-8 shows tabulation of roll to lateral cyclic transfer functions for each of these cases. For the completely open-loop dynamics (first column) as rate of climb increases, dutch roll damping decreases and becomes approximately netural at maximum rate of climb. This trend can be observed in flight test data; however, what cannot be observed directly is a variation in coupling among the roll, spiral, and dutch roll modes. For level flight, the coupling is nearly zero, but for non-level flight the coupling takes on differing forms. Figure III-9 shows dutch roll root locus along with roll and spiral for various rates of climb, $\dot{h}$, based on the data from Volume One.

The pitch-regulated roll response in column 2 of Table III-8 helps us to sort out the modes more easily. The same trends are visible in the roll, spiral, and dutch roll modes for increasing rate of climb, that is, the roll and spiral modes tend to become more coupled and the dutch roll less damped. The effect of pitch regulation on lateral-directional modes in general is to reduce dutch roll damping and to alter roll-spiral modes somewhat.

The implication of the high rate of climb effect on roll response is illustrated by the closed-loop step responses in Fig. III-10. These show that for pure gain regulation of roll attitude in the presence of good pitch regulation there is no problem in level flight, but for maximum climb, a troublesome dutch roll oscillation is present. The deterioration of dutch roll damping with increased rate of climb is observable in the AH-1G, SCAS off according to the flight data presented in Ref. 26.

TABLE III-8

AH-1G ROLL RESPONSE, 60 KT, SCAS OFF

	$\frac{\varphi}{\delta_A}$	$\frac{\varphi}{\delta_A}\Big\vert_\theta$
AUTO ROTATION (-1860fpm)	$\frac{.44[.076;.276][.672;.923][.378;1.20]}{(-.185)(.855)[.051;.265][.368;1.20][.961;1.24]}$ S R P D SP	$\frac{.44(-.009)(.878)\quad[.396;1.22]}{(-.008)(-.162)(.812)(1.81)[.479;1.20]}$ SD S H R D
LEVEL FLIGHT	$\frac{.49\quad[-.152;.319][.389;1.25][.838;.788]}{(.072)(1.44)[-.06;.264][.337;1.23][.705;.82]}$ S R P D SP	$\frac{.49(.0073)(.909)\quad[.398;1.25]}{(.0042)(.069)(.922)(1.34)[.33;1.23]}$ SD S R D
MAXIMUM CLIMB (+2340 fpm)	$\frac{.60\quad[-.088;.168][.435;1.10][.491;1.29]}{(.64)(1.01)[-.313;.139][.052;.964][.413;1.17]}$ S R P D SP	$\frac{.60(.016)(.977)\quad[.508;1.17]}{(.013)(.487)[.997;1.04][-.018;.883]}$ SD S R/H D

KEY TO MODE IDENTIFICATION

S — Spiral
R — Roll Damping
D — Dutch Roll
P — Phugoid
SP — Short Period
H — Heave Damping
SD — Speed Damping

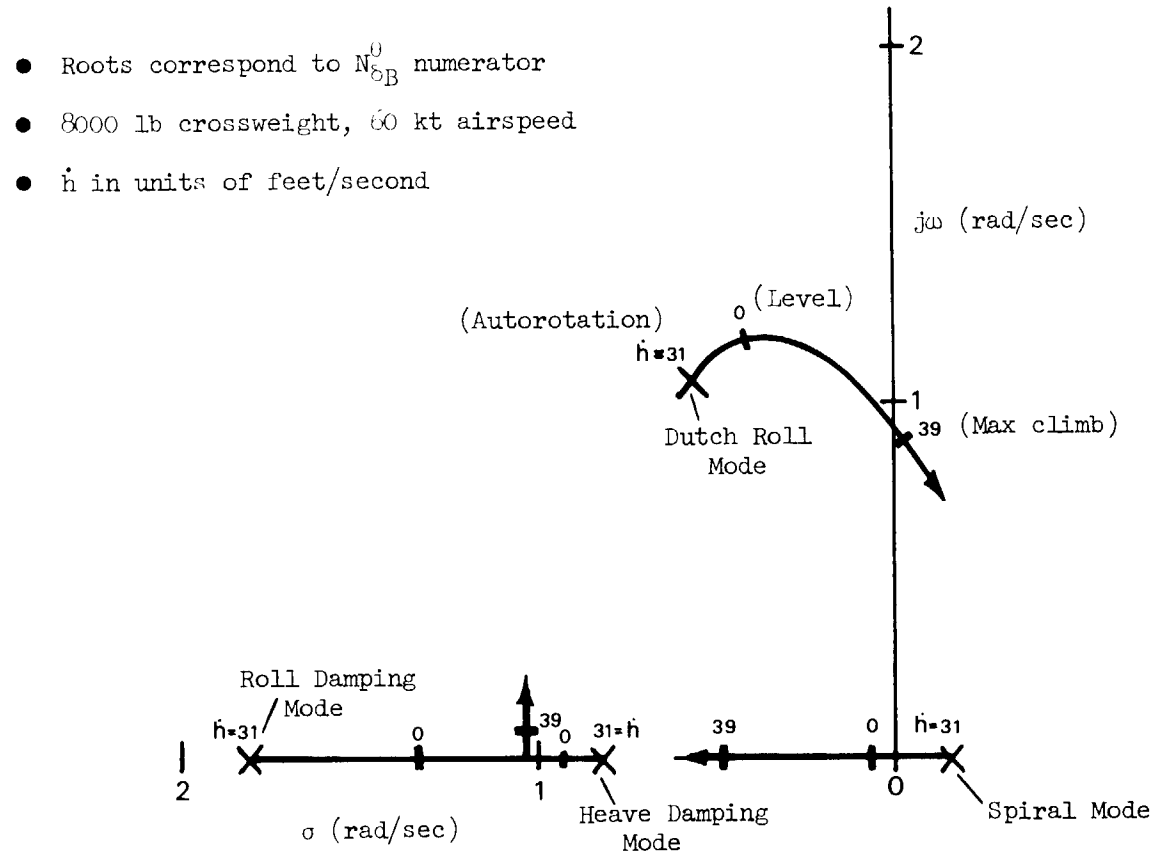

Figure III-9. Root Locus of Lateral-Directional Modes for Varying Vertical Velocity

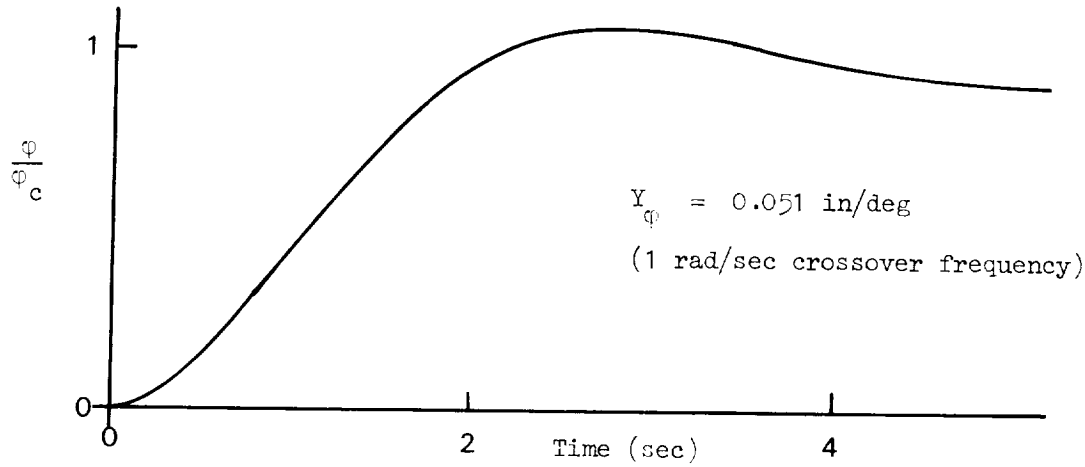

a. Level Flight, Normal Roll Response for Step φ_c

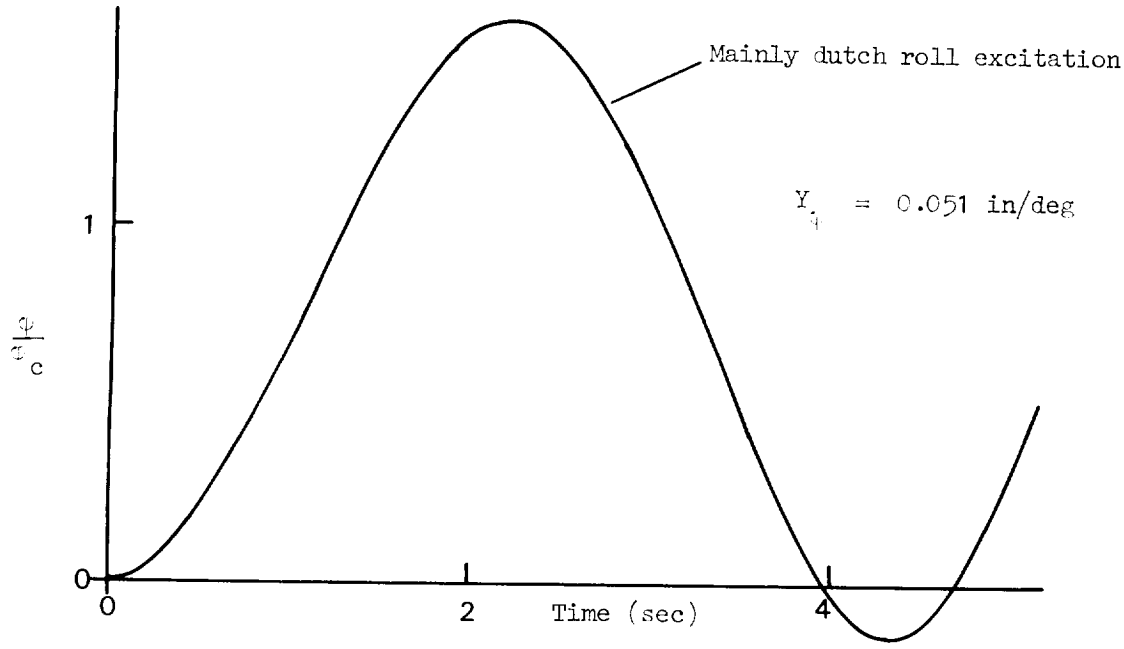

b. Maximum Climb, Pathological Roll Response with Same Pilot Action as in a.

Figure III-10. Closed Loop Responses to Step φ_c
(AH-1G, 60 kt, SCAS Off)

c. Summary

Based on the analysis presented, the key points regarding roll control response are therefore:

- The predominant roll control response features and procedures for analyzing them are strongly analogous to those of the pitch axis.
- The essential φ/δ_A controlled element features can be factored from a high order transfer function and identified in conventional terms (e.g., lateral phugoid, spiral, and roll damping).
- Appropriate numerator ratios can be used to imbed the effects of off-axis regulation, but the impact of pitch on roll response is generally less than for roll on pitch response.
- Roll damping, L'_p, is the prime differentiating feature in roll response among vehicles. Like pitch damping it is invariant with airspeed but, unlike pitch damping, does vary with vertical velocity.

3. Yaw Regulation

Yaw regulation through use of rudder pedals is required when sideslip stiffness is inadequate such as in hover or backward flight. In addition, yaw control is involved in providing turn coordination when needed.

The general form of the ψ/δ_p transfer function varies somewhat depending on whether roll and pitch loops are closed. If we consider the case of roll and pitch inner loops closed, ψ/δ_p is relatively simple in form and allows some degree of insight, i.e.,

$$\left.\frac{\psi}{\delta_p}\right|_{\varphi,\theta} = \frac{N^{\psi}_{\delta_p}\, \dot{\varphi}^{\theta}_{\delta_A\delta_B}}{N^{\dot{\varphi}^{\theta}}_{\delta_A\delta_B}}$$

$$\doteq \frac{A_{\psi}\left(\ \right)^{LD}_{YD}}{(0)\left(\ \right)^{LD}_{YD}} \quad \text{in hover} \qquad \text{(III-28)}$$

and

$$\doteq \frac{A_{\psi}\left(\ \right)^{LD}_{D}}{\left[\ \right]_{D}} \quad \text{in forward flight}$$

Note that the numerator form is the same between hover and forward flight. The denominator also is actually the same form if we recognize it as the quadratic containing yaw damping, N'_r, and sideslip stiffness, N'_β $(= VN'_v)$. This can be shown with a set of reduced equations of motion having only r and v degrees of freedom:

$$\begin{bmatrix} s - N'_r & -N'_v \\ V & s - Y_v \end{bmatrix} \begin{bmatrix} \psi s \\ v \end{bmatrix} \doteq \begin{bmatrix} N'_{\delta_p} \\ Y_{\delta_p} \end{bmatrix} \begin{bmatrix} \delta_p \end{bmatrix} \qquad \text{(III-29)}$$

Thus,

$$\frac{\psi}{\delta_p} \doteq \frac{N'_{\delta_p}\left(s - Y_v + \frac{Y_{\delta_p}}{N_{\delta_p}} N'_v\right)}{s\left[s^2 - (N'_r + Y_v)\, s + VN'_v + N'_r\, Y_v\right]} \qquad \text{(III-30)}$$

or, more simply, if we neglect small terms

$$\doteq \frac{N'_{\delta_p}\,(s - Y_v)}{s\left[s^2 - N'_r\, s + VN'_v\right]}$$

The last expression is instructive for it shows that the yaw control varies primarily as a function of airspeed to the extent that N'_{δ_p}, Y_v, N'_r, and N'_v are invariant which can be confirmed by inspection of the compiled data in Volume One.

The above form is useful in computing the relief from the need for yaw regulation as forward velocity is increased from a hover flight condition. Consider the two root loci in Fig. III-11 for the second order portion of the ψ/δ_p denominator, one corresponding to a pure gain regulation of ψ, and the other corresponding to a forward velocity-induced variation:

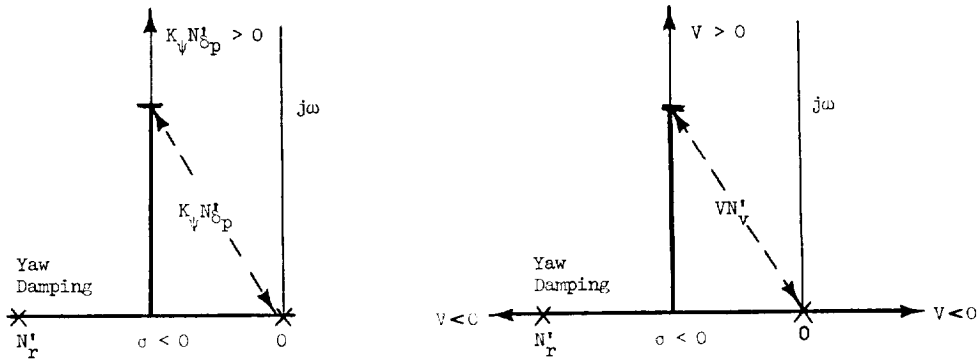

a. Pure Gain Regulation of Yaw Angle

b. Forward Velocity-Induced Oscillation

Figure III-11. Root Loci for the Dutch Roll

These show an equivalence in terms of the effect on the ψ/δ_p denominator although not in terms of active yaw regulation (VN'_v represents active sideslip regulation rather than yaw angle regulation). Nevertheless, we can utilize this to compute the forward velocity for which active yaw regulation becomes unnecessary.

Assuming a pure gain pilot, we can directly estimate the K_ψ for a given crossover frequency, ω_{c_ψ}, according to:

$$1 = \left|Y_p Y_c\right| \doteq \left|\frac{K_\psi N'_{\delta_p}}{s^2 - N'_r s + VN'_v}\right|_{s=j\omega_{c_\psi}} \qquad \text{(III-31)}$$

or

$$K_\psi N'_{\delta_p} \doteq \sqrt{\left(VN'_v - \omega_{c_\psi}{}^2\right)^2 + \left(N'_r\,\omega_{c_\psi}\right)^2} \qquad \text{(III-32)}$$

Hence, for hover:

$$K_\psi N'_{\delta_p} \doteq \omega_{c_\psi} \sqrt{\omega_{c_\psi}^2 + N_r'^2} \qquad \text{(III-33)}$$

Thus, the forward velocity which yields the equivalent directional stiffness is:

$$V \doteq \frac{\omega_{c_\psi} \sqrt{\omega_{c_\psi}^2 + N_r'^2}}{N'_v} \qquad \text{(III-34)}$$

Figure III-12 shows a plot of sideslip stiffness, N'_β, versus airspeed, V, for the five helicopters studied. Superimposed are approximate levels of equivalent yaw regulation at hover. In the case of the OH-6A a forward velocity of 22 kt provides a level of directional stability equivalent to a pilot-generated yaw crossover frequency equal to 1 rad/sec at hover. Thus, if $\omega_{c_\psi} = 1$ rad represented the desired level of yaw regulation, active regulation would be unnecessary above 22 kt. Note that the two examples having the lowest level of N'_β utilize yaw stability augmentation (the effect of which will be discussed in Section VI).

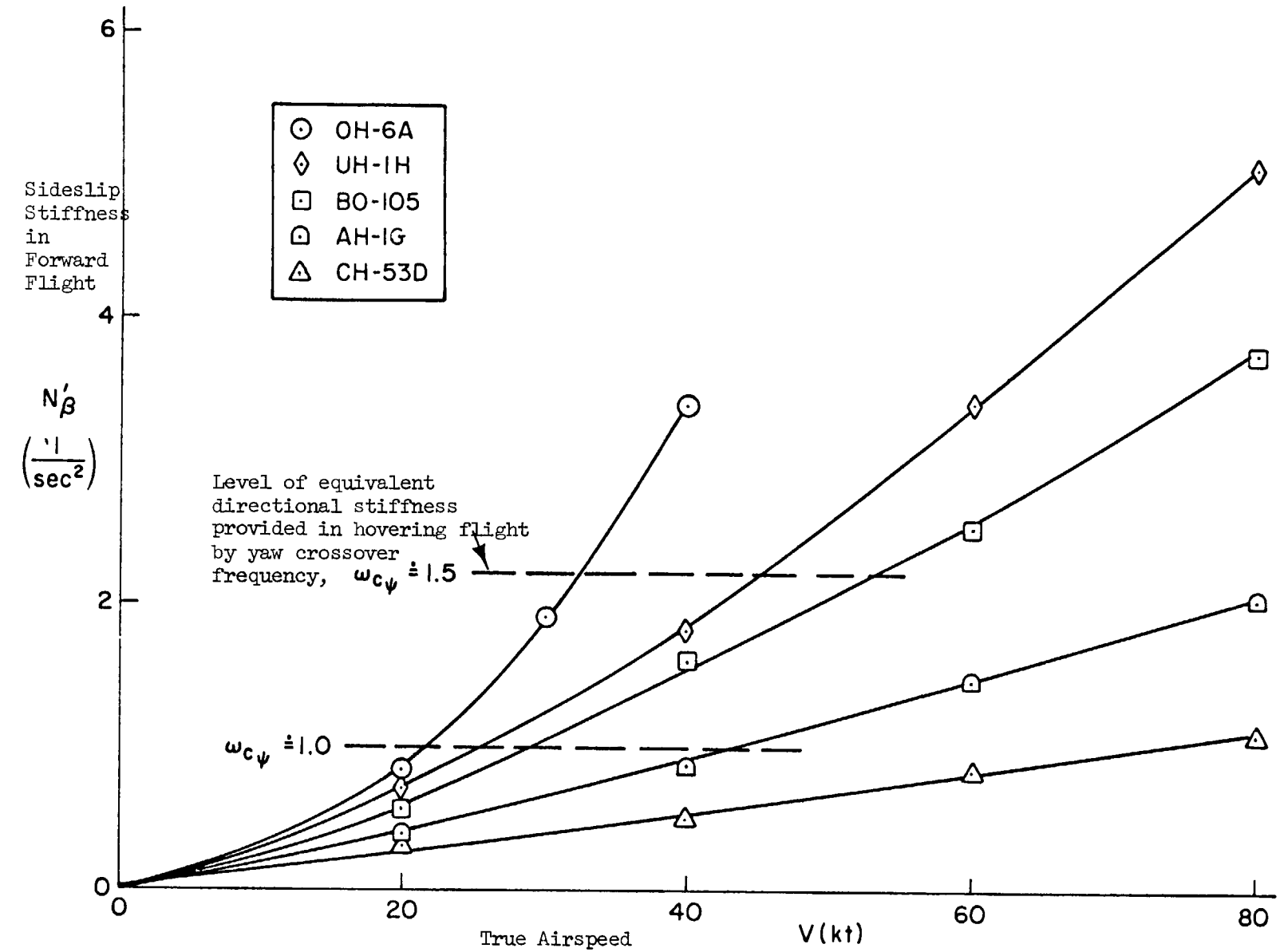

Figure III-12. Sideslip Stiffness as a Function of Airspeed for Five Helicopters with Two Superimposed Levels of Equivalent Directional Stiffness Provided by Active Yaw Regulation in Hovering Flight

A survey of approximate yaw control response in hover is shown in Table III-9. A progression of off-axis regulation includes ψ/δ_p with open loops, with $\theta \longrightarrow \delta_B$, and finally with $\varphi \longrightarrow \delta_A$ as well. One feature common to all cases is that heave damping appears coupled to yaw response. This is most directly observable in the ψ/δ_p response with perfect φ and θ regulation. In the case of the OH-6A $\psi \longrightarrow \delta_p$ degrades heave damping and in the UH-1H and AH-1G it enhances heave damping. In the case of the BO-105 any effect is obscured because heave damping and yaw damping cannot be distinguished positively. Finally, in the CH-53D we have an example of how off-axis regulation ($\varphi \longrightarrow \delta_A$) noticeably improves the predominant yaw response mode from about 0.3 rad/sec to 0.4 rad/sec.

The essential features of the yaw controlled element at hover or very low speeds are analogous to pitch and roll. That is, the controlled element in each case is like a K/s system which is bandwidth limited by the respective rate damping level. Thus, for yaw control to be good, yaw damping, i.e., N'_r, should be commensurate with the desired crossover frequency range and whatever effective control lags are present.

Reference 21 suggests that the minimum yaw damping level for NOE operation be about 5/sec. While this would provide a good controlled element, it is in sharp contrast with the lower levels indicated by the data from Volume One.

C. CROSS COUPLING

The term cross coupling can refer to a variety of specific features connected with helicopter dynamics. The limit on this variety is dependent only upon the model degrees of freedom. The features to be considered here, of course, fall within the range of a six-degrees-of-freedom quasi-static description, but the general approach could be applied to more complex systems.

Cross coupling can manifest itself in at least two ways. First, it can alter the direct primary control response by changing dominant mode characteristics. For example, in the preceding subsection, roll regulation was shown sometimes to affect dominant modes involved in pitch and

TABLE III-9. SURVEY OF APPROXIMATE* YAW RESPONSE TRANSFER FUNCTIONS (HOVER)

	OH-6A	BO-105	AH 1G (SCAS OFF)	UH-1H (WITHOUT STABILIZER BAR)	CH-53D (SAS OFF)
Open Loop: $\frac{N^{\psi}_{\delta_p}}{\Delta}$	$\doteq \frac{-2.56(.30)[-.19,.48][.05,.53]}{(0)(.82)(.23)[0,.41][-.03,.51]}$ (HD; P; PL / YD; HD; P; PL)	$\doteq \frac{1.39(.33)}{(0)(.28)(.35)}$ (HD / YD, HD)	$\doteq \frac{-.81\ (.72)[-.46,.42][-.04,.40]}{(0)(.44)(.82)[-.24,.54][-.29,.36]}$ (PL; P / PL; P)	$\doteq \frac{-1.20(.70)\ [-.46,.48][-.10,.43]}{(0)(.47)(.94)[-.15,.55][-.37,.46]}$ (PL; P / PL; P)	$\doteq \frac{-.35(.31)}{(0)(.29)(.32)}$ (HD / YD, HD)
Pitch Perfectly Regulated: $\frac{N^{\psi}_{\delta_p}{}^{\theta}_{\delta_B}}{N^{\theta}_{\delta_B}}$	$\doteq \frac{-2.58\ (.34)}{(0)(.89)(.25)}$ (HD / YD; HD)	$\doteq \frac{1.40(.33)}{(0)(.28)(.35)}$ (HD / YD, HD)	$\doteq \frac{-.82\ (.33)\ [-.13,.40]}{(0)[.98,.47][-.21,.53]}$ (PL / PL)	$\doteq \frac{-1.20(.28)\ [-.15,.41]}{(0)[.96,.42][.14,.55]}$ (PL)	$\doteq \frac{-.35(.30)}{(0)(.28)(.33)}$ (HD / YD, HD)
Pitch and Roll Perfectly Regulated: $\frac{N^{\psi}_{\delta_p}{}^{\theta}_{\delta_B}{}^{\phi}_{\delta_A}}{N^{\theta}_{\delta_B}{}^{\phi}_{\delta_A}}$	$\doteq \frac{-2.55\ (.34)}{(0)(.89)(.25)}$ (HD / YD; HD)	$\doteq \frac{1.40(.33)}{(0)(.27)(.39)}$ (HD / YD, HD)	$\doteq \frac{-.83(.021)\ (.39)}{(0)(.073)[.99,.45]}$ (LD; HD / PD-HD)	$\doteq \frac{-1.25(.007)\ (.39)}{(0)(.062)(.62)(.44)}$ (LD; HD / YD; HD)	$\doteq \frac{-.37\ (.30)}{(0)(.39)(.28)}$ (HD / YD; HD)
Remarks:	• Yaw damping fairly high • Transfer function not changed much with off-axis regulation • Heave-related dipole involved — $\psi \rightarrow \delta_p$ regulation decreases heave damping. • Phugoid excitation in open loop transfer function.	• Not possible to discriminate between yaw damping and heave damping.	• Modes not well defined — yaw coupled with heave.	• Similar to AH-1G but better definition of yaw damping mode	• Not much effect of off-axis regulation except that $\zeta \rightarrow \delta_A$ increases yaw damping.

*Approximately cancelling dipole factors are omitted from 6 DOF quasi-static transfer function expressions shown.

( ) first order factor, [ ] second order factors, {( )}...[ ] approximately cancelling dipole factors.

$\binom{\ }{X}$ mode label according to the following key: P - phugoid, PL - lateral phugoid, PD - pitch damping, R - roll damping, YD - yaw damping, SP - short period, D - dutch roll, S - spiral, SD - surge damping, LD - sway damping, HD - heave damping.

yaw response. A second form of cross coupling is the direct production of unwanted motion from a given control or commanded motion. The most common example of this in a helicopter is the unwanted yawing motion due to a collective control input.

To a large extent we have addressed the first of the above coupling effects in Subsection B, for it is closely connected with direct control response itself. Therefore, in the following pages our attention will center on the "unwanted response" aspects of cross coupling. We shall address the procedures for computing it and demonstrate examples relevant to helicopter vehicles.

One way of systematically approaching the many kinds of cross coupling possibilities is to consider various motions resulting from various controls. Ideally, a pure, direct motion should be produced from each of the four flight controls, i.e.:

- Heave from collective
- Pitch from longitudinal cyclic
- Roll from lateral cyclic
- Yaw from rudder pedals

Table III-10 shows how these four motions can be produced in ways other than from the respective direct control. Note that the desired level of cross coupling is not always zero, however. Good turn coordination, for example, requires that a yaw rate be produced for a given bank angle in the proportion of g/V. Also, vertical velocity due to pitch motion should be equal to V, especially where flight path is controlled by pitch attitude.

In the following pages we shall address three of the twelve interactions identified in Table III-10. The first two include roll-due-to-pitch control and pitch-due-to-roll control and represent cross coupling phenomena which require for their description at least the complexity of a six-degree-of-freedom quasi-static model. It will be demonstrated that selected stability

TABLE III-10

DESIRED CONTROL INTERACTION

	HEAVE	PITCH	ROLL	YAW
Collective	———	$\frac{\theta}{\delta_c} = 0$	$\frac{\varphi}{\delta_c} = 0$	$\frac{\psi}{\delta_c} = 0$
Longitudinal Cyclic	$\frac{\dot{h}}{\theta} = V$	———	$\frac{\varphi}{\theta} = 0$	$\frac{\psi}{\theta} = 0$
Lateral Cyclic	$\frac{\dot{h}}{\varphi} = 0$	$\frac{\theta}{\varphi} = 0$	———	$\frac{\dot{\psi}}{\varphi} = \frac{g}{V}$
Rotary Rudder	$\frac{\dot{h}}{\psi} = 0$	$\frac{\theta}{\psi} = 0$	$\frac{\varphi}{\psi} = 0$	———

derivative parameters, while providing insight, do not completely describe important coupling effects. The third form of cross coupling we shall consider is uncoordinated yaw due to roll command. In this case multiloop effects are more easily reduced to a few key derivatives.

1. Pitch-Roll Cross Coupling

We shall consider the mutual cross coupling effects between pitch and roll axes in the context of multiloop manual control. Thus, instead of viewing coupling terms of a control response, say φ/δ_B, let us look at coupling relative to a commanded response, i.e., φ/θ_c. This will be not only more direct in terms of visually perceived relationships, but also mathematically simpler and more general.

To the extent that cross coupling does not meet the ideal levels shown in Table III-10, the pilot must minimize it through compensatory tracking or by utilizing appropriate pursuit control crossfeed paths. An example involving pitch regulation with roll cross coupling is shown in Fig. III-13.

Regardless of the pilot control strategy, the key transfer function to describing cross coupling is the appropriate modal response ratio. For example, for roll-due-to-pitch we would compute:

$$\frac{\varphi}{\theta} = \frac{N^{\varphi}_{\delta_B}}{N^{\theta}_{\delta_B}} \qquad \text{(III-35)}$$

This expression is relevant to the compensatory tracking strategy because it represents the unwanted off-axis response which must be regulated out by the roll loop. In the pursuit crossfeed situation, the above numerator indicates the crossfeed required to minimize uncommanded roll. To see this, consider the general transfer function for φ/θ_c:

$$\frac{\varphi}{\theta_c} = \frac{Y_\theta N^{\varphi}_{\delta_B} + Y_{cf} Y_\varphi N^{\varphi}_{\delta_A}}{\Delta + Y_\theta N^{\theta}_{\delta_B} + Y_\varphi N^{\varphi}_{\delta_A} + Y_\theta Y_\varphi N^{\theta\ \varphi}_{\delta_B \delta_A}} \qquad \text{(III-36)}$$

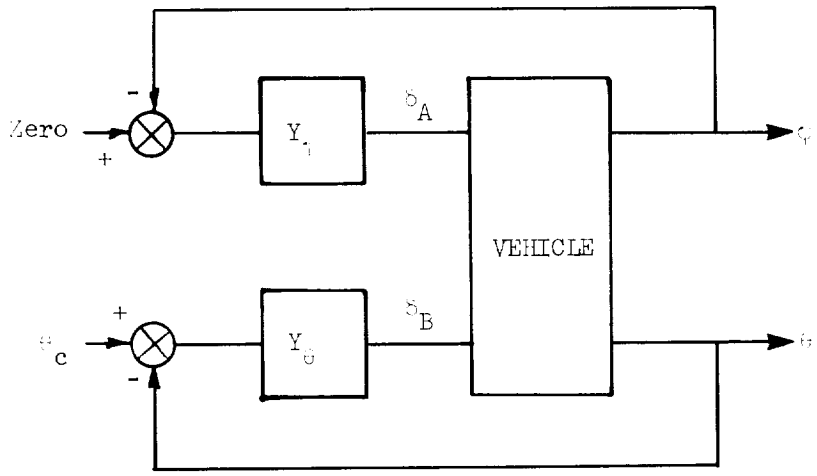

a. Compensatory Loop Structure

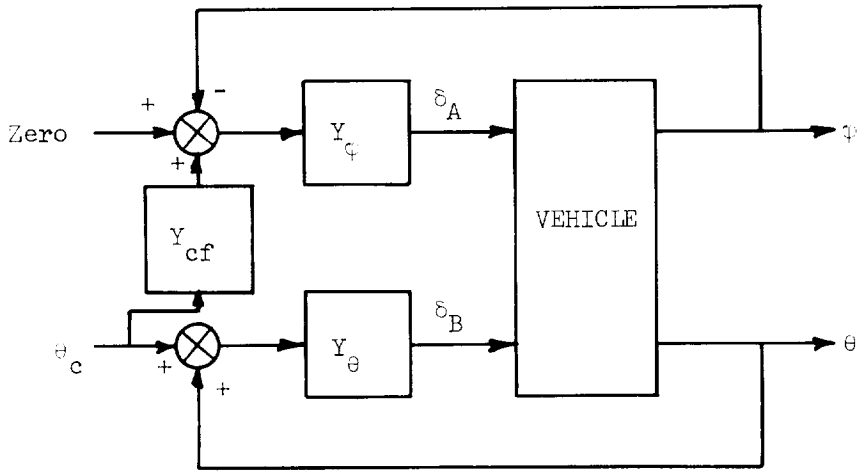

b. Compensatory Loop Structure with Pursuit Crossfeed

Figure III-13. Block Diagrams Comparing Compensatory Loop Structures with and without Pursuit Crossfeed for Pitch and Roll Control

For φ/θ_c to be zero,

$$Y_{cf} = -\frac{Y_\theta N^{\varphi}_{\delta_B}}{Y_\varphi N^{\varphi}_{\delta_A}} \qquad \text{(III-37)}$$

But, according to the crossover model:

$$\frac{Y_\varphi N^{\varphi}_{\delta_A}}{\Delta} \doteq \frac{\omega_{c_\varphi}}{s} e^{-\tau_{e_\varphi} s} \qquad \text{(III-38)}$$

and

$$\frac{Y_\theta N^{\theta}_{\delta_B}}{\Delta} \doteq \frac{\omega_{c_\theta}}{s} e^{-\tau_{e_\theta} s} \qquad \text{(III-39)}$$

Substituting these into the crossfeed expression gives:

$$Y_{cf} = -\frac{\omega_{c_\theta}}{\omega_{c_\varphi}} \frac{N^{\varphi}_{\delta_B}}{N^{\theta}_{\delta_B}} e^{-(\tau_{e_\theta} - \tau_{e_\varphi})} \qquad \text{(III-40)}$$

Note that the effective delays cancel, if $\tau_{e_\theta} = \tau_{e_\varphi}$.

If, in addition, the pitch and roll loops were closed at the same crossover frequency, then the pursuit crossfeed required to decouple the roll from pitch would be exactly:

$$Y_{cf} = -\frac{N^{\varphi}_{\delta_B}}{N^{\theta}_{\delta_B}} \qquad \text{(III-41)}$$

For strictly compensatory tracking the level φ/θ_c cannot be made exactly zero, rather the effect is minimized depending upon the tightness of the roll loop. This can be shown by substituting crossover model functions into the general equation for φ/θ_c. For the sake of simplicity the effective delays can be neglected, without loss of generality, and reinstated later if desired; therefore:

$$\frac{Y_\varphi N^\varphi_{\delta_A}}{\Delta} \doteq \frac{\omega_{c_\varphi}}{s} \qquad \text{(III-42)}$$

and

$$\frac{Y_\theta N^\theta_{\delta_B}}{\Delta} \doteq \frac{\omega_{c_\theta}}{s} \qquad \text{(III-43)}$$

Thus:

$$\frac{\varphi}{\theta_c} = \frac{Y_\theta N^\varphi_{\delta_B}}{\Delta + Y_\theta N^\theta_{\delta_B} Y_\varphi N^\varphi_{\delta_A} + Y_\theta Y_\varphi N^{\theta\ \varphi}_{\delta_B \delta_A}}$$

$$= \frac{N^\varphi_{\delta_B}}{N^\theta_{\delta_B}} \frac{Y_\theta N^\theta_{\delta_B}}{\Delta} \frac{1}{1 + \frac{Y_\theta N^\theta_{\delta_B}}{\Delta} + \frac{Y_\varphi N^\varphi_{\delta_A}}{\Delta} + \frac{Y_\theta Y_\varphi N^{\theta\ \varphi}_{\delta_B \delta_A}}{\Delta}}$$

$$= \frac{N^\varphi_{\delta_B}}{N^\theta_{\delta_B}} \frac{\omega_{c_\theta}}{s} \frac{1}{1 + \frac{\omega_{c_\theta}}{s} + \frac{\omega_{c_\varphi}}{s} + \frac{\omega_{c_\theta}}{s}\frac{\omega_{c_\varphi}}{s}\left(1 - \frac{N^\varphi_{\delta_B}}{N^\theta_{\delta_B}} \frac{N^\theta_{\delta_A}}{N^\varphi_{\delta_A}}\right)} \qquad \text{(III-44)}$$

or, after eliminating higher order effects

$$\frac{\varphi}{\theta_c} \doteq \frac{N^\varphi_{\delta_B}}{N^\theta_{\delta_B}} \underbrace{\frac{\omega_{c_\theta}\, s}{\left(s + \omega_{c_\theta}\right)\left(s + \omega_{c_\varphi}\right)}}_{\text{Bandpass Filter Between } \omega_{c_\theta} \text{ and } \omega_{c_\varphi}} \qquad \text{(III-45)}$$

Note that for no active roll regulation ($\omega_{c_\varphi} = 0$) the amount of φ/θ_c is exactly equal to the numerator ratio out to the pitch crossover frequency (as shown previously in Section II).

Again, the main point to be made is that for roll due to pitch the numerator ratio $N^{\varphi}_{\delta_B}/N^{\theta}_{\delta_B}$ describes the level of coupling which must be overcome regardless of the pilot's control strategy — whether purely compensatory or involving a pursuit crossfeed.

A general survey of cross coupling in terms of roll-due-to-pitch and pitch-due-to-roll was made for the various subject helicopters in order to search for consistent trends and to try to develop simple approximate factors relationships for this variety of cross coupling. Hover and 60 kt flight conditions were considered. The modal response ratios used as indicators were:

$$\frac{\varphi}{\theta_c} = \frac{N^{\varphi}_{\delta_B}}{N^{\theta}_{\delta_B}} \text{ for forward flight} \qquad \text{(III-46)}$$

In hover, where yaw regulation must also be provided, we constrain ψ, thus:

$$\frac{\varphi}{\theta_c} = \frac{N^{\varphi\ \psi}_{\delta_B \delta_p}}{N^{\theta\ \psi}_{\delta_B \delta_p}} \text{ for hover} \qquad \text{(III-47)}$$

Similarly, for pitch-due-to-roll:

$$\frac{\theta}{\varphi_c} = \begin{cases} \dfrac{N^{\theta}_{\delta_A}}{N^{\varphi}_{\delta_A}} \text{ for forward flight} \\ \dfrac{N^{\theta\ \psi}_{\delta_A \delta_p}}{N^{\varphi\ \psi}_{\delta_B \delta_p}} \text{ for hover} \end{cases} \qquad \text{(III-48)}$$

By considering a time history corresponding to a unit step input, we obtain a direct indication of the magnitude of unwanted roll excursion which must be countered by the pilot.

Figures III-14 and III-15 show step input time histories for the two varieties of coupling. This covers each subject helicopter at hover and

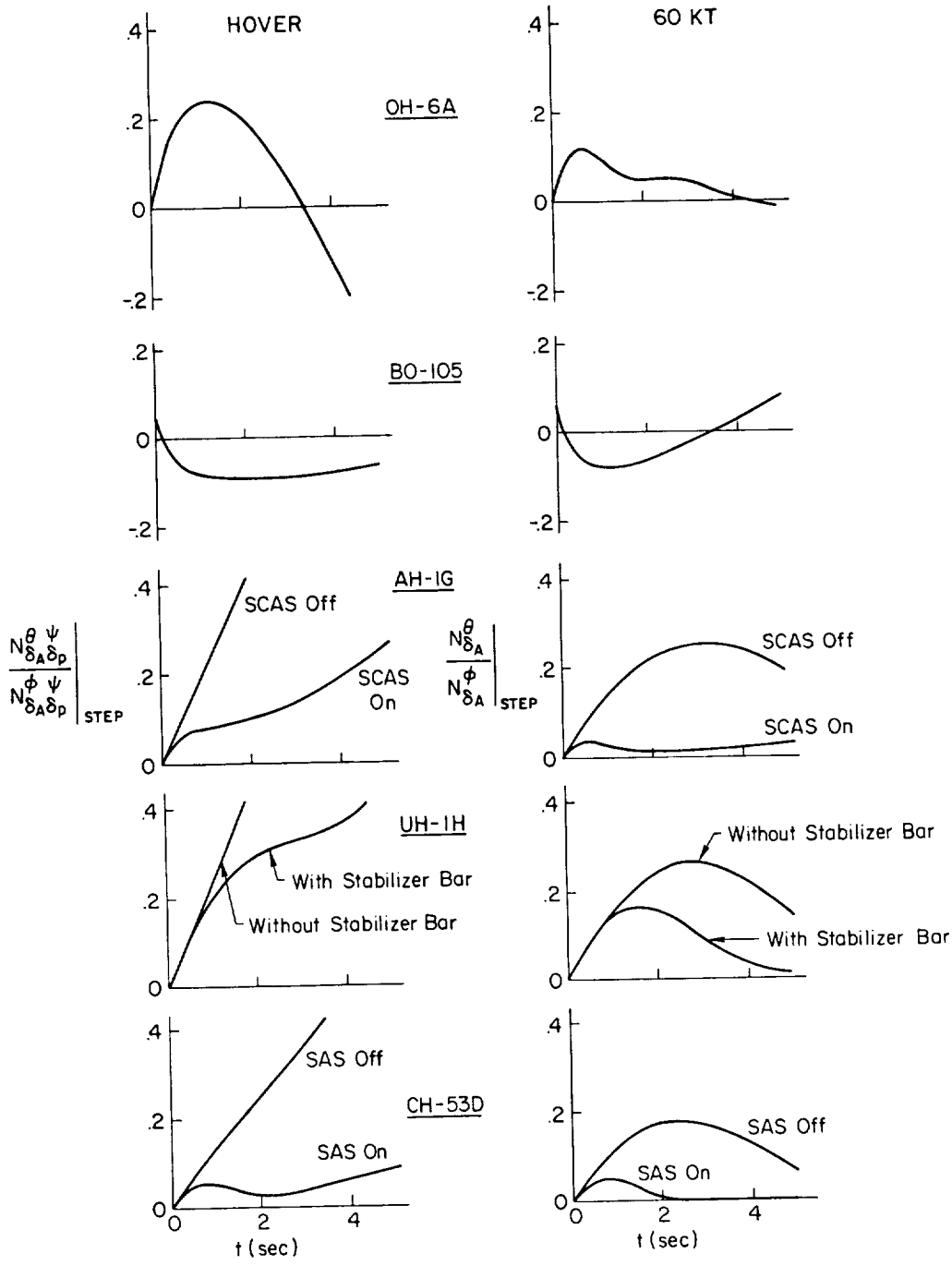

Figure III-14. $\varphi_c \longrightarrow \theta$ Cross Coupling Effect

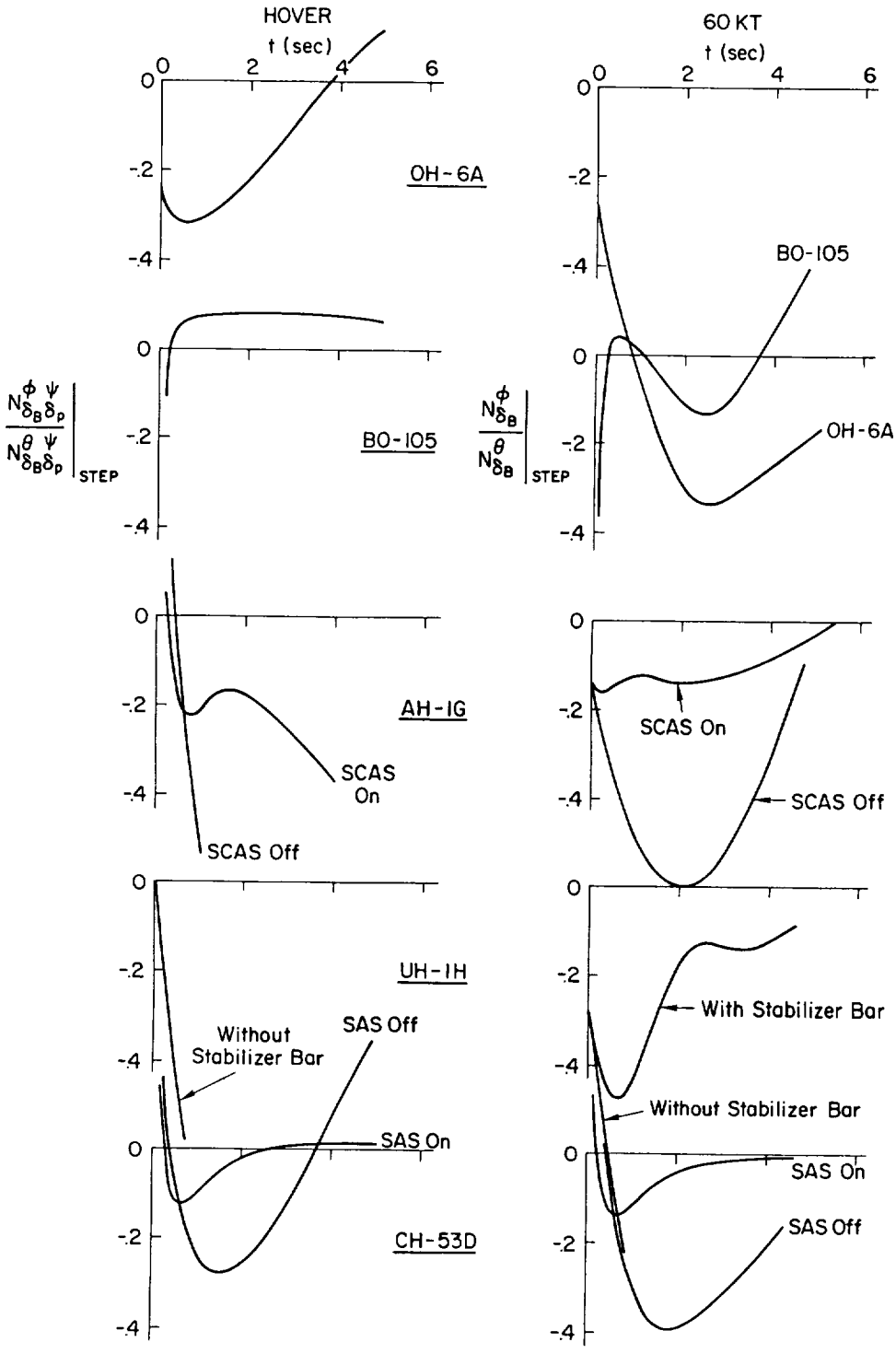

Figure III-15. $\theta_c \longrightarrow \varphi$ Cross Coupling Effect

60 kt, with and without augmentation. For pitch-due-to-roll ($\varphi_c \rightarrow \theta$) in Fig. III-14:

- Hover involves more coupling than 60 kt
- The sense is nose up for right roll except for the BO-105
- Augmentation is effective in reducing the coupling.

For roll-due-to-pitch ($\theta_c \rightarrow \varphi$) in Fig. III-15:

- 60 kt is worse than hover
- The sense is left roll for nose up (again, except for the BO-105)
- Augmentation reduces coupling
- The magnitude is generally larger than for pitch-due-to-roll.

The results obtained in the foregoing exercise are generally representative of the respective main rotor designs involved. According to Ref. 22 the roll-due-to-pitch and pitch-due-to-roll depend upon various rotor system parameters discussed previously in connection with pitch damping. A sketch of the effects of hinge offset and Lock No. on important cross coupling stability derivatives is shown in Fig. III-16. Recall that the level of roll-due-to-pitch and pitch-due-to-roll ranged from one extreme with the teetering designs (UH-1H and AH-1G) through articulated (OH-6A and CH-53D) to the other extreme with a hingeless design (BO-105).

It is convenient to express the roll-due-to-pitch and pitch-due-to-roll in terms of appropriate stability derivative ratios as done in Ref. 22. For example, roll-due-to-pitch could be expressed in terms of:

$$\frac{L_q}{L_p} \text{ or } \frac{M_{\delta_B}}{M_q}\frac{L_q}{L_p} \qquad \text{(III-49)}$$

An alternative, however, is to utilize the appropriate numerator ratio with some sacrifice in computational ease but with added value in terms of

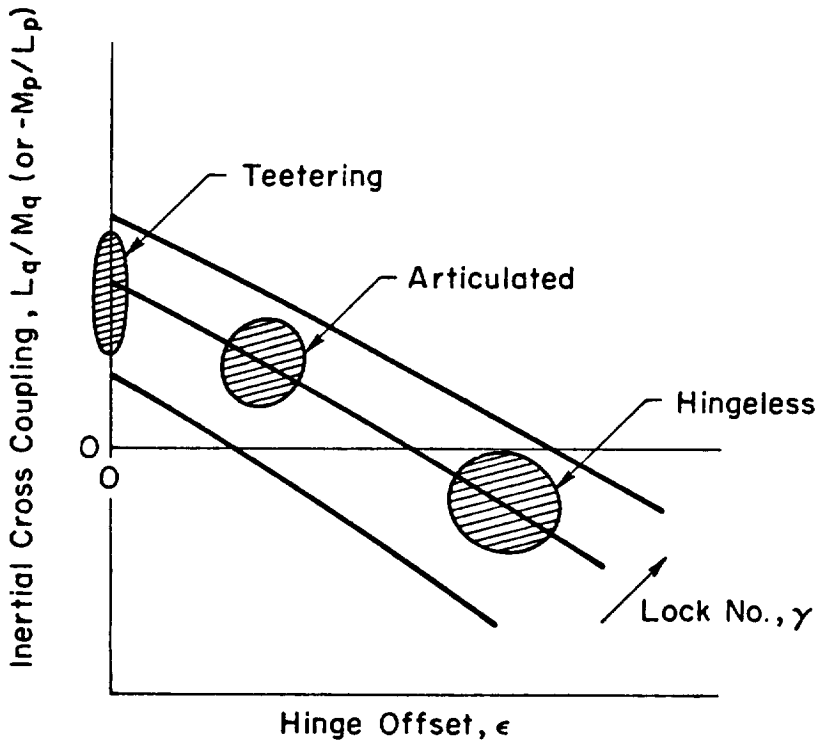

Figure III-16. Sketch of How Key Rotor System Parameters Affect Inertial Cross Coupling (Based on Material From Ref. 22)

pilot-vehicle effects. Figure III-17 illustrates roll-due-to-pitch coupling as a function of airspeed using three parameters:

- $-\frac{M_{\delta_B}}{M_q}\frac{L_q}{L_p}$
- $-\frac{L_q}{L_p}$
- Peak φ following a unit step θ_c (with and without ψ regulated).

Note that the two stability derivative-based parameters show a reasonable trend in the low speed range but do not reveal the extreme level of coupling in hover nor the increasing level of coupling at higher airspeeds.

The above is a demonstration of how cross coupling can be put in a multiloop manual control context such as φ/θ_c or θ/φ_c. Key stability derivatives such as M_p and L'_q are used in a supporting role to indicate origins of the phenomena, but the derivatives themselves may not necessarily adequately describe the overall effect.

2. Turn Coordination

Another form of cross coupling which we shall consider is turn coordination or lack thereof. According to Ref. 25 adverse yaw (turn coordination) can be especially detrimental to NOE operation if too extreme. In this variety of coupling it is possible to identify the potential problem source well enough to speculate on how it may arise for given rotor system designs, particularly the hingeless variety.

None of the helicopter examples from Volume One exhibit significant adverse yaw, however, their characteristics are used to verify a simplified form of the closed loop transfer relationship.

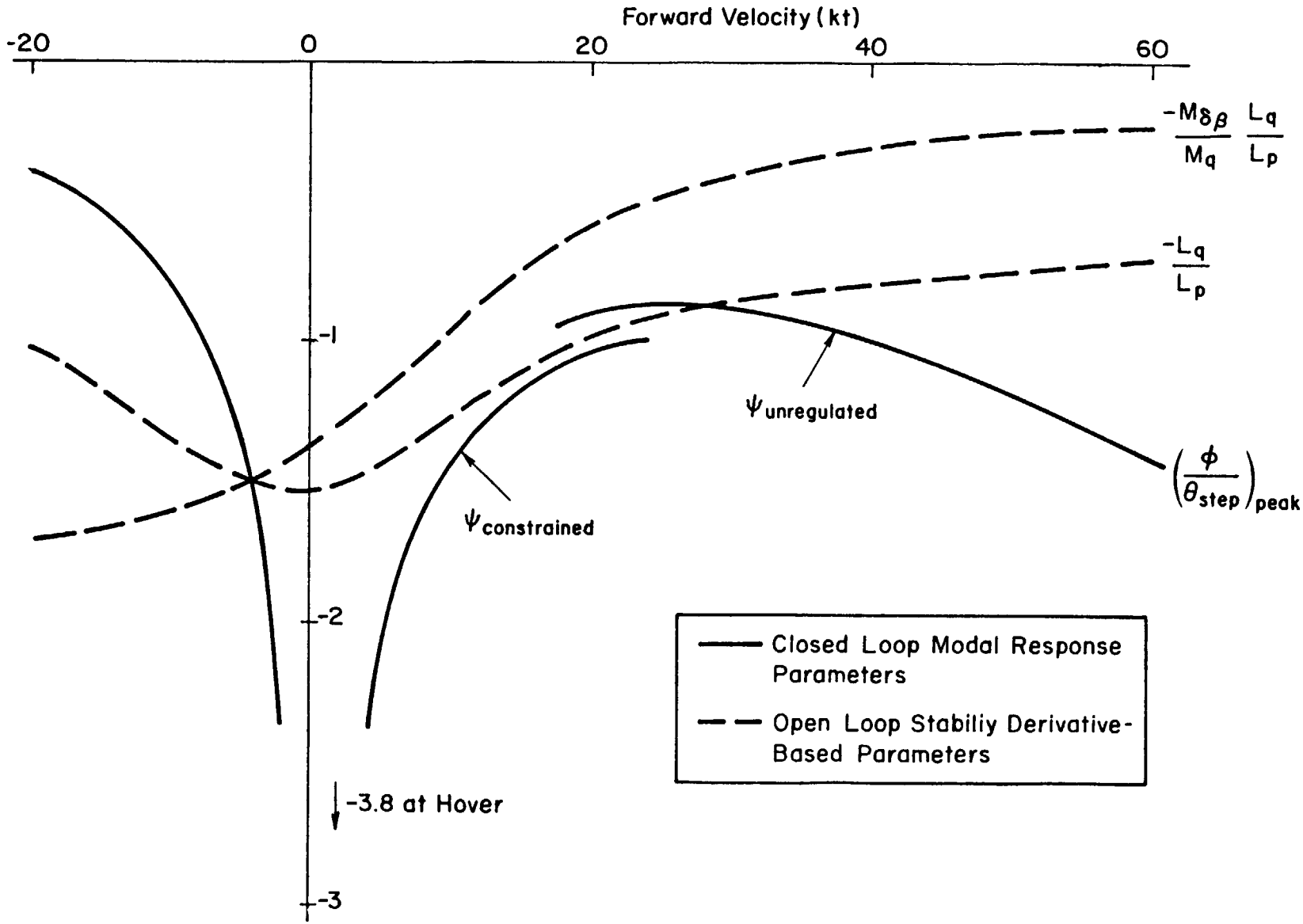

Figure III-17. Survey of $\theta_c \longrightarrow \varphi$ Cross Coupling

The closed loop dynamic response relationship considered most meaningful is $\dot{\psi}/\varphi$ since we have only to check how closely it equals g/V with use of roll and pitch controls only. Hence, the appropriate transfer function is:

$$\frac{\dot{\psi}}{\varphi} = \frac{s\, N^{\dot{\psi}\ \theta}_{\delta_A \delta_B}}{N^{\varphi\ \theta}_{\delta_A \delta_B}} \qquad \text{(III-50)}$$

The above expression contains all the cross coupling effects among longitudinal, lateral, and directional axes describable by the basic six-degree-of-freedom model. In addition, it represents the pilot's crossfeed between roll and yaw loops if he were to apply manual coordination. (This is analogous to the pursuit crossfeeds of φ/θ and θ/φ modal response ratios discussed previously.) This is illustrated in the following block diagram:

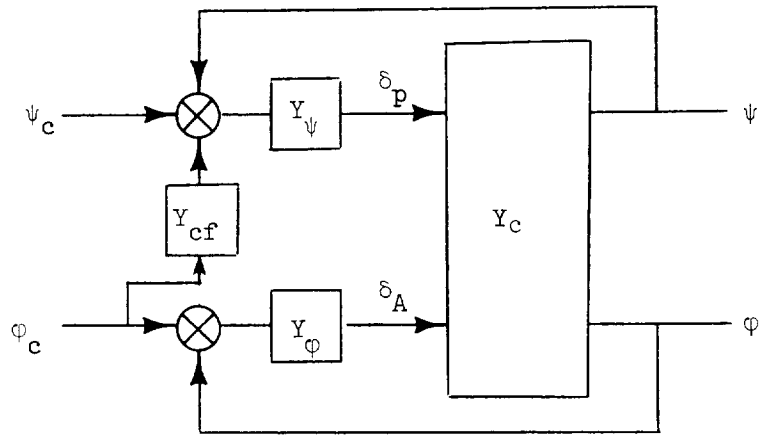

$$\text{where } Y_{cf} = \frac{1}{s}\left(\frac{g}{V} - \frac{s\, N^{\dot{\psi}\ \theta}_{\delta_A \delta_B}}{N^{\varphi\ \theta}_{\delta_A \delta_B}}\right) \qquad \text{(III-51)}$$

To gain insight we can solve for an approximation of $\dot{\psi}/\varphi$ using a simplified set of directional equations of motion similar to that introduced in the discussion of yaw control response, i.e.,

$$\begin{bmatrix} \doteq 0 \\ s-\cancel{Y_v} & -\frac{g}{V} & 1 \\ -L'_\beta & s(s-L'_p) & -L'_r \\ -N'_\beta & -N'_p\, s & s-N'_r \end{bmatrix} \begin{matrix} \beta \\ \varphi \\ s\psi \end{matrix} \doteq \begin{bmatrix} 0 \\ L'_{\delta_A} \\ N'_{\delta_A} \end{bmatrix} \delta_A \qquad \text{(III-52)}$$

The approximation is:

$$\frac{\dot{\psi}}{\varphi} \doteq \frac{s\, N^{\psi}_{\delta_A}}{N^{\varphi}_{\delta_A}} \doteq \frac{\begin{vmatrix} s & -\frac{g}{V} & 0 \\ -L'_\beta & s(s-L'_p) & 1 \\ -N'_\beta & -N'_p\, s & N'_{\delta_A}/L'_{\delta_A} \end{vmatrix}}{\begin{vmatrix} s & 0 & 1 \\ -L'_\beta & 1 & -L'_r \\ -N'_\beta & N'_{\delta_A}/L'_{\delta_A} & s-N'_r \end{vmatrix}} \qquad \text{(III-53)}$$

$$\doteq \frac{\frac{N'_{\delta_A}}{L'_{\delta_A}} s^3 + \left(N'_p - \frac{N'_{\delta_A}}{L'_{\delta_A}} L'_p\right) s^2 + \frac{g}{V} N'_\beta}{s^2 - N'_r\, s + N'_\beta}$$

if $$\left| \frac{N'_{\delta_A}}{L'_{\delta_A}} L'_\beta \right| << \left| N'_\beta \right| \qquad \text{(III-54)}$$

and $$\left| \frac{N'_{\delta_A}}{L'_{\delta_A}} L'_r \right| << \left| N'_r \right| \qquad \text{(III-55)}$$

both are valid assumptions according to the data in Volume One. Equation III-51 can be further manipulated into the following useful form if $N'_\beta > 0$, $N'_p - (L'_{\delta_A}/N'_{\delta_A})L'_p < 0$ and $(N'_{\delta_A}/L'_{\delta_A})s^3 \doteq 0$:

$$\frac{\dot{\psi}}{\varphi} \doteq \frac{\left(N'_p - \frac{N'_{\delta_A}}{L'_{\delta_A}} L'_p\right)\left(s - a\right)\left(s + a\right)}{\left[s^2 - N'_r\, s + N'_\beta\right]} \qquad \text{(III-56)}$$

where

$$a^2 = \frac{\frac{g}{V} N'_\beta}{\left| N'_p - \frac{N'_{\delta_A}}{L'_{\delta_A}} L'_p \right|} \qquad \text{(III-57)}$$

Thus, the $\dot{\psi}/\varphi$ transfer function is composed of a high frequency gain equal to $N'_p - (N'_{\delta_A}/L'_{\delta_A})L'_p$, a non-minimum phase zero, a denominator consisting of the dutch roll approximation, and a low frequency gain equal to g/V. Therefore the magnitude of $N'_p - (N'_{\delta_A}/L'_{\delta_A})L'_p$ directly determines the adverse yaw excitation of dutch roll. If $N'_p - (N'_{\delta_A}/L'_{\delta_A})L'_p$ equaled g/V, an unlikely occurrence, then $\dot{\psi}/\varphi$ would be very nearly g/V in the dynamic sense. Let us consider, then, the composition of $N'_p - (N'_{\delta_A}/L'_{\delta_A})L'_p$.

First, let us view the adverse yaw in terms of unprimed derivatives, i.e.,

$$N'_p - \frac{N'_{\delta_A}}{L'_{\delta_A}} L'_p \doteq N_p + \frac{I_{xz}}{I_z} L_p - \frac{N'_{\delta_A}}{L'_{\delta_A}} L_p \qquad \text{(III-58)}$$

According to the compiled data the first and third terms above are normally small. It is the second term, $(I_{xz}/I_z)L_p$, which could be potentially troublesome if the cross product of inertia and basic roll damping were both large. The first condition is strictly a function of mass distribution, but the second one is heavily dependent on the rotor system design. We would expect L_p to be large for, say, hingeless rotors. It is not surprising, then, that the adverse yaw problems encountered in the NOE flight tests reported in Ref. 25 involved a hingeless rotor helicopter. Unfortunately data describing inertial and roll damping characteristics were not available.

It is important to note that the BO-105 hingeless rotor data compiled in Volume One did exhibit a very large L'_p but did not involve a non-zero I_{xz}, therefore the adverse yaw characteristics of the modeled vehicle are probably unrealistically low.

A survey of the turn coordination of the various helicopters is shown in Fig. III-18. Time histories of $\dot{\psi}/\varphi_c$ are plotted for a step φ_c and an assumed roll crossover frequency of 1 rad/sec. The dashed line in each plot represents $g/V \cdot \varphi/\varphi_c$, i.e., perfect turn coordination. When the solid line is below the dashed line, inadequate turn rate (adverse yaw) is present and, conversely, when above it, excessive turn rate (proverse yaw). Note that the AH-1G SCAS tends to produce worse adverse yaw than the bare airframe, but the CH-53D SAS produces perfect coordination. These features will be further discussed in Section VI.

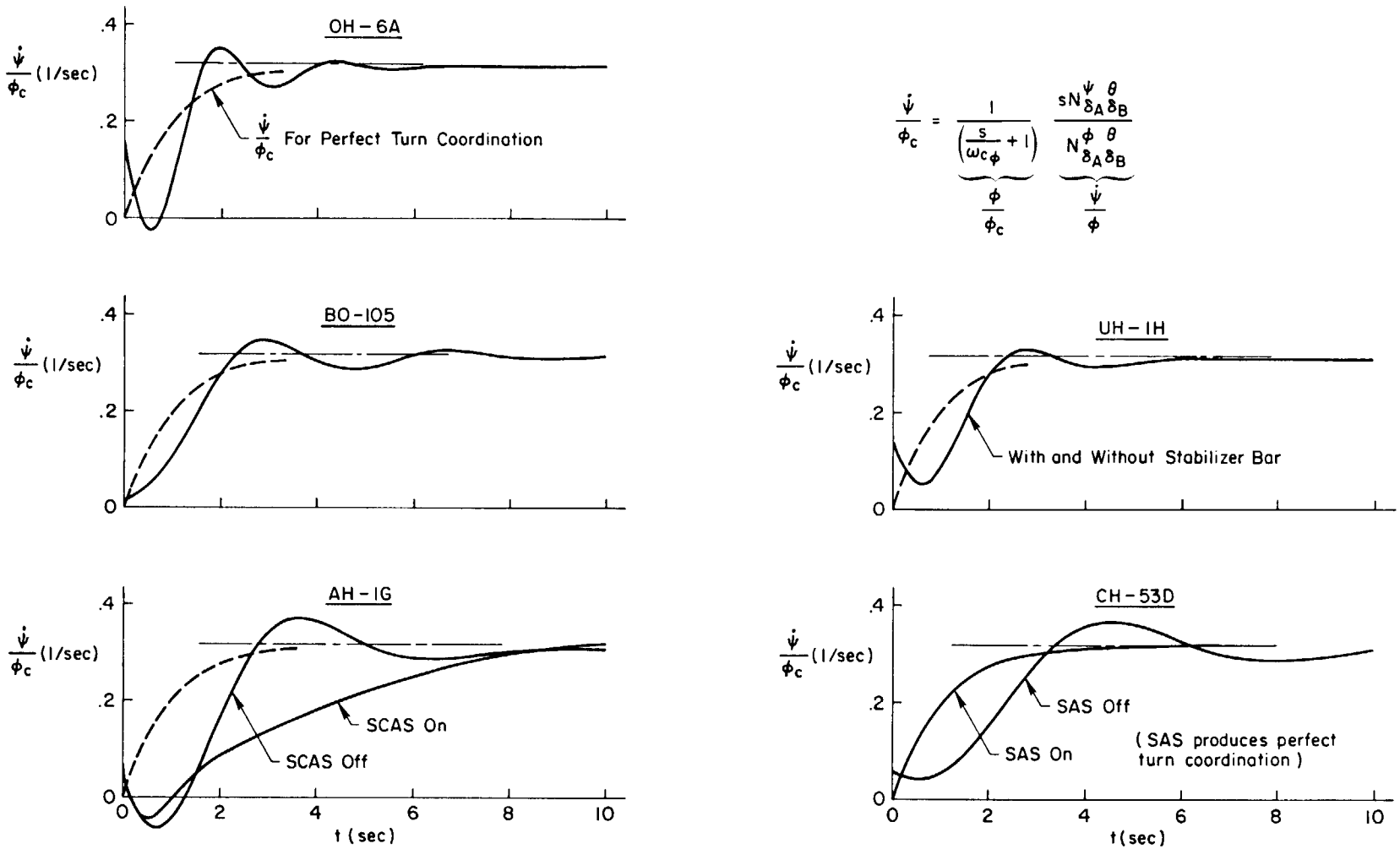

Figure III-18. Turn Coordination Characteristics

SECTION IV

OUTER LOOP REGULATION

A. BACKGROUND

In this section we shall explore the closed-loop dynamics of the outer manual control loops involving position or translational velocity.

The ability to control a vehicle's position in space or its flight path is an important factor in completion of its mission. The traditional handling qualities parameters that pertain to position and/or velocity control such as stable stick force characteristics with respect to velocity, positive effective dihedral (stable spiral), etc., are often parameters defined by static or open-loop vehicle characteristics. However, it is possible to view position and/or velocity as the outer loops of our six-degrees-of-freedom model, and to evaluate the total dynamic and static characteristics for each case. The benefits to be gained by doing so are an increased understanding of the total vehicle response and a better understanding of the parameters which may affect the vehicle's response.

In segregating the six parameters of our model into inner (ϑ, φ, ψ) and outer ($\dot{x}$, $\dot{y}$, $\dot{z}$) loops, we have to appreciate fully the impact of the inner loop closures on outer loop responses: that the basic modes of the outer loop responses are derived largely from the inner loop closures. Thus, outer loop characteristics such as response time constants, steady state gains, and damping ratios, are strongly affected by inner loop closures. In this study, many of the outer loop characteristics will be examined for the cases where inner loop regulation is assumed because it removes the complexities of pilot behavior while retaining the key vehicle-related characteristics.

B. PRIMARY CONTROL RESPONSE

According to the overall pilot-vehicle loop structure in Section II, the primary outer loop controls are:

- Collective stick for heave
- Pitch attitude for surge (or forward speed)
- Roll attitude for sway (or lateral flight path).

We shall begin our discussion of these by developing a general expression for outer loop response given the regulation of inner loops with finite bandwidth. This will be followed by specific applications to surge, sway, and heave control.

The main objective in the following pages is to demonstrate the use of appropriate numerator ratios in estimating outer loop control response. Let us begin by considering the example of surge control ($\dot{x}/\theta_c$) for forward flight specifically including the effects of pitch and roll regulation but neglecting yaw regulation.

1. Surge (Longitudinal) Control

The general expression for $\dot{x}/\theta_c$ can be written directly from the block diagram, i.e.,

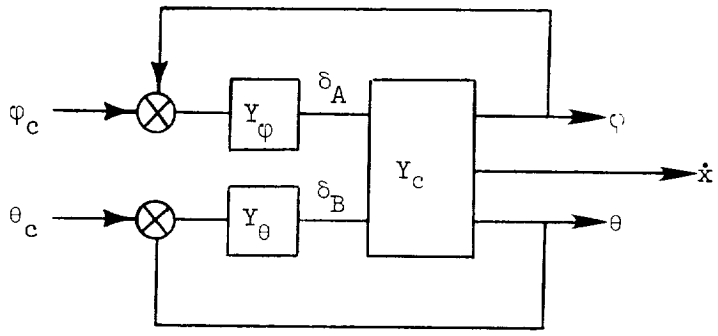

$$\frac{\dot{x}}{\theta_c} = \frac{Y_\theta \left(N^{\dot{x}}_{\delta_B} + Y_\varphi N^{\dot{x}\ \varphi}_{\delta_B \delta_A} \right)}{\Delta + Y_\theta N^{\theta}_{\delta_B} + Y_\varphi N^{\varphi}_{\delta_A} + Y_\theta Y_\varphi N^{\theta\ \varphi}_{\delta_B \delta_A}} \qquad \text{(IV-1)}$$

After rearranging and expanding coupling numerators, we have

$$\frac{\dot{x}}{\theta_c} = \frac{N^{\dot{x}}_{\delta_B}{}^{\varphi}_{\delta_A}}{N^{\theta}_{\delta_B}{}^{\varphi}_{\delta_A}} \frac{\dfrac{Y_\theta N^{\theta}_{\delta_B}}{\Delta}\left(1 - \dfrac{N^{\varphi}_{\delta_B} N^{\theta}_{\delta_A}}{N^{\varphi}_{\delta_B} N^{\theta}_{\delta_A}}\right)\left[\dfrac{Y_\varphi N^{\varphi}_{\delta_A}}{\Delta} + \dfrac{1}{1 - \dfrac{N^{\dot{x}}_{\delta_A} N^{\varphi}_{\delta_B}}{N^{\varphi}_{\delta_A}{}^{\dot{x}}_{\delta_B}}}\right]}{\left(1 + \dfrac{Y_\theta N^{\theta}_{\delta_B}}{\Delta}\right)\left(1 + \dfrac{Y_\varphi N^{\varphi}_{\delta_A}}{\Delta}\right) - \dfrac{Y_\varphi N^{\varphi}_{\delta_A}}{\Delta}\dfrac{Y_\theta N^{\theta}_{\delta_B}}{\Delta}\dfrac{N^{\varphi}_{\delta_B} N^{\theta}_{\delta_A}}{N^{\varphi}_{\delta_A} N^{\theta}_{\delta_B}}} \tag{IV-2}$$

Under the conditions of weak cross coupling, i.e.,

$$N^{\dot{x}}_{\delta_A} N^{\varphi}_{\delta_B} \ll N^{\dot{x}}_{\delta_B} N^{\varphi}_{\delta_A} \tag{IV-3}$$

and

$$N^{\theta}_{\delta_A} N^{\varphi}_{\delta_B} \ll N^{\theta}_{\delta_B} N^{\varphi}_{\delta_A} \tag{IV-4}$$

then

$$\frac{\dot{x}}{\theta_c} \doteq \frac{N^{\dot{x}}_{\delta_B}{}^{\varphi}_{\delta_A}}{N^{\theta}_{\delta_B}{}^{\varphi}_{\delta_A}} \frac{\dfrac{Y_\theta N^{\theta}_{\delta_B}}{\Delta}}{1 + \dfrac{Y_\theta N^{\theta}_{\delta_B}}{\Delta}} \tag{IV-5}$$

Notice that explicit terms involving $\varphi - \delta_A$ disappear, and only $\theta - \delta_B$ terms remain. After substituting an appropriate crossover model approximation such as $(Y_\theta N^{\theta}_{\delta_B}/\Delta) \doteq (\omega_{c_\theta}/s)$ (we can choose to neglect the effective delay τ_e, since it is a high frequency effect) we have

$$\frac{\dot{x}}{\theta_c} \doteq \frac{N^{\dot{x}}_{\delta_B}{}^{\varphi}_{\delta_A}}{N^{\theta}_{\delta_B}{}^{\varphi}_{\delta_A}} \frac{1}{\left(\dfrac{s}{\omega_{c_\theta}} + 1\right)}$$

$$\doteq \frac{N^{\dot{x}}_{\delta_B}{}^{\varphi}_{\delta_A}}{N^{\theta}_{\delta_B}{}^{\varphi}_{\delta_A}} \quad \text{for } |s| < \omega_{c_\theta} \tag{IV-6}$$

Using a similar argument, if roll and yaw loops are closed:

$$\frac{\dot{x}}{\theta_c} \doteq \frac{N^{\dot{x}}_{\delta_B}\,{}^{\varphi}_{\delta_A}\,{}^{\psi}_{\delta_p}}{N^{\theta}_{\delta_B}\,{}^{\varphi}_{\delta_A}\,{}^{\psi}_{\delta_p}} \frac{1}{\left(\frac{s}{\omega_{c_\theta}} + 1\right)} \doteq \frac{N^{\dot{x}}_{\delta_B}\,{}^{\varphi}_{\delta_A}\,{}^{\psi}_{\delta_p}}{N^{\theta}_{\delta_B}\,{}^{\varphi}_{\delta_A}\,{}^{\psi}_{\delta_p}} \text{ provided } |s| < \omega_{c_\theta} \tag{IV-7}$$

The foregoing is important because it essentially separates all inner loop features from outer loop ones except for the primary inner loop cross-over frequency (ω_{c_θ} in the case of $\dot{x}/\theta_c$). Similar relationships can be developed for the other outer loops.

2. Sway (Lateral) Control

In the case of lateral position control:

$$\frac{\dot{y}}{\varphi_c} \doteq \frac{N^{\dot{y}}_{\delta_A}\,{}^{\theta}_{\delta_B}}{N^{\varphi}_{\delta_A}\,{}^{\theta}_{\delta_B}} \frac{1}{\left(\frac{s}{\omega_{c_\theta}} + 1\right)} \doteq \frac{N^{\dot{y}}_{\delta_A}\,{}^{\theta}_{\delta_B}}{N^{\varphi}_{\delta_A}\,{}^{\theta}_{\delta_B}} \text{ provided } |s| < \omega_{c_\theta} \tag{IV-8}$$

or, with pitch and yaw loops:

$$\frac{\dot{y}}{\varphi_c} \doteq \frac{N^{\dot{y}}_{\delta_A}\,{}^{\theta}_{\delta_B}\,{}^{\psi}_{\delta_p}}{N^{\varphi}_{\delta_A}\,{}^{\theta}_{\delta_B}\,{}^{\psi}_{\delta_p}} \text{ provided } |s| < \omega_{c_\varphi} \tag{IV-9}$$

Pitch loop effects can usually be assumed negligible because they enter in the form of higher order effects as shown previously for the $\dot{x}/\theta_c$ transfer function. Yaw regulation, however, may involve a less negligible cross coupling effect. It can be included, though, in a direct way:

$$\frac{\dot{y}}{\varphi_c} \doteq \frac{N^{\dot{y}\ \psi\ \theta}_{\delta_A \delta_p \delta_B}}{N^{\varphi\ \psi\ \theta}_{\delta_A \delta_p \delta_B}} \frac{\dfrac{Y_\varphi N^{\varphi\ \theta}_{\delta_A \delta_B}}{N^{\theta}_{\delta_B}} \left[\dfrac{Y_\psi N^{\psi\ \theta}_{\delta_p \delta_B}}{N^{\theta}_{\delta_B}} + \dfrac{1}{1 - \dfrac{N^{\dot{y}\ \theta}_{\delta_p \delta_B} N^{\psi\ \theta}_{\delta_A \delta_B}}{N^{\dot{y}\ \theta}_{\delta_A \delta_B} N^{\psi\ \theta}_{\delta_p \delta_B}}} \right]}{\left(1 + \dfrac{Y_\varphi N^{\varphi\ \theta}_{\delta_A \delta_B}}{N^{\theta}_{\delta_B}}\right)\left(1 + \dfrac{Y_\psi N^{\psi\ \theta}_{\delta_p \delta_B}}{N^{\theta}_{\delta_B}}\right)} \qquad \text{(IV-10)}$$

Thus, to the extent that $\dot{y}$ responds to rudder pedals, ψ responds to lateral cyclic, and a yaw loop is closed, there will be a corresponding modification of the first order sway control response.

3. Heave Control

Heave response due to collective control requires consideration of an inner pitch loop, i.e.,

$$\frac{\dot{z}}{\delta_c} = \frac{N^{\dot{z}}_{\delta_c} + Y_\theta N^{\dot{z}\ \theta}_{\delta_c \delta_B}}{\Delta + Y_\theta N^{\theta}_{\delta_B}}$$

$$= \frac{N^{\dot{z}\ \theta}_{\delta_c \delta_B}}{N^{\theta}_{\delta}} \frac{\left(\dfrac{Y_\theta N^{\theta}_{\delta_B}}{\Delta} + \dfrac{1}{1 - \dfrac{N^{\theta}_{\delta_B} N^{\dot{z}}_{\delta_c}}{N^{\theta}_{\delta_B} N^{\dot{z}}_{\delta_c}}} \right)}{\left(1 + \dfrac{Y_\theta N^{\theta}_{\delta_B}}{\Delta}\right)} \qquad \text{(IV-11)}$$

or, with φ and ψ regulated

$$\frac{\dot{z}}{\delta_c} \doteq \frac{N^{\dot{z}\ \theta\ \varphi\ \psi}_{\delta_c\delta_B\delta_A\delta_p}}{N^{\theta\ \varphi\ \psi}_{\delta_B\delta_A\delta_p}} \frac{\left(\frac{Y_\theta N^{\theta\ \varphi\ \psi}_{\delta_B\delta_A\delta_p}}{N^{\varphi\ \psi}_{\delta_A\delta_p}} + \frac{1}{1 - \frac{N^{\theta\ \varphi\ \psi}_{\delta_c\delta_A\delta_p} N^{\dot{z}\ \varphi\ \psi}_{\delta_B\delta_A\delta_p}}{N^{\theta\ \varphi\ \psi}_{\delta_B\delta_A\delta_p} N^{\dot{z}\ \varphi\ \psi}_{\delta_c\delta_A\delta_p}}}\right)}{\left(1 + \frac{Y_\theta N^{\theta\ \varphi\ \psi}_{\delta_B\delta_A\delta_p}}{N^{\varphi\ \psi}_{\delta_A\delta_p}}\right)} \qquad \text{(IV-12)}$$

and if pitch-heave coupling is low with collective and longitudinal cyclic controls, i.e.,

$$N^{\theta\ \varphi\ \psi}_{\delta_c\delta_A\delta_p} N^{\dot{z}\ \varphi\ \psi}_{\delta_B\delta_A\delta_p} << N^{\theta\ \varphi\ \psi}_{\delta_B\delta_A\delta_p} N^{\dot{z}\ \varphi\ \psi}_{\delta_c\delta_A\delta_p} \qquad \text{(IV-13)}$$

then

$$\frac{\dot{z}}{\delta_c} \doteq \frac{N^{z\ \theta\ \varphi\ \psi}_{\delta_c\delta_B\delta_A\delta_p}}{N^{\theta\ \varphi\ \psi}_{\delta_B\delta_A\delta_p}} \text{ provided } |s| < \omega_{c_\theta} \qquad \text{(IV-14)}$$

C. ANALYSIS USING APPROXIMATE FACTORS

The expressions shown for outer loop primary control response appear more formidible than they really are, especially when approximately cancelling dipoles are omitted. For example, consider the AH-1G at 60 kt including SCAS effects. While seven first order roots and two second order roots are present in the denominator ($N^{\theta\ \varphi}_{\delta_B\delta_A}$), they all approximately cancel except for the following:

$$\frac{\dot{x}}{\theta} \doteq \frac{N^{\dot{x}\ \varphi}_{\delta_B\delta_A}}{N^{\theta\ \varphi}_{\delta_B\delta_A}} \doteq \frac{-7.6(0.85)[0.02;2.1]}{(0.007)(0.90)} \doteq \frac{-32.3}{(0.007)} \qquad \text{(IV-15)}$$

$$\frac{\dot{y}}{\varphi} \doteq \frac{N^{\dot{y}\ \theta}_{\delta_A\delta_B}}{N^{\varphi\ \theta}_{\delta_A\delta_B}} \doteq \frac{1.73[0.03;4.3]}{(0)} \doteq \frac{31.4}{(0)} \qquad \text{(IV-16)}$$

$$\frac{\dot{z}}{\delta_c} \doteq \frac{N^{\dot{z}\ \theta\ \varphi}_{\delta_c\delta_B\delta_A}}{N^{\theta\ \varphi}_{\delta_B\delta_A}} \doteq \frac{-14.4(0.009)}{(0.9)(0.007)} \doteq \frac{-14.4}{(0.9)} \qquad \text{(IV-17)}$$

The simplicity of the above expressions can be shown more formally by considering reduced order longitudinal-vertical and lateral-directional equations of motion, i.e.,

Longitudinal-Vertical Equations of Perturbed Motions

$$\begin{bmatrix} s - X_u & \overset{\doteq 0}{\cancel{-X_w}} \\ -Z_u & s - Z_w \end{bmatrix} \begin{bmatrix} \dot{x} \\ \dot{z} \end{bmatrix} \doteq \begin{bmatrix} \overset{\doteq 0}{\cancel{(X_\alpha}} - g) & \overset{\doteq 0}{\cancel{X_{\delta_c}}} \\ Z_\alpha & Z_{\delta_c} \end{bmatrix} \begin{bmatrix} \theta \\ \delta_c \end{bmatrix} \qquad \text{(IV-18)}$$

$$\text{or} \qquad \Delta \doteq \begin{vmatrix} s - X_u & 0 \\ -Z_u & s - Z_w \end{vmatrix} = \underset{SD}{(s - X_u)}\underset{HD}{(s - Z_w)} \qquad \text{(IV-19)}$$

$$\text{and} \qquad N^{\dot{x}}_{\theta} \doteq \begin{vmatrix} -g & 0 \\ Z_\alpha & s - Z_w \end{vmatrix} = \underset{HD}{-g\,(s - Z_w)} \qquad \text{(IV-20)}$$

$$\text{whence} \qquad \frac{\dot{x}}{\theta} \doteq \frac{-g}{\underset{SD}{(s - X_u)}} \qquad \text{(IV-21)}$$

Likewise $$N^{\dot{z}}_{\delta_c} \doteq \begin{vmatrix} s - X_u & 0 \\ -Z_u & Z_{\delta_c} \end{vmatrix} = \underset{SD}{Z_{\delta_c}\,(s - X_u)} \qquad \text{(IV-22)}$$

whence $$\frac{\dot{z}}{\delta_c} \doteq \frac{Z_{\delta_c}}{\underset{HD}{\left(s - Z_w\right)}} \qquad \text{(IV-23)}$$

Lateral-Directional Equations of Perturbed Motions

$$\begin{bmatrix} s - Y_v & Y_\beta \\ -N_v & s^2 - N'_r s + N'_\beta \end{bmatrix} \begin{bmatrix} \dot{y} \\ \psi \end{bmatrix} = \begin{bmatrix} g \\ N'_p s \end{bmatrix} \begin{bmatrix} \varphi \end{bmatrix} \qquad \text{(IV-24)}$$

or $$\Delta \doteq \begin{vmatrix} s - Y_v & Y_\beta \\ -N_v & s^2 - N'_r s + N'_\beta \end{vmatrix} \doteq \underset{D}{s\left[s^2 - \left(N'_r + Y_v\right)s + N'_\beta + Y_v N'_r\right]} \qquad \text{(IV-25)}$$

and $$N^{\dot{y}}_{\varphi} = \begin{vmatrix} g & Y_\beta \\ N'_p s & s^2 - N'_r s + N'_\beta \end{vmatrix} = \underset{D}{g\left[s^2 - \left(N'_r + \frac{VY_v N'_p}{g}\right)s + N'_\beta\right]} \qquad \text{(IV-26)}$$

whence $$\underset{\varphi}{\underset{\sim\sim}{\frac{\dot{y}}{}}} \doteq \underset{s}{\underset{\sim\sim}{\frac{g}{}}} \qquad \text{(IV-27)}$$

and, if ψ is constrained

$$\underset{\varphi}{\underset{\sim\sim}{\frac{\dot{y}}{}}} \doteq \underset{\underset{LD}{s - Y_v}}{\underset{\sim\sim}{\frac{g}{}}} \qquad \text{(IV-28)}$$

The accuracy of the above approximations is demonstrated in the survey of outer loop control characteristics shown in Table IV-1. Further, the validity over a range of forward velocities is shown in Table IV-2 using the OH-6A as an example.

a. Surge Regulation. The nature of outer loop regulation is easily shown using the foregoing relationships along with a crossover model for the inner loop regulation by the pilot. First, consider the surge loop.

$$\frac{x}{\theta_c} \doteq \frac{-g}{s\left(s - X_u\right)} \frac{1 - \frac{\tau_e}{2} s}{\left(\frac{s}{\omega_{c_\theta}} + 1\right)\left(1 + \frac{\tau_e}{2} s\right)} \qquad \text{(IV-29)}$$

The root locus is thus:

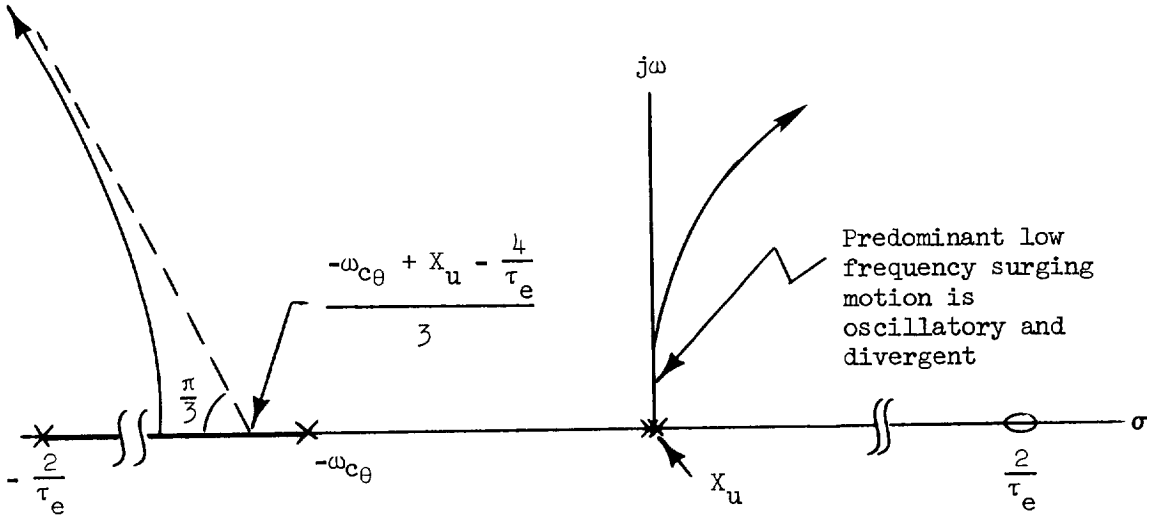

This sketch indicates that surge control is essentially a K/s^2 system in which the attitude loop tightness, represented by ω_{c_θ}, plays a relatively weak role. According to the root locus some degree of lead or velocity feedback is required for a stable loop closure as shown in the sketch. This lead requirement is effectively addressed by the extended crossover model described in Ref. 12 in which the parameter α represents a lead compensation zero placement.

TABLE IV-1

SURVEY OF OUTER LOOP CONTROL CHARACTERISTICS

at 60 kt

	OH-6A	BO-105	AH-1G	UH-1H	CH-53D	
$\frac{\dot{x}}{\theta_c} \doteq \frac{N^{\dot{x}}_{\delta_B} N^{\varphi}_{\delta_A}}{N^{\theta}_{\delta_B} N^{\varphi}_{\delta_A}}$	$\frac{-32.1}{(0.022)}$	$\frac{-32.0}{(0.022)}$	$\frac{-32.1}{(0.0073)}$	$\frac{-32.5}{(0.0047)}$	$\frac{-32.3}{(0.015)}$	$\doteq \frac{-g}{(1/T_{\theta_1})}$
$\frac{\dot{y}}{\varphi_c} \doteq \frac{N^{\dot{y}}_{\delta_A} N^{\theta}_{\delta_B}}{N^{\varphi}_{\delta_A} N^{\theta}_{\delta_B}}$	$\frac{32.1}{(0)}$	$\frac{31.8}{(0)}$	$\frac{30.6}{(0)}$	$\frac{31.3}{(0)}$	$\frac{31.1}{(0)}$	$\doteq \frac{g}{(0)}$
$\frac{\dot{h}}{\delta_c} \doteq \frac{-N^{\dot{z}}_{\delta_c} N^{\theta}_{\delta_B} N^{\varphi}_{\delta_A}}{N^{\theta}_{\delta_B} N^{\varphi}_{\delta_A}}$	$\frac{7.0}{(0.74)}$	$\frac{10.2}{(0.76)}$	$\frac{13.7}{(0.91)}$	$\frac{11.2}{(0.92)}$	$\frac{7.15}{(0.65)}$	$\doteq \frac{-Z_{\delta_c}}{(1/T_{\theta_2})}$

TABLE IV-2

SURVEY OF OUTER LOOP CONTROL CHARACTERISTICS

VARYING AIRSPEED

OH-6A

	-20 kt	Hover	20 kt	40 kt	60 kt
$\frac{\dot{x}}{\delta_c}$	$\frac{-33.3}{(0.025)}$	$\frac{-32.2}{(0.011)}$	$\frac{-32.3}{(0.0067)}$	$\frac{-30.5}{(0.016)}$	$\frac{-32.1}{(0.022)}$
$\frac{\dot{y}}{\varphi_c}$	$\frac{31.8}{(0.0043)}$ with $(\psi \rightarrow \delta_p)$	$\frac{32.2}{(0.022)}$ with $(\psi \rightarrow \delta_p)$	$\frac{31.8}{(0.011)}$ with $(\psi \rightarrow \delta_p)$	$\frac{32.1}{(0)}$	$\frac{32.1}{(0)}$
$\frac{\dot{h}}{\delta_c}$	$\frac{7.07\ [0.81;0.0135]}{(0.0043)(0.0248)(0.407)}$	$\frac{7.4}{(0.34)}$	$\frac{6.9(0.013)}{(0.011)(0.429)}$	$\frac{6.7(0.020)}{(0.016)(0.65)}$	$\frac{7.0}{(0.74)}$

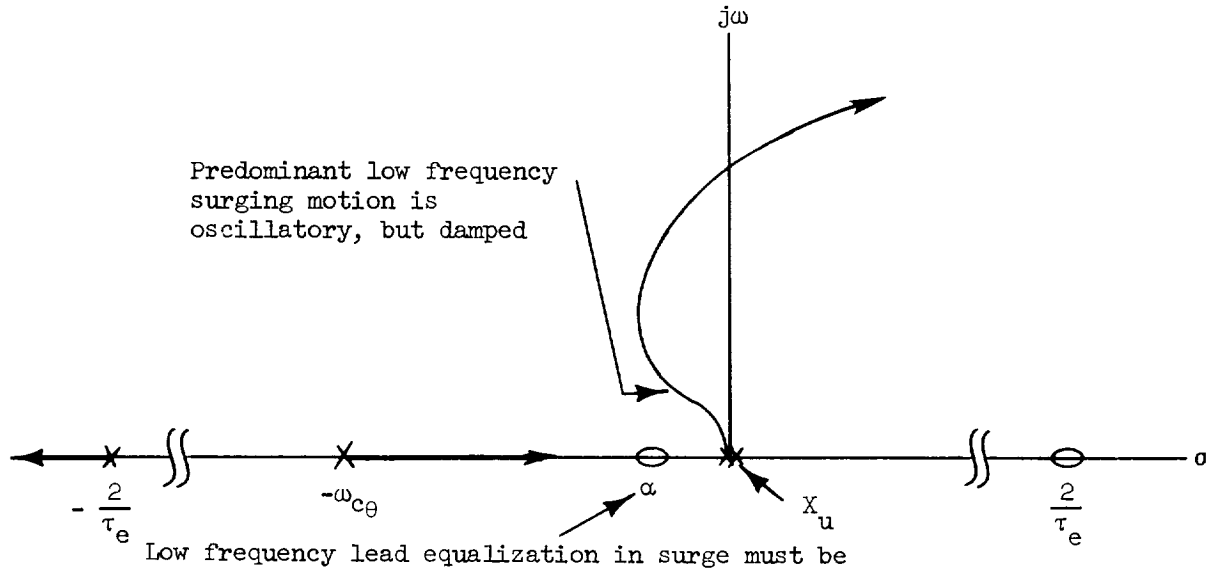

Low frequency lead equalization in surge must be supplied either by the pilot at great cost in workload or by automatic surge velocity-aided augmentation

If velocity rather than position were being regulated as in forward flight, the controlled element would be more like K/s and the closed loop bandwidth would exhibit a stronger dependence on ω_{c_θ}, i.e.,

$$\frac{\dot{x}}{\theta_c} \doteq \frac{-g}{\left(s - X_u\right)} \frac{1 - \frac{\tau_{e_\theta}}{2} s}{\left[2 \frac{\tau_{e_\theta}}{\omega_{c_\theta}} s^2 + \left(\frac{1}{\omega_{c_\theta}} + \frac{\tau_{e_\theta}}{2}\right) s + 1\right]} \qquad \text{(IV-30)}$$

The corresponding root locus is shown in the following sketch.

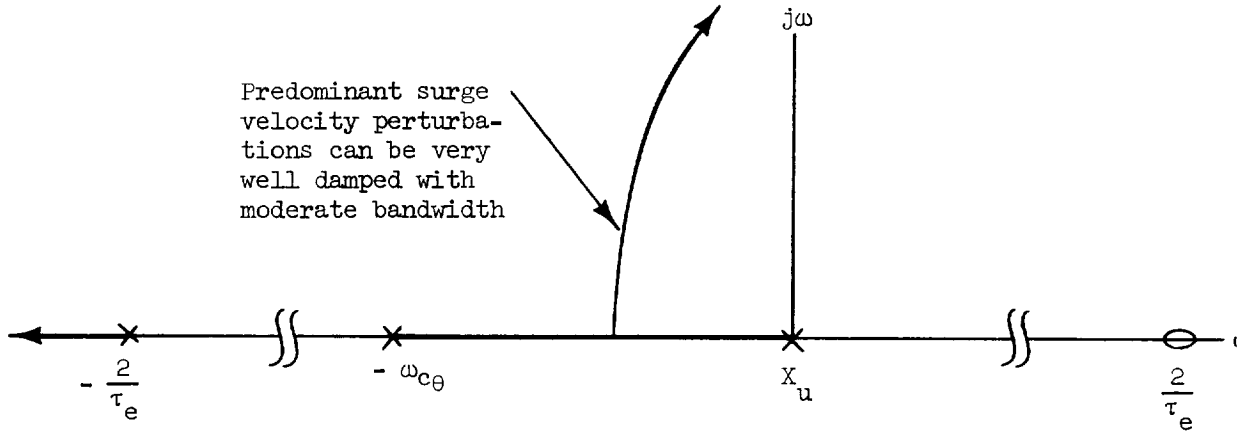

According to Ref. 11 the difference between K/s^2 and $K/s(s+1)$ or $K/s(s+2)$ controlled elements (hence position versus velocity) can amount to one or two points on the Cooper-Harper rating scale.

b. Sway Regulation. The above discussion of longitudinal control applies equally to lateral position and velocity control, since the respective controlled elements for both axes are essentially the same in hovering flight. Hence, lateral position,

$$\frac{y}{\varphi_c} \doteq \frac{g\left(1 - \frac{\tau_{e_\varphi}}{2} s\right)}{s^2\left(\frac{s}{\omega_{c_\varphi}} + 1\right)\left(1 + \frac{\tau_{e_\varphi}}{2} s\right)} \qquad \text{(IV-31)}$$

$$\left(\text{or } \frac{g\left(1 - \frac{\tau_{e_\varphi}}{2} s\right)}{s\left(s - Y_v\right)\left(\frac{s}{\omega_{c_\varphi}} + 1\right)\left(1 + \frac{\tau_{e_\varphi}}{2} s\right)} \text{ with } \psi \text{ regulation} \right) \qquad \text{(IV-32)}$$

is like K/s^2. Lateral velocity (also lateral flight path angle),

$$\frac{\dot{y}}{\varphi_c} = \frac{g\left(1 - \frac{\tau_{e_\varphi}}{2} s\right)}{s\left(\frac{s}{\omega_{c_\varphi}} + 1\right)\left(1 + \frac{\tau_{e_\varphi}}{2} s\right)} \qquad \text{(IV-33)}$$

is a $K/s(s+1)$ or $K/s(s+2)$ controlled element, and therefore somewhat easier to control than lateral position.

The x and y axes do not involve strong aerodynamic effects. Only X_u and Y_v appear explicitly, and they are both very small. For example X_u represents an inverse time constant for surge damping which is typically much less than the crossover frequency for x-axis regulation. Only in the z-axis does a significant vehicle aerodynamic effect appear.

c. Heave Regulation. From the simplified $\dot{z}/\delta_c$ transfer function we see that the heave damping, Z_w predominates, i.e.,

$$\frac{\dot{z}}{\delta_c} \doteq \frac{Z_{\delta_c}}{s - Z_w} \qquad \text{(IV-34)}$$

According to Ref. 14 the value of Z_w in hover is inversely proportional to the square root of disk loading*. As airspeed is increased heave damping grows as shown in Fig. IV-1 for various helicopter examples.

The essential features of the manual pure gain compensation heave loop are shown in the following root locus sketch for:

$$\frac{z}{\delta_c} \doteq \frac{Z_{\delta_c}}{s\left(s - Z_w\right)} \qquad \text{(IV-35)}$$

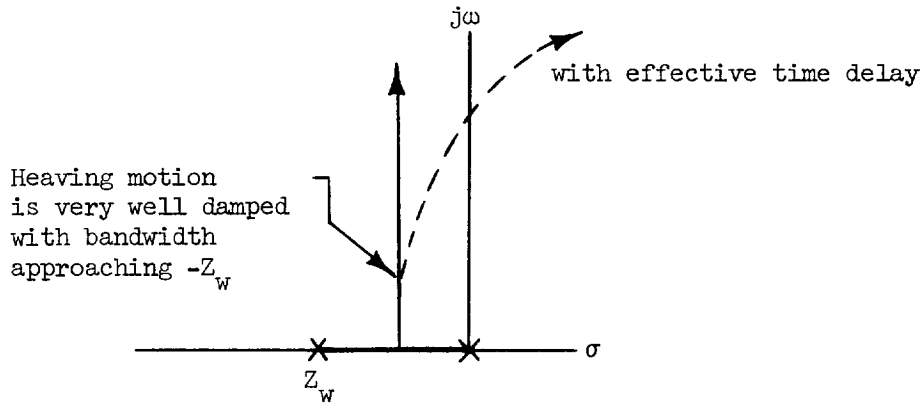

Note that the heave loop is primarily bandwidth-limited by Z_w. This implies that a somewhat higher crossover frequency is possible for vertical position regulation than for horizontal position in either the x or y axis.

---

* Ref. 14 indicates the $Z_w \doteq g\sqrt{\frac{\rho}{2\ W/A}}$

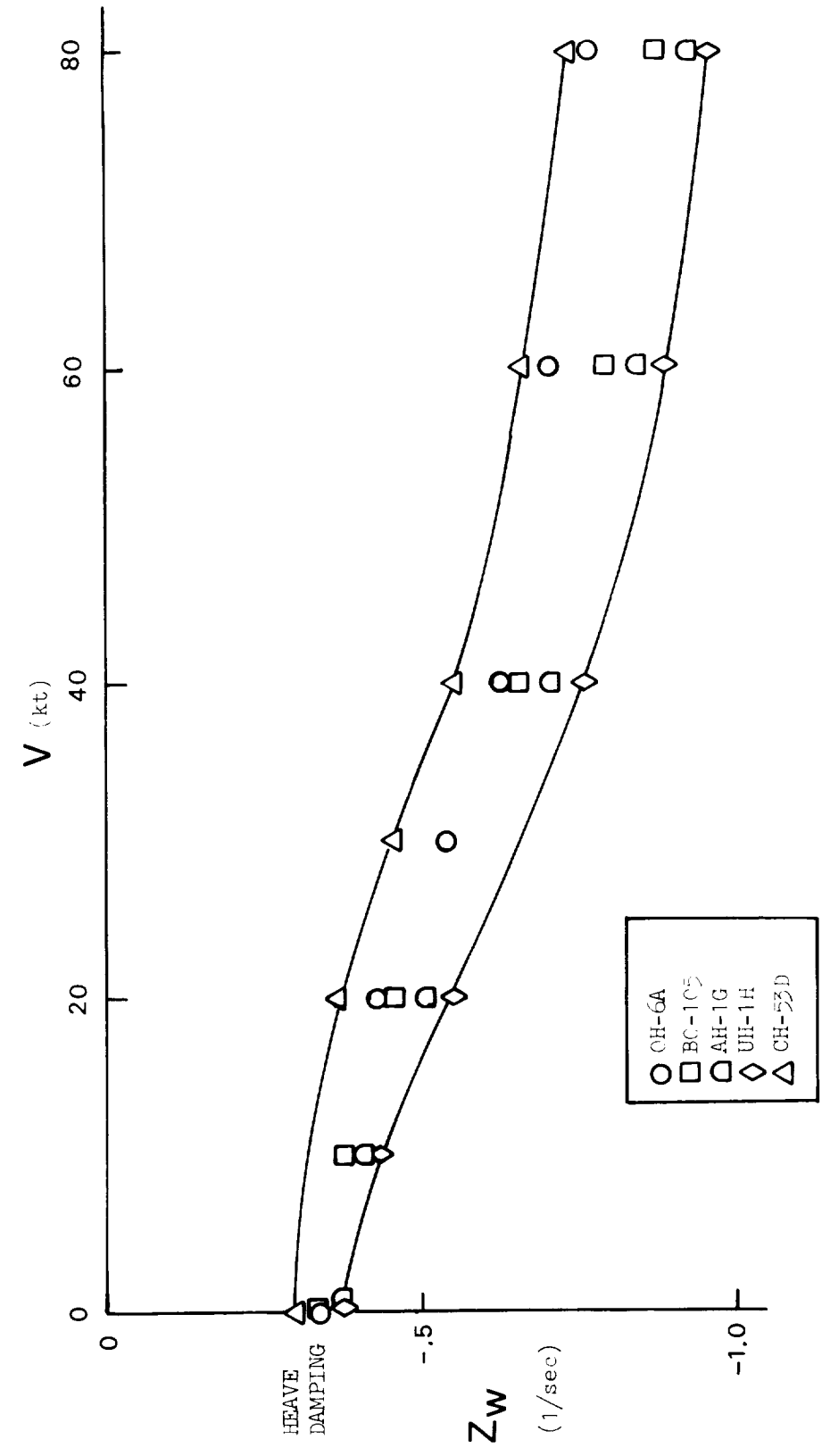

Figure IV-1. Variation in Heave Damping with Airspeed

d. Summary. The outer loop control features which have been exposed by the application of multiloop analysis and interpretation by simplified pilot-vehicle equations of motion are summarized by the following:

- Outer loop control characteristics can be effectively divorced from inner loop vehicle dynamics by use of appropriate numerator ratios.
- For x and y-axis regulation the controlled element is primarily like K/s^2 with the respective inner-loop crossover frequencies acting as effective control lags — aerodynamic effects (surge and sway damping) are neglible.
- For z-axis regulation the controlled element is bandwidth limited by heave damping, a characteristic determined mainly by disk loading and airspeed.

The helicopter examples considered demonstrate the relative invariance of outer loop control response which is suggested by the various generic approximations.

To a limited extent, outer loop regulation is aided by good inner loop control characteristics. For example, x-axis regulation benefits from a tight θ loop which reduces the surge control lag and which, in turn, depends upon easy manual regulation of θ or effective automatic regulation.

This indirect impact of inner loop control on x and y-axis outer loop control is the means by which current handling qualities specifications (MIL-H-8501A and MIL-F-83300) address outer loop control features. The weakness of purely aeroydnamic effects (surge and sway damping) appears to be acknowledged in the current specifications.

In the z-axis the very important aerodynamically-determined heave damping is subject to some variation due to disk loading. Unfortunately it too is not addressed by current handling specifications although it should be.

For operation in the NOE environment it may also be advisable to assess the need for explicit outer loop control requirements, namely, by specifying effective levels of augmented surge, sway, and heave damping. This could have the effect of imposing direct x, y, and z-force augmentation.

SECTION V

ATMOSPHERIC DISTURBANCES

A. INTRODUCTION

The purpose of this section is to take advantage of the foregoing method of closed-loop pilot-vehicle analysis in order to expose some properties of coupled longitudinal-lateral-directional helicopter dynamics. Two specific topics are considered. First, we shall explore the relative effects of individual gust components on each of the inner loop states. This will reveal the nature of interactions between the normally partitioned longitudinal and lateral-directional dynamics. The second topic we consider is related to outer loop states. In particular, we treat the interaction of the pilot-vehicle combination with terrain-dependent disturbances and find that helicopters are susceptible to the disturbances under certain conditions.

The compiled data in Volume One contain gust numerators for flight conditions at hover and 60 kt forward flight. In addressing the two topics just mentioned we shall demonstrate the use of the gust numerators given.

Note that the compiled data are broken down into translational and rotary gust components. That is, the effects of q_g and r_g components are not imbedded in the u_g and v_g transfer functions as is traditionally done (e.g., Ref. 1). Therefore, it is unnecessary to apply the frozen field gust assumption (Ref. 27). This allows the introduction of rotary gusts at zero airspeed without a singularity appearing in gust numerators.

Another feature of the compiled data is that gust components are taken with respect to an earth-fixed reference frame, not the usual body-fixed reference frame. This was believed to be of more general use in a low speed, low altitude environment especially where gusts can be terrain-dependent.

Presently there appears not to be a completely satisfactory gust model for nap-of-the-earth environment especially at or near hover. Nevertheless, the MIL-F-8785B turbulence model (Ref. 28) is frequently applied in this

flight regime, and we shall make limited use of it here for the purpose of estimating the size of various gust components and their relative frequency content. In addition, we shall make use of simple deterministic gust inputs such as step translational gusts and step rotary gusts. The main objective in doing so will be to establish the important gust components in each of the inner and outer loops for a given vehicle and flight condition.

B. INNER LOOP GUST RESPONSE

In the following pages we demonstrate the method for obtaining gust response relationships for the inner-loop regulated variables (pitch, roll, and yaw). This method is then applied to an example to investigate the gust sensitivity in low speed flight and especially the nature of axis cross coupling.

We begin by describing the insertion of pilot feedback loops, compute a set of gust transfer functions, then apply two kinds of gust inputs. In one case a random gust model is used to show rms motion excursions, in the other case step inputs are applied for each gust component. These results are correlated with stability derivatives to provide for a method of easily estimating significant gust components in each inner loop axis.

Computation of inner closed-loop gust responses can be accomplished by making the following assumptions:

1. Outer loops are open (no position or velocity regulation).
2. Off-axis inner loops are perfectly regulated (e.g., in considering θ response, φ and possibly ψ are constrained).
3. A realistic pilot loop closure is adopted for regulation of the axis in question (e.g., for θ response to gusts, assume a pure gain feedback of $\theta \longrightarrow \delta_B$ at a given crossover frequency).

These steps, each of which was justified in previous sections, permit an easy formulation of a gust transfer function from the data presented in Volume One.

Consider an example. The OH-6A open loop θ/u_g transfer function in the presence of perfect roll and yaw regulation and without outer loop regulation (Steps 1 and 2 above) yields:

$$\left.\frac{\theta}{u_g}\right|_{\varphi,\psi} \doteq \frac{N^{\theta\ \varphi\ \psi}_{u_g\delta_A\delta_p}}{N^{\varphi\ \psi}_{\delta_A\delta_p}} = \frac{0.0409(0)(0.022)(0.37)}{-3.27(0.022)(0.36)(1.85)[-.125;0.471]}$$

LD HD PD P

Note that this response is unstable. Clearly, any consideration of gust characteristics must account for the effects of the pilot to regulate divergent responses. This forces us to model the pilot's pitch attitude regulation. We shall assume that the effects of pilot compensation can be suitably modeled by a pure gain set for a 1 rad/sec crossover frequency. This type of pilot model retains the basic features of a human pilot, while keeping the model simple enough to use without ambiguity. Thus, the closed loop θ/u_g transfer function is:

$$\left.\frac{\theta}{u_g}\right|_{\substack{\varphi,\psi \\ \theta \rightarrow \delta_B}} = \frac{N^{\theta\ \varphi\ \psi}_{u_g\delta_A\delta_p} + Y_\theta\ N^{\theta\ \theta\ \varphi\ \psi}_{u_g\delta_p\delta_A\delta_p}}{N^{\varphi\ \psi}_{\delta_A\delta_p} + Y_\theta\ N^{\theta\ \varphi\ \psi}_{\delta_B\delta_A\delta_p}}$$

where $\left|\frac{Y_\theta\ N^{\theta\ \varphi\ \psi}_{\delta_B\delta_A\delta_p}}{N^{\varphi\ \psi}_{\delta_A\delta_p}}\right| = -1$ at $s = j\omega_{c_\theta} = j\ 1$ rad/sec

Table V-1 lists the gust transfer functions which result from assuming each primary axis to be closed by a pure gain at 1 rad/sec and the other two axes perfectly regulated.

By using the transfer functions of Table V-1 and the gust power spectral density models of MIL-F-8785B, we can compute the rms gust responses which are shown in Table V-2 and determine the predominant gust components in each axis.

TABLE V-1

SURVEY OF ATTITUDE RESPONSE DUE TO GUSTS
FOR OH-6A IN HOVER (CASE 4)

NUMERATORS	φ	θ	ψ
u_g	-.0042(0)(0.031)(0.39)	-.0125(0)(0.022)(0.37)	0.025(0)(0.022)(0.41)
v_g	0.047(0)(0.011)(0.33)	0.0017(0)[0.81;0.094]	-.007(0)[0.68;0.069]
w_g	0.0021(0)(0.011)(-.33)	0.0063(0)(0.012)(0.031)	-.031(0)(0.012)(0.026)
p_g	4.8(0.011)(0.026)(0.34)	-.52(0.001)(0.023)(0.34)	0.32(0.024)(-.024)(0.33)
q_g	1.58(0.34)[0.90;0.014]	1.72(0.015)(0.023)(0.34)	0.087(0.021)(-.23)(0.34)
r_g	0.0196(0.016)(-.045)(0.62)	-.16(0.28)[0.99;0.022]	0.80(0.016)(0.021)(0.28)
DENOMINATORS			
(open loop) Δ	(0.011)(0.34)(4.9)[-.03;0.56] SD HD R PL	(0.022)(0.36)(1.85)[-.125;0.47] LD HD PD P	(0)(0.016)(0.022)(0.25)(0.89) SD LD HD YD
	$\varphi \rightarrow \delta_A$	$\theta \rightarrow \delta_B$	$\psi \rightarrow \delta_p$
(closed loop) Δ'	(0.011)(0.33)(4.1)[0.63;0.63] SD HD R	(0.022)[0.95;0.36][0.65;1.1] LD	(0.011)(0.022)(0.35)[0.35;1.1] SD LD HD

TABLE V-2

RMS GUST RESPONSE

(MIL-F-8785B Dryden model applied to OH-6A
in hover at 40 ft altitude, σ_{u_g} = 4.5 ft/sec
and mean wind 10 ft/sec)

COMPONENT	σ_φ (deg)	σ_θ (deg)	σ_ψ (deg)
u_g	0.8	0.65	4.9
v_g	1.0	0.07	0.6
w_g	0.05	0.5	1.2
p_g	2.0	0.6	0.6
q_g	0.5	1.3	0.1
r_g	0.02	0.2	1.9

Considering the translational gusts first, we see that θ is most influenced by u_g and w_g; φ by v_g; and ψ by u_g. The only real surprise in this data is the large effect of u_g on ψ. For the rotary gusts, we see that p_g has a strong effect on φ, θ, and ψ.

As an alternative to examining inner loop gust sensitivity by applying random gust inputs, a systematic application of deterministic gust inputs was also considered. The same example was used, i.e., the OH-6A in hover flight condition.

The procedure for viewing the response to deterministic gust inputs was to consider one inner loop axis at a time and to apply a unit step for each of the six gust components. For example, in the roll axis, pitch and yaw were assumed to be perfectly regulated and a 1 rad/sec crossover frequency was used for roll loop regulation. Time histories were then generated for the closed-loop φ response resulting from a 1 kt step input of u_g, v_g, and w_g, then a 1 kt per rotor diameter step in p_g, q_g, and r_g. The same procedure was then applied to the pitch axis and finally to the yaw axis. Results are plotted in Fig. V-1.

A third and much simpler way of estimating the significant gust components in each axis is to compare directly the appropriate stability derivatives. For example, the relative effect of u_g, v_g, and w_g on pitch attitude should be visible from the relative values of M_u, M_v, and M_w, respectively.

The danger in using stability derivatives in the manner suggested is that axis transformations (body axis to earth axis) are not strictly accounted for, and the effects of predominant response modes are neglected. Nevertheless, reasonably good agreement with the two previous methods is obtained. Table V-3 shows the relative magnitudes of gust response computed using random gusts, deterministic (step) gusts, and stability derivative ratios. Thus, any one of three methods could be used to determine the main gust component contributions for each axis.

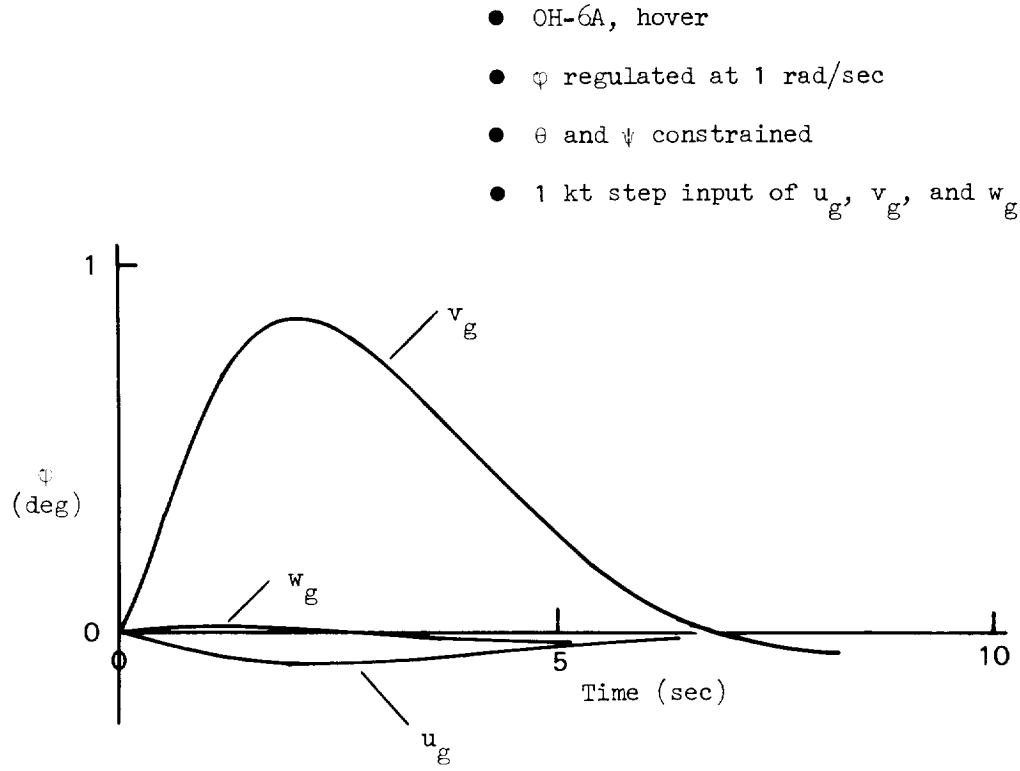

a. φ response to translational gust components

Figure V-1. Attitude Response to Step Gust Inputs

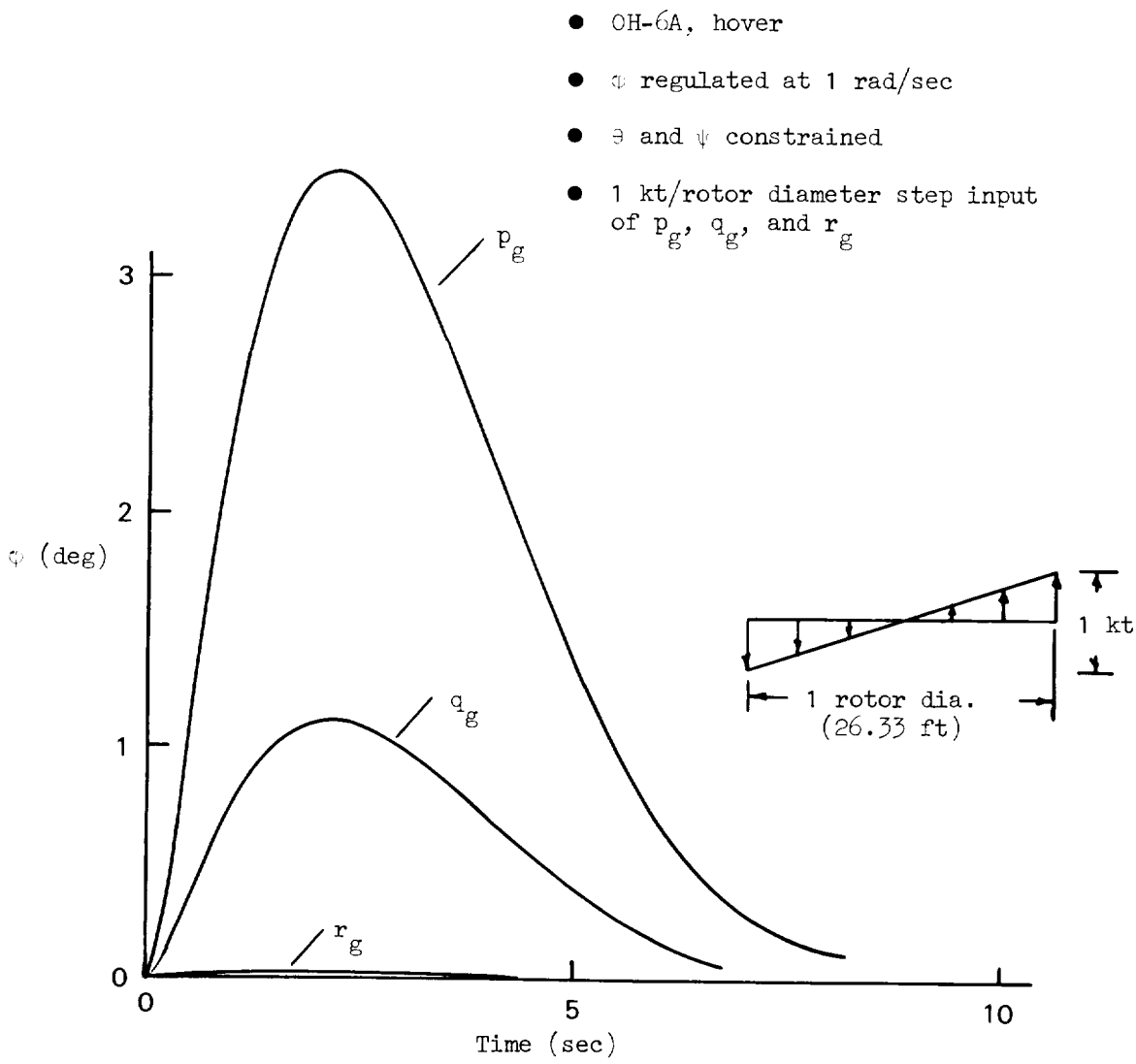

b. φ response to rotary gust components

Figure V-1 (Continued)

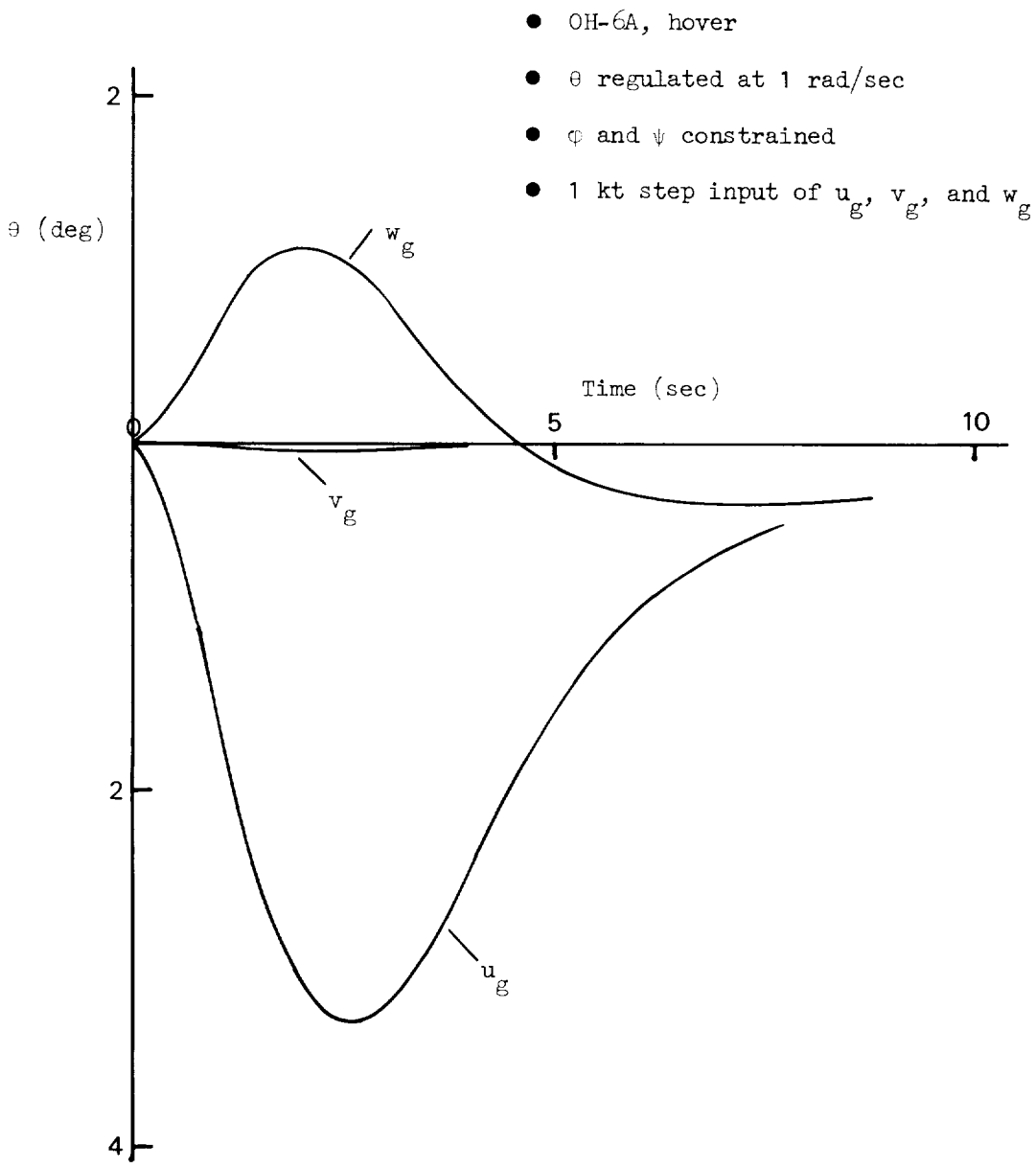

c. θ response to translational gust components

Figure V-1 (Continued)

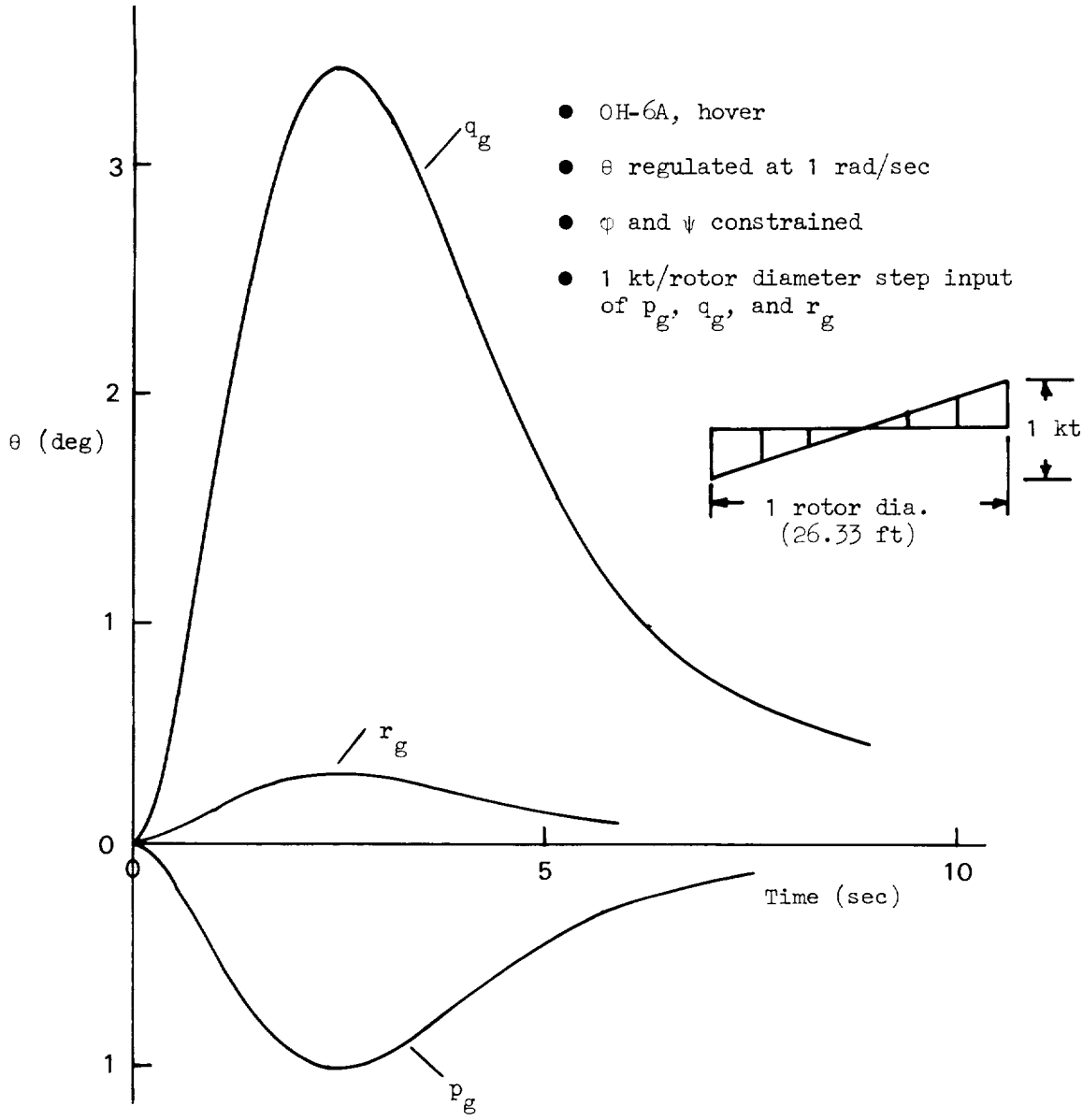

d. θ response to rotary gust components

Figure V-1 (Continued)

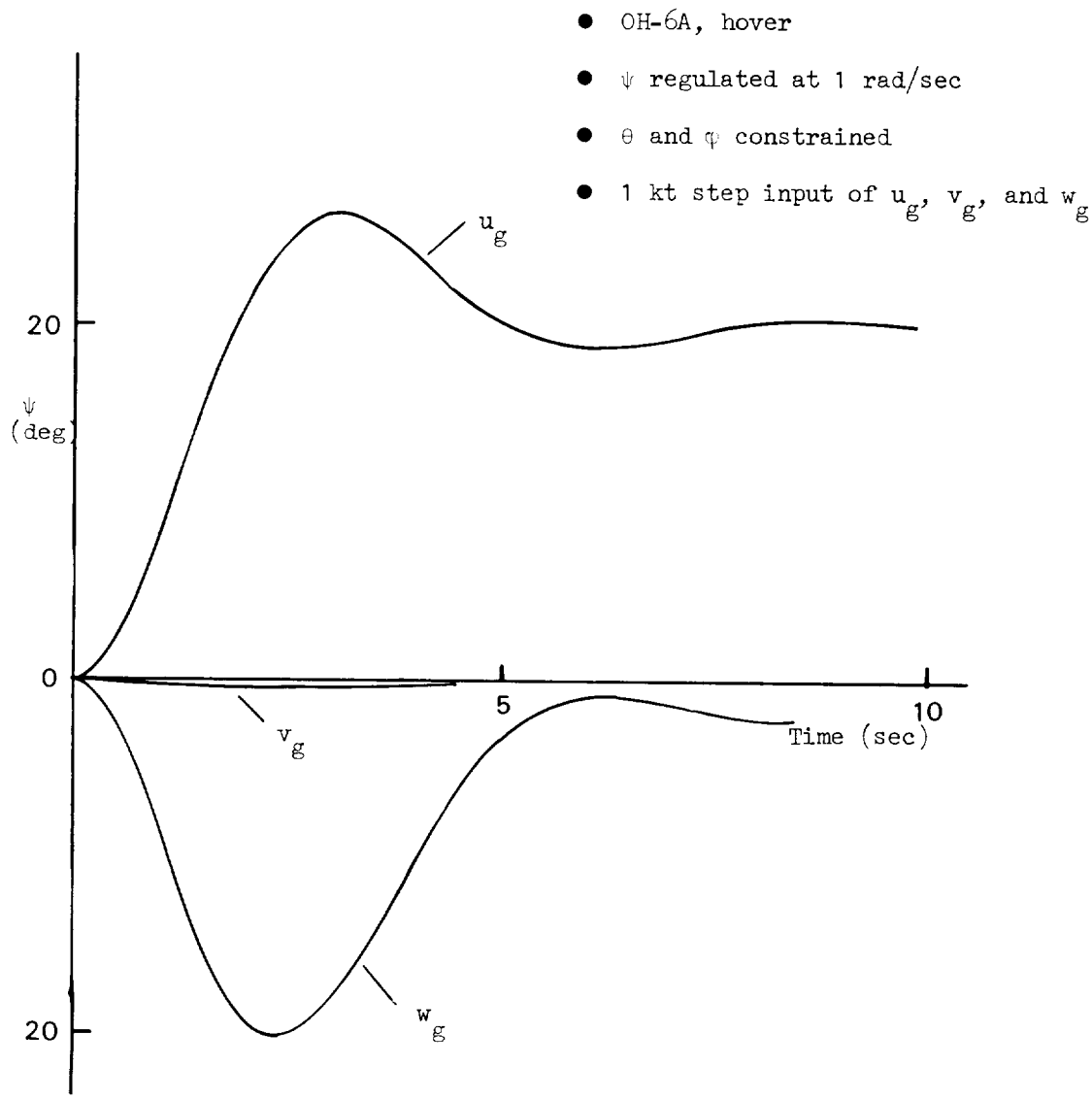

e. ψ response to translational gust components

Figure V-1 (Continued)

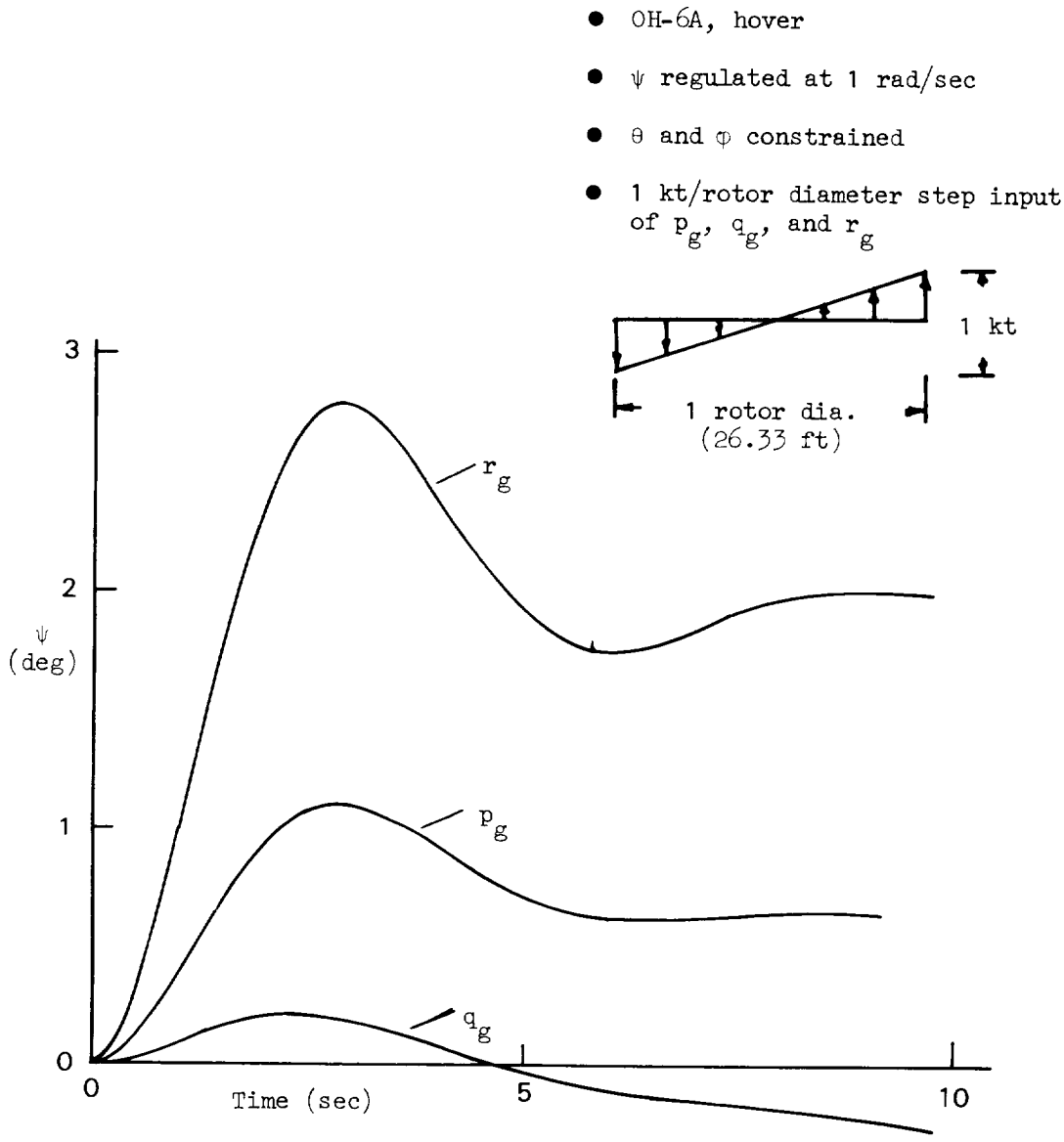

f. ψ response to rotary gust components

Figure V-1 (Concluded)

TABLE V-3

RELATIVE EFFECT OF INDIVIDUAL GUST COMPONENTS
FOR RANDOM GUSTS/DETERMINISTIC (STEP) GUSTS/AND STABILITY DERIVATIVES
(OH-6A, HOVER)

	φ	θ	ψ
u_g	0.1/—/—*	1/1/1	1/1/1
v_g	1/1/1	0.1/—/0.2	0.1/—/0.1
w_g	—/—/—	0.7/0.3/0.5	0.3/0.8/1.2
p_g	1/1/1	0.4/0.3/0.2	0.3/0.4/1.2
q_g	0.2/0.3/0.2	1/1/1	0.1/0.1/0.2
r_g	—/—/0.1	0.2/0.1/—	1/1/1

* Each element shows the magnitude of motion for one gust component relative to the predominant gust component. The order of numerical entries in each element, set off by slant lines, is:

Relative rms from MIL-F-8785B model / Relative peak due to step gust / Relative moment from stability derivatives corresponding to each element

For the specific example considered, namely the OH-6A in hover, the response to on-diagonal gust components is direct as expected. Significant off-diagonal results include:

- Roll response due to q_g
- Pitch response due to p_g
- Yaw response due to u_g, w_g, and p_g.

In general, any given vehicle would require a survey to determine important gust components for an individual axis. Based on the foregoing, however, such a survey could easily be conducted by a direct comparison of stability derivatives with reasonable assurance of success.

C. OUTER LOOP GUST RESPONSE

In order to observe the effects of atmospheric disturbances on outer loop states it is necessary to stabilize inner loops suitably. And, in doing so we can develop simplified expressions for outer loop gust transfer functions in a manner similar to that used for expressing outer loop control response.

To illustrate the general approach for obtaining the essential outer loop gust response, consider heave motion due to a horizontal gust component with pitch attitude regulation:

$$\left.\frac{\dot{z}}{u_g}\right|_{\theta \rightarrow \delta_B} = \frac{N^{\dot{z}}_{u_g} + Y_\theta N^{\theta}_{\delta_B} N^{\dot{z}}_{u_g}}{\Delta + Y_\theta N^{\theta}_{\delta_B}}$$

$$= \frac{N^{\theta}_{\delta_B} N^{\dot{z}}_{u_g}}{N^{\theta}_{\delta_B}} \frac{\left(\frac{Y_\theta N^{\theta}_{\delta_B}}{\Delta} + \frac{1}{1 - \frac{N^{\theta}_{u_g} N^{\dot{z}}_{\delta_B}}{N^{\theta}_{\delta_B} N^{\dot{z}}_{u_g}}} \right)}{\left(\frac{Y_\theta N^{\theta}_{\delta_B}}{\Delta} + 1 \right)}$$

or, with the addition of φ and ψ regulation:

$$\left.\frac{\dot{z}}{u_g}\right|_{\substack{\varphi,\psi \\ \theta \rightarrow \delta_B}} \doteq \frac{N^{\dot{z}\ \theta\ \varphi}_{u_g \delta_B \delta_A}\Big|^{\psi}_{\delta_p}}{N^{\theta\ \varphi}_{\delta_B \delta_A}\Big|^{\psi}_{\delta_p}} \left(\frac{\dfrac{Y_\theta N^{\theta\ \varphi}_{\delta_B \delta_A}\Big|^{\psi}_{\delta_p}}{N^{\varphi}_{\delta_A}\Big|^{\psi}_{\delta_p}}}{\left(\dfrac{Y_\theta N^{\theta\ \varphi}_{\delta_B \delta_A}\Big|^{\psi}_{\delta_p}}{N^{\varphi}_{\delta_A}\Big|^{\psi}_{\delta_p}} + 1\right)} \right) \left(\frac{1}{1 - \dfrac{N^{\theta\ \varphi}_{u_g \delta_A}\Big|^{\psi}_{\delta_p}\ N^{\dot{z}\ \varphi}_{\delta_B \delta_A}\Big|^{\psi}_{\delta_p}}{N^{\theta\ \varphi}_{\delta_B \delta_A}\Big|^{\psi}_{\delta_p}\ N^{\dot{z}\ \varphi}_{u_g \delta_A}\Big|^{\psi}_{\delta_p}}} \right)^{*}$$

$$\doteq \frac{N^{\dot{z}\ \theta\ \varphi}_{u_g \delta_B \delta_A}\Big|^{\psi}_{\delta_p}}{N^{\theta\ \varphi}_{\delta_B \delta_A}\Big|^{\psi}_{\delta_p}}$$

$$\text{if} \quad N^{\theta\ \varphi}_{u_g \delta_A}\Big|^{\psi}_{\delta_p}\ N^{\dot{z}\ \varphi}_{\delta_B \delta_A}\Big|^{\psi}_{\delta_p} \ll N^{\theta\ \varphi}_{\delta_B \delta_A}\Big|^{\psi}_{\delta_p}\ N^{\dot{z}\ \varphi}_{u_g \delta_A}\Big|^{\psi}_{\delta_p}$$

This applies similarly to $\dot{z}/w_g$ if we replace u_g with w_g numerators. Further, $\dot{x}/u_g$, $\dot{x}/w_g$, and $\dot{y}/v_g$ transfer function relationships can also be so inferred and are listed in Appendix A.

It is advantageous to express the simplified longitudinal and lateral equations of motion to reveal generic properties and to compare with the complete quasi-static six-degree-of-freedom transfer functions. Following the forms used in Section IV, we can write:

---

* If yaw regulation is not involved, the vertical dashed line partitions the φ-constrained numerators from the ψ-constrained numerators.

Longitudinal-Vertical Equations of Perturbed Motion

$$\begin{bmatrix} s-X_u & \cancel{-X_w} \\ -Z_u & s-Z_w \end{bmatrix} \begin{bmatrix} \dot{x} \\ \dot{z} \end{bmatrix} \doteq \begin{bmatrix} -X_u & \cancel{-X_w} \\ -Z_u & -Z_w \end{bmatrix} \begin{bmatrix} u_g \\ w_g \end{bmatrix}$$

$\doteq 0$ $\doteq 0$

or

$$\Delta \doteq \begin{vmatrix} s-X_u & \cancel{-X_w} \\ -Z_u & s-Z_w \end{vmatrix} = \left(s-X_u\right)\left(s-Z_w\right)$$

$\doteq 0$

$$N^{\dot{x}}_{u_g} \doteq \begin{vmatrix} -X_u & \cancel{-X_w} \\ -Z_u & s-Z_w \end{vmatrix} = -X_u\left(s-Z_w\right)$$

$$N^{\dot{x}}_{w_g} \doteq \begin{vmatrix} 0 & 0 \\ -Z_w & s-Z_w \end{vmatrix} = 0$$

$$N^{\dot{z}}_{u_g} \doteq \begin{vmatrix} s-X_u & -X_u \\ -Z_u & -Z_u \end{vmatrix} \doteq -Z_u\, s$$

$$N^{\dot{z}}_{w_g} \doteq \begin{vmatrix} s-X_u & 0 \\ -Z_u & -Z_w \end{vmatrix} \doteq -Z_w\left(s-X_u\right)$$

and,

$$\left.\frac{\dot{x}}{u_g}\right|_{\theta,\varphi,\psi} \doteq \frac{-X_u}{s - X_u} \doteq \frac{N^{\dot{x}\ \theta\ \varphi}_{u_g\delta_B\delta_A}\Big|^{\psi}_{\delta_p}}{N^{\theta\ \varphi}_{\delta_B\delta_A}\Big|^{\psi}_{\delta_p}}$$

$$\left.\frac{\dot{x}}{w_g}\right|_{\theta,\varphi,\psi} \doteq 0 \doteq \frac{N^{\dot{x}\ \theta\ \varphi}_{w_g\delta_B\delta_A}\Big|^{\psi}_{\delta_p}}{N^{\theta\ \varphi}_{\delta_B\delta_A}\Big|^{\psi}_{\delta_p}}$$

$$\left.\frac{\dot{z}}{u_g}\right|_{\theta,\varphi,\psi} \doteq \frac{-Z_u\ s}{\left(s - X_u\right)\left(s - Z_w\right)} \doteq \frac{N^{\dot{z}\ \theta\ \varphi}_{u_g\delta_B\delta_A}\Big|^{\psi}_{\delta_p}}{N^{\theta\ \varphi}_{\delta_B\delta_A}\Big|^{\psi}_{\delta_p}}$$

$$\left.\frac{\dot{z}}{w_g}\right|_{\theta,\varphi,\psi} \doteq \frac{-Z_w}{\left(s - Z_w\right)} \doteq \frac{N^{\dot{z}\ \theta\ \varphi}_{w_g\delta_B\delta_A}\Big|^{\psi}_{\delta_p}}{N^{\theta\ \varphi}_{\delta_B\delta_A}\Big|^{\psi}_{\delta_p}}$$

Lateral-Directional Equations of Perturbed Motion

$$\begin{bmatrix} s-Y_v & Y_\beta \\ -N_v & s^2-N'_r s+N'_\beta \end{bmatrix}\begin{bmatrix} \dot{y} \\ \psi \end{bmatrix} = \begin{bmatrix} -Y_v \\ -N_v \end{bmatrix}\begin{bmatrix} v_g \end{bmatrix}$$

$$\Delta \doteq s\left[s^2 - N'_r\ s + N'_\beta\right]$$

$$N^{\dot{y}}_{v_g} \doteq \begin{vmatrix} -Y_v & Y_\beta \\ -N_v & s^2 - N'_r s + N'_\beta \end{vmatrix} = -Y_v \, s \left(s - N'_r \right)$$

and

$$\frac{\dot{y}}{v_g} \doteq \frac{-Y_v\left(s - N'_r\right)}{\left[s^2 - N'_r \, s + N'_\beta\right]} \doteq \frac{N^{\dot{y}}_{u_g} \Big|^{\varphi \; \theta}_{\delta_A \delta_B} \Big|^{\psi}_{\delta_p}}{N^{\varphi \; \theta}_{\delta_A \delta_B} \Big|^{\psi}_{\delta_p}}$$

Based on the relative magnitudes of predominant stability derivatives, the two major outer loop disturbance transfer functions in the above list are:

$$\frac{\dot{z}}{u_g} \quad \text{and} \quad \frac{\dot{z}}{w_g}$$

The first of these is of particular interest because of the relative importance of height regulation and the likelihood of strong u_g gust or shear components when near the ground. In fact, a significant degree of $\dot{z}/u_g$ sensitivity occurs in a critical range of airspeeds which can contribute to an adverse pilot-vehicle-gust interaction.

Reference 29 describes a hypothetical situation for CTOL aircraft flying in an altitude-dependent wind shear where a significant level of destabilization can occur in closed-loop flight path response modes. The relationships are shown in block diagram form in Fig. V-2. A direct analogy can be made for a helicopter operating at low altitudes where a terrain-dependent wind shear can occur from the wind shadowing effect of trees or other obstacles.

A simple example of pilot-vehicle-gust interaction is shown in Fig. V-3. We consider a helicopter hovering in a spatially-dependent wind consisting of a linear shear with altitude. If the pilot is simply regulating his height,

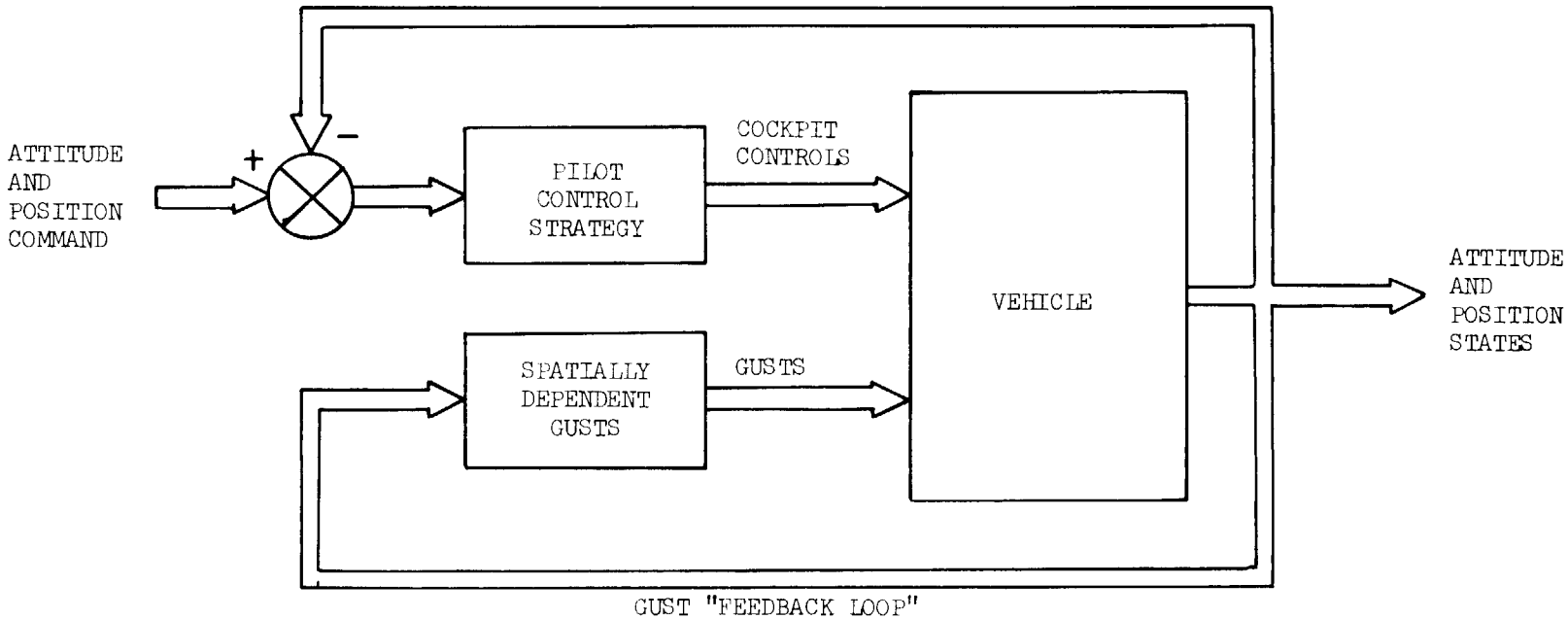

Figure V-2. Closed Loop Aspect of Spatially-Dependent Gusts

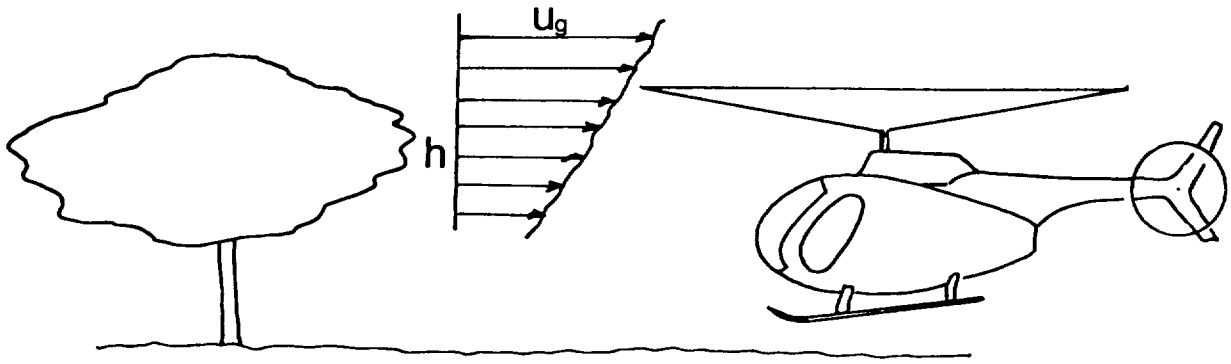

BLOCK DIAGRAM

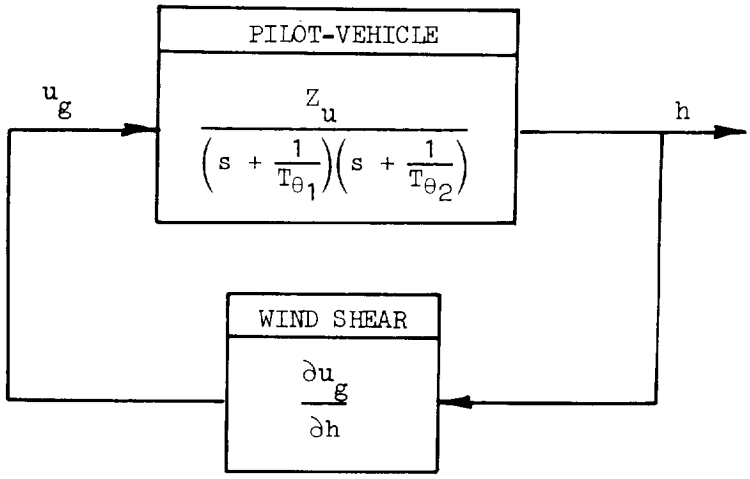

ROOT LOCUS

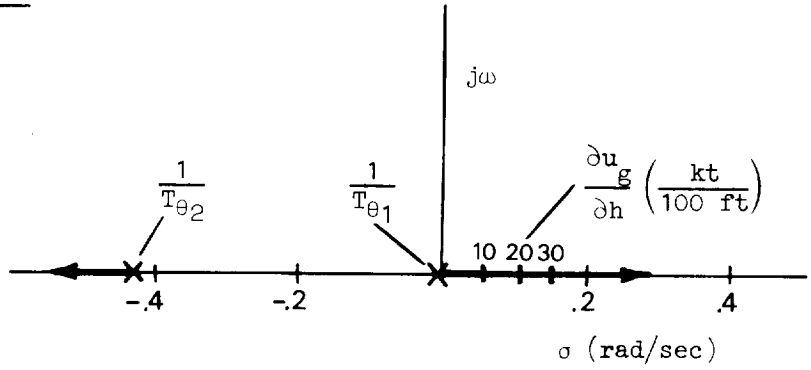

Figure V-3. Hover in a Spatially-Dependent Wind

$$\frac{h}{u_g} = \frac{Z_u}{\left(s + \frac{1}{T_{\theta_1}}\right)\left(s + \frac{1}{T_{\theta_2}}\right)}$$

where $1/T_{\theta_1}$ and $1/T_{\theta_2}$ are the closed loop pilot-vehicle modes dominant in surge and heave, respectively.

The wind shear can act to modify the pilot-vehicle stability as shown in the block diagram and root locus plot of Fig. V-3. Note that the stability derivative Z_u combines with the wind shear gradient $\partial u_g/\partial h$ to produce a divergence — a feature which can be directly associated with additional pilot workload.

Several factors make the above example interesting:

- The value of Z_u is most critical for helicopters (approximately -0.2/sec in magnitude) at airspeeds of 20 to 30 kt as shown in Fig. V-4
- The critical shear corresponds to a headwind decreasing with altitude
- A shear such as this can be found in the altitude segment between the ground and the top of a canopy formed by trees as indicated by wind tunnel velocity profile measurements from Ref. 30.

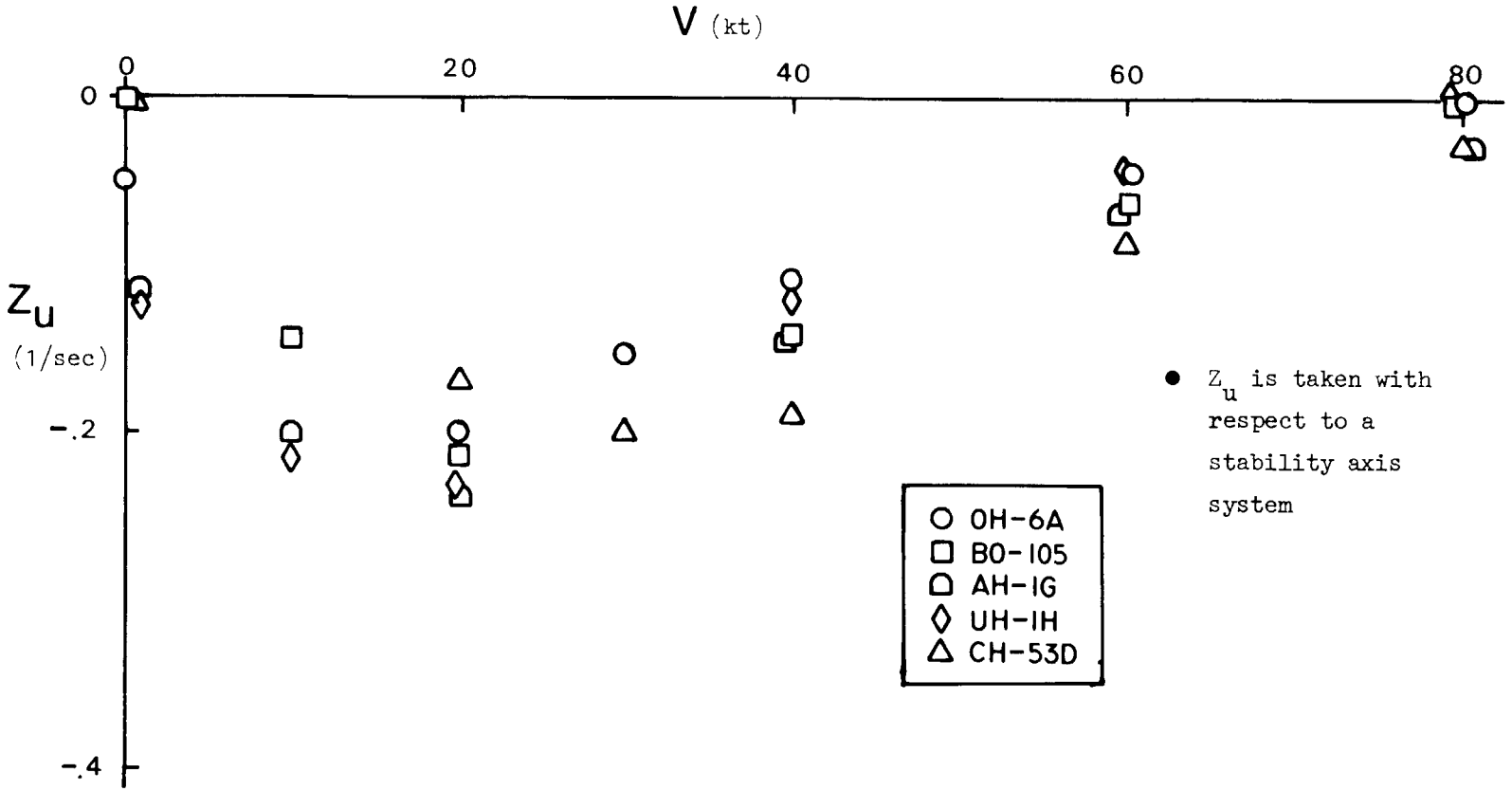

Figure V-4. Variation of Z_u with Airspeed

SECTION VI

AUGMENTATION SYSTEMS

Of the five vehicles included in the data compilation in Volume One, three employ forms of stability and control augmentation systems. The examples involved span the range of complexity from a simple mechanical, two-axis stability augmentor (UH-1H stabilizer bar) to a three-axis eletronic rate and attitude feedback with command augmentation and turn coordination (CH-53D). A system having an intermediate degree of complexity involves angular rate damping about three axes with command augmentation (AH-1G). In the following pages we shall describe each of the three examples in order of their increasing complexity. Then, we shall briefly examine how each augmentation system example influences the basic handling qualities by considering the inner loop and outer loop relationships as described previously in Sections III and IV.

A. SYSTEMS DESCRIPTIONS

Each of the three augmentation systems is described in Volume One by a system block diagram and each was implemented in the equations of motion accordingly. Some additional discussion of important features, however, will aid in our examination of resulting handling qualities.

1. UH-1H Stabilizer Bar

The stabilizer bar employed by the UH-1H is a mechanical stability augmentor which operates at all times. As described in Ref. 17 the Bell stabilizer bar is pivoted to the rotor shaft and coupled with a viscous damper. Gyroscopic, inertial, and damping torques are involved, but only the last two directly determine feedback angles to the main rotor feathering controls.

A derivation of stabilizer bar equations of motion is given in Table VI-1. From this, it is apparent that the stabilizer bar senses pitch and roll rates relative to the main rotor shaft axis, and that by gearing the

TABLE VI-1. STABILIZER BAR DYNAMICS

The UH-1H stabilizer bar equations of motion can be derived from the following diagram:

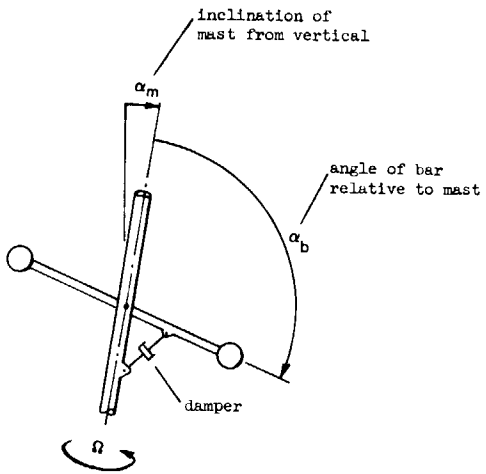

Thus the basic equation of motion in a mast-fixed reference frame is:

$$\ddot{\alpha}_b + \frac{2}{T}\dot{\alpha}_b + \Omega\ \alpha_b = \ddot{\alpha}_m + \Omega\ \alpha_m \qquad \text{(VI-1)}$$

where $\alpha_b \triangleq$ bar angle with respect to the mast

$\alpha_m \triangleq$ mast angle with respect to vertical

$2/T \triangleq$ ratio of damping torque to moment of inertia

$\Omega \triangleq$ mast rotation rate

Resolution of α_b and α_m in a non-rotating reference frame is:

$$\alpha_b = -c \cos \Omega t + d \sin \Omega t \qquad \text{(VI-2)}$$

$$\alpha_m = -\theta_m \cos \Omega t + \varphi_m \sin \Omega t \qquad \text{(VI-3)}$$

where $c \triangleq$ bar pitch tip path plane with respect to the mast

$d \triangleq$ bar roll tip path plane with respect to the mast

$\theta_m \triangleq$ mast pitch angle

$\varphi_m \triangleq$ mast roll angle

TABLE VI-1 (Concluded)

Decoupling of the basic equation of motion (substitution of Eqs. VI-2 and VI-3 and their derivatives into Eq. VI-1):

$$-\ddot{c} - \frac{2}{T}\dot{c} + 2\Omega\dot{d} + \frac{2}{T}\Omega d = -\ddot{\theta}_m + 2\Omega\dot{\varphi}_m$$

and $$2\Omega\dot{c} + \frac{2}{T}\Omega c + \ddot{d} + \frac{2}{T}d = 2\Omega\dot{\theta}_m + \ddot{\varphi}_m$$

or rearranging in matrix form:

$$\begin{bmatrix} s\left(s + \frac{2}{T}\right) & -2\Omega\left(s + \frac{1}{T}\right) \\ s\Omega\left(s + \frac{1}{T}\right) & s\left(s + \frac{2}{T}\right) \end{bmatrix} \begin{matrix} c \\ d \end{matrix} = \begin{bmatrix} s & -2\Omega \\ 2\Omega & s \end{bmatrix} \begin{matrix} q_m \\ p_m \end{matrix}$$

where $q_m \triangleq$ mast pitch rate, i.e., $\dot{\theta}_m$

$p_m \triangleq$ mast roll rate, i.e., $\dot{\varphi}_m$

Solving for transfer functions:

$$\Delta = s^2\left(s + \frac{2}{T}\right)^2 + 4\Omega^2\left(s + \frac{1}{T}\right)^2 \doteq \left(s + \frac{1}{T}\right)^2\left[s^2 + \frac{2}{T}s + 4\Omega^2\right]$$

$$N^c_{q_m} = \det\begin{bmatrix} s & -2\Omega\left(s + \frac{1}{T}\right) \\ 2\Omega & s\left(s + \frac{2}{T}\right) \end{bmatrix} \doteq \left(s + \frac{1}{T}\right)\left[s^2 + \frac{1}{T}s + 4\Omega^2\right]$$

$$N^c_{p_m} = \det\begin{bmatrix} -2\Omega & -2\Omega\left(s + \frac{1}{T}\right) \\ s & s\left(s + \frac{1}{T}\right) \end{bmatrix} \doteq \frac{-2\Omega s}{T}$$

For the lateral tip path plane angle, d, the transfer functions are symmetric. Thus:

$$\frac{c}{q_m} = \frac{d}{p_m} \doteq \frac{1}{\left(\frac{1}{T}\right)} \frac{\left[\frac{1}{4\Omega T},\ 2\Omega\right]}{\left[\frac{1}{2\Omega T},\ 2\Omega\right]} \doteq \frac{1}{\left(\frac{1}{T}\right)}$$

$$\frac{c}{p_m} = \frac{d}{q_m} \doteq \frac{-\frac{2\Omega}{T}(0)}{\left(\frac{1}{T}\right)^2\left[\frac{1}{2\Omega T},\ 2\Omega\right]} \doteq 0$$

For the UH-1H, 0.16 deg of cyclic control results in the same blade feathering angle as 1 deg of stabilizer bar angle, and the damping time constant is 3 sec. Hence, the effective

$$\frac{\Delta B_1}{q_m} = \frac{0.16}{s + 0.333}$$

and $$\frac{\Delta A_1}{p_m} = \frac{0.16}{s + 0.333}$$

stabilizer bar directly to main rotor feathering controls, rate feedback can be effected. Finally, the lag in rate feedback can be adjusted by the time constant in viscous damping between the main rotor shaft and stabilizer bar.

The stabilizer bar equations of motion involve high frequency dynamics and some pitch-roll cross coupling. These effects, however, are clearly negligible within the constraints of this study. For the normal 324 rpm of the UH-1H rotor, the natural frequency of the oscillatory mode occurs far outside our range of interest at 69 rad/sec. The cross coupling is small compared to the direct feedback effect as shown by the following stabilizer bar tip path plane modal response ratio:

$$\frac{\frac{d}{q_m}}{\frac{c}{q_m}} \doteq \frac{-2\,\Omega\,s}{T\left(s + \frac{1}{T}\right)4\,\Omega^2} \doteq \frac{-.015\,s}{(3\,s + 1)} \doteq 0 \qquad \text{(VI-4)}$$

In analyzing the effects of the stabilizer bar feedback it is convenient to take advantage of closed loop analysis methods, especially where high order equations of motion are involved. For example, to examine the effects of the pitch augmentation loop ($q_m \longrightarrow B_{1_s}$) on the pilot's pitch response we shall use the following:

$$\left.\frac{\theta}{\delta_B}\right|_{\text{BAR ON}} \doteq \frac{N^{\theta}_{\delta_B} N^{\varphi}_{\delta_A} N^{\psi}_{\delta_p} + Y_{q_m} N^{\theta}_{\delta_B} N^{q_m}_{B_{1_s}} N^{\varphi}_{\delta_A} N^{\psi}_{\delta_p}}{N^{\varphi}_{\delta_A} N^{\psi}_{\delta_p} + Y_{q_m} N^{q_m}_{B_{1_s}} N^{\varphi}_{\delta_A} N^{\psi}_{\delta_p}} \qquad \text{(VI-5)}$$

where Y_{q_m} is the stabilizer bar feedback compensation, $\Delta B_1/q_m$. This minimizes complication of lateral-directional effects. One further simplifying step is to recognize that $q_m = \dot{\theta}$ and $B_{1_s} = K\,\delta_B$. Hence:

$$N^{\theta\ q_m}_{\delta_B B1_s}\ \begin{matrix}\cdots\\ \cdots\end{matrix} = 0 \qquad \text{(VI-6)}$$

and $$N^{q_m\ \varphi}_{B1_s \delta_A}\ \begin{matrix}\cdots\\ \cdots\end{matrix} = K_s N^{\theta\ \varphi}_{\delta_B \delta_A}\ \begin{matrix}\cdots\\ \cdots\end{matrix}$$

In other words, only the θ/δ_B denominator is modified, and we can make direct use of the tabulated transfer function data in Volume One. The roll axis is analogous.

The effect of the stabilizer bar can be demonstrated by considering each response in hover. According to the relationships stated above in Eq. VI-6, Eq. VI-5 becomes:

$$\frac{\theta}{\delta_B} \doteq \frac{N^{\theta\ \varphi\ \psi}_{\delta_B \delta_A \delta_p} + Y_{q_m} \cancelto{=0}{N^{\theta\ \theta}_{\delta_B B1_s}} \cdots}{N^{\varphi\ \psi}_{\delta_A \delta_p} + Y_{q_m} K_s N^{\theta\ \varphi\ \psi}_{\delta_B \delta_A \delta_p}} \qquad \text{(VI-7)}$$

Thus, the θ/δ_B numerator is unchanged, but the denominator does vary. The following root locus shows how the denominator is modified by the stabilizer bar:

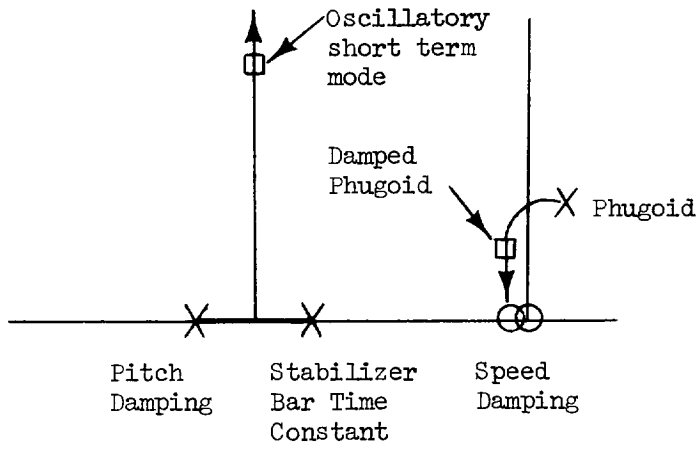

The phugoid is stabilized by the washout and speed damping zeros, the pitch damping mode couples with the stabilizer bar pole and becomes oscillatory. This general trend occurs in both pitch and roll axes and for hover and forward flight conditions. We shall consider specific results shortly in Section VI.B.

The basic feedback loops involved in the pitch and roll axes can be rearranged from Volume One to the following forms shown in Fig. VI-1. The stabilizer bar provides a lagged angular rate feedback, or alternatively, a washed-out attitude feedback. Because of the relatively large time constant (3 sec) the latter interpretation is perhaps more meaningful.

2. AH-1G SCAS

The AH-1G SCAS involves angular rate feedback and control feedforward about all three axes. The nature of compensation, however, varies among the axes.

a. Pitch Axis. The pitch axis involves feedback and feedforward loops as shown in Volume One. The feedback consists of a pitch rate-to-longitudinal cyclic path which is compensated to emphasize the mid-frequency region near 0.4 rad/sec, i.e.,

$$\frac{B_{1_s}}{q} \doteq K \frac{(0.22)(0.74)}{(0.42)(0.43)} \qquad \text{(VI-8)}$$

Hence, the system augments the basic vehicle pitch damping which, in hover,

- Increases the frequency of the pitch damping mode
- Decreases the frequency of the phugoid mode
- Increases the damping of the phugoid mode.

This is shown in the following comparison of the SCAS off and SCAS on θ/δ_B (i.e., $N^{\theta}_{\delta_B} N^{\varphi}_{\delta_A} N^{\psi}_{\delta_p} / N^{\dot{\varphi}}_{\delta_A} N^{\psi}_{\delta_p}$) transfer functions:

LONGITUDINAL

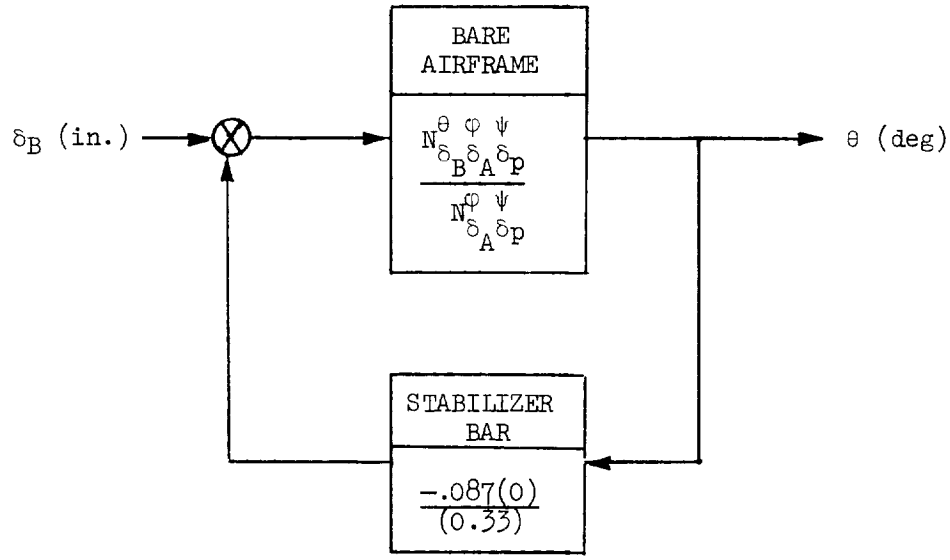

LATERAL

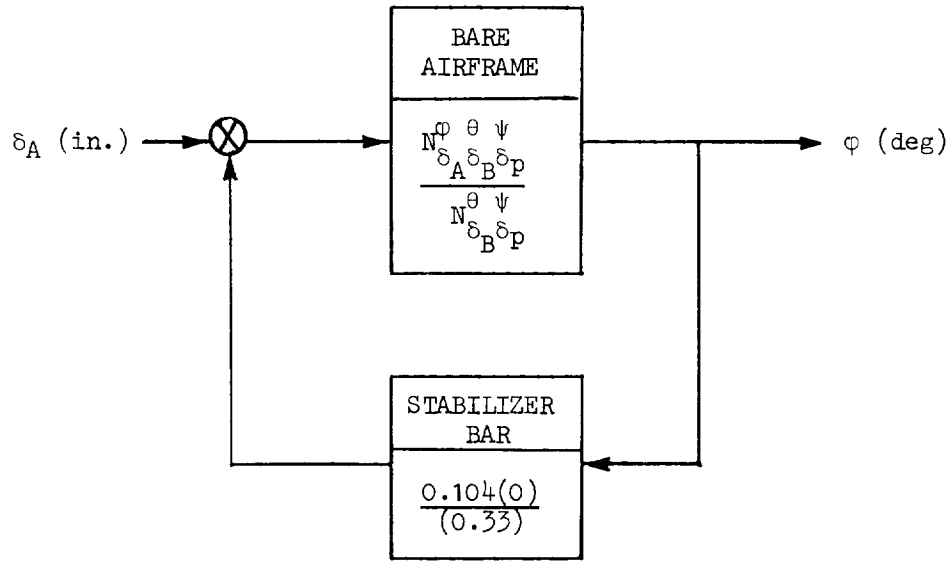

Figure VI-1. Approximate Equivalent Feedback Loops for UH-1H Stabilizer Bar

Pitch Response in Hovering Flight:

SCAS Off:

$$\left.\frac{\theta}{\delta_B}\right|_{\varphi,\psi} \doteq \frac{\overset{SD}{-.146}(\overset{HD}{-.001})(0.39)}{[-.43;0.28][0.90;0.47]} \qquad \text{(VI-9)}$$
$$\qquad\qquad\quad P \qquad\quad HD \quad PD$$

SCAS On:

$$\left.\frac{\theta}{\delta_B}\right|_{\varphi,\psi} \doteq \frac{\overset{SD}{-.146}(\overset{HD}{-.001})(0.07)(0.39)\qquad (2.6)}{[-.16;0.13]\ (0.26)(0.39)(0.80)(2.5)} \qquad \text{(VI-10)}$$
$$\qquad\qquad\quad P \qquad\qquad\quad HD$$

From Feedforward Compensation

From Feedback Compensation

The Bode root locus plot for each condition is shown in Figs. VI-2 and VI-3. Note that the net favorable effect of the longitudinal SCAS is to separate phugoid and pitch damping modes and to create a controlled element more nearly like K/s.

In forward flight the AH-1G pitch SCAS also augments pitch damping and produces the same general effects as in hover. In fact, the effect of the SCAS on pitch response in forward flight is nearly identical numerically to that of the hover condition. (Cf. Eq. VI-12 with VI-10.)

Pitch Response in Forward Flight at 60 kt:

SCAS Off:

$$\left.\frac{\theta}{\delta_B}\right|_{\varphi} \doteq \frac{\overset{SD}{-.16}(\overset{HD}{0.01})(0.91)}{[-.15;0.32][0.84;0.79]} \qquad \text{(VI-11)}$$
$$\qquad\qquad\quad P \qquad\quad SP$$

SCAS On:

$$\left.\frac{\theta}{\delta_B}\right|_{\varphi} \doteq \frac{-.16(0.01)(0.07)(0.90)}{[-.04;0.14](0.26)(0.68)(1.2)} \qquad \text{(VI-12)}$$

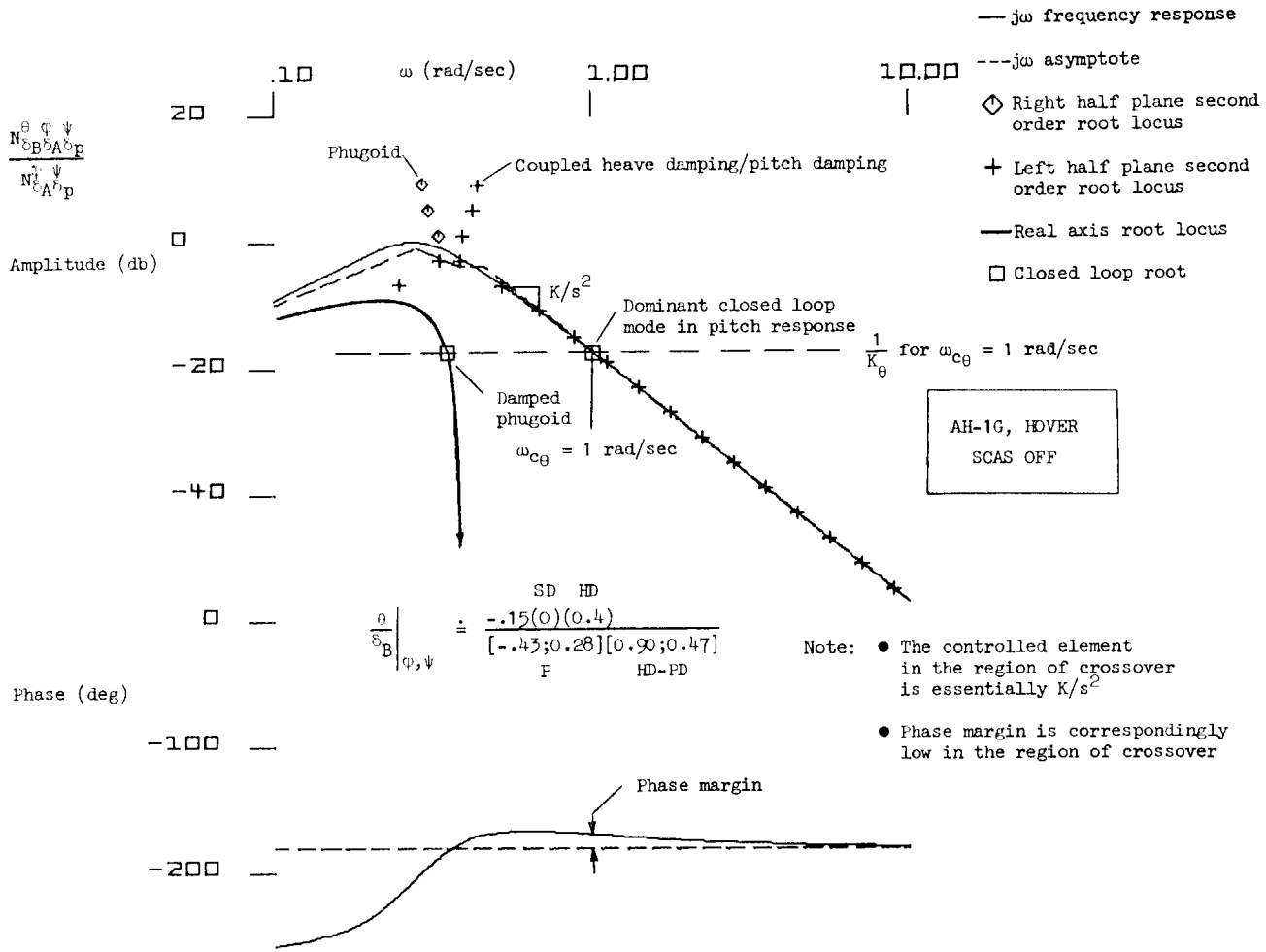

Figure VI-2. SCAS Off Pitch Response (AH-1G in Hover)

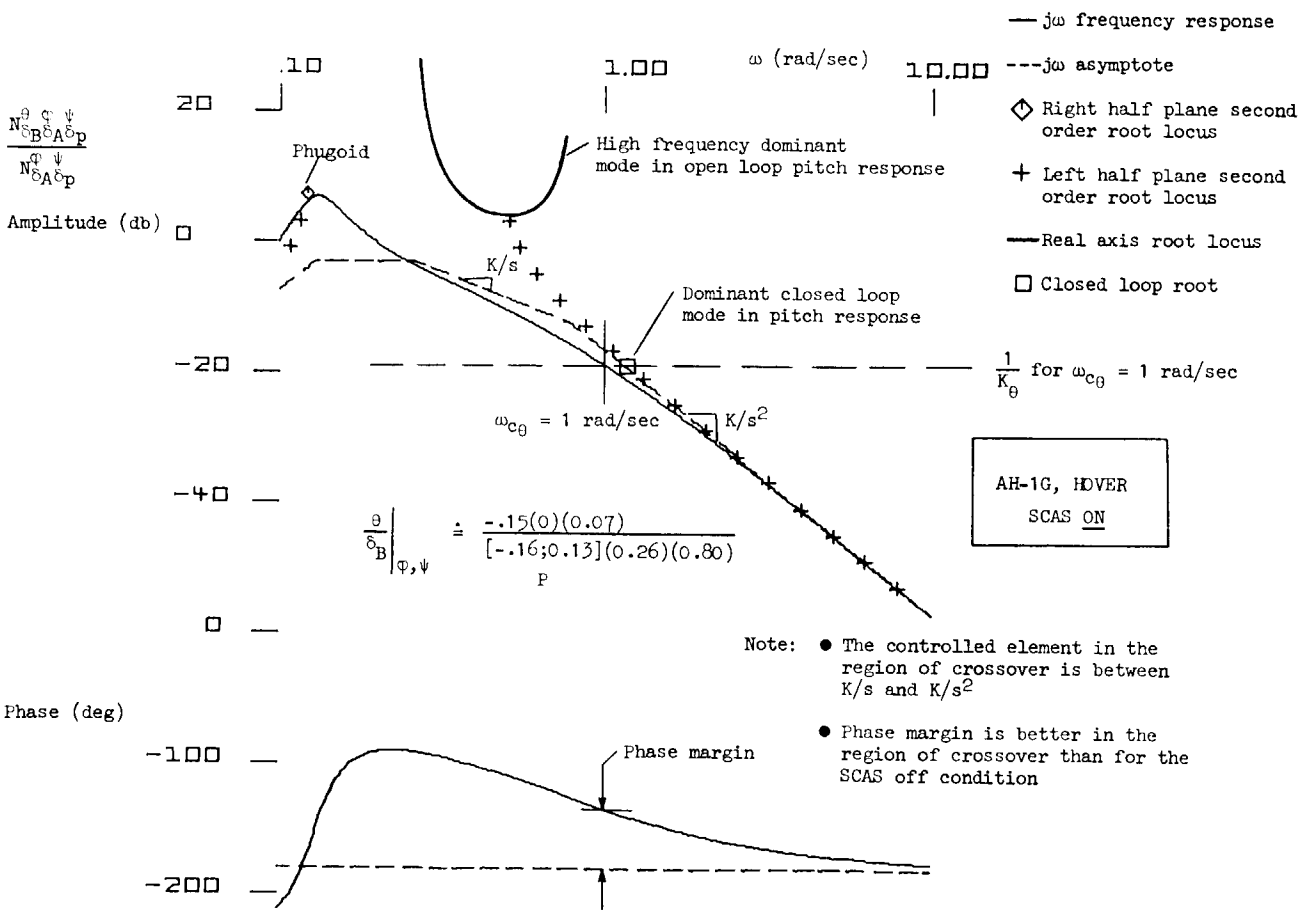

Figure VI-3. SCAS On Pitch Response (AH-1G in Hover)

b. Roll Axis. The AH-1G roll axis SCAS, as in the pitch axis, involves feedforward and feedback loops. There is an important difference, however, in the form of feedback compensation, i.e., a low frequency washout.

$$\frac{A_{1_S}}{p} \doteq \frac{K\,(0)(3.6)}{(0.37)(1)} \qquad \text{(VI-13)}$$

The result is that, in hover, the lateral phugoid is not improved; in fact, it is slightly degraded. But, the ability to damp manually the lateral phugoid remains effective and, most importantly, roll phase margin is improved in the region of crossover as shown in the comparative roll response Bode root locus plots in Figs. VI-4 and VI-5.

In forward flight the lateral SCAS provides the same controlled element as in hover, just as did the pitch SCAS.

Roll Response in Hover, SCAS On:

$$\left.\frac{\varphi}{\delta_A}\right|_{\theta,\psi} \doteq \frac{0.48(0)(0.06)(5.75)}{[-.28;0.19](0.15)[0.75;3.3]} \qquad \text{(VI-14)}$$

Roll Response at 60 kt, SCAS On:

$$\left.\frac{\varphi}{\delta_A}\right|_{\theta,\psi} \doteq \frac{0.48(0)(0.06)(5.75)}{[-.28;0.19](0.15)[0.75;3.3]} \qquad \text{(VI-15)}$$

c. Yaw Axis. The AH-1G yaw axis SCAS is similar in form to the pitch and roll axes with a combination of feedforward command augmentation, feedback stability augmentation. The feedback loop in the yaw axis consists of compensation which is very nearly a washout followed by a lag.

$$\frac{\theta_{TR}}{r} = \frac{K\,(0.04)(3.3)}{(0.54)(0.59)} \qquad \text{(VI-16)}$$

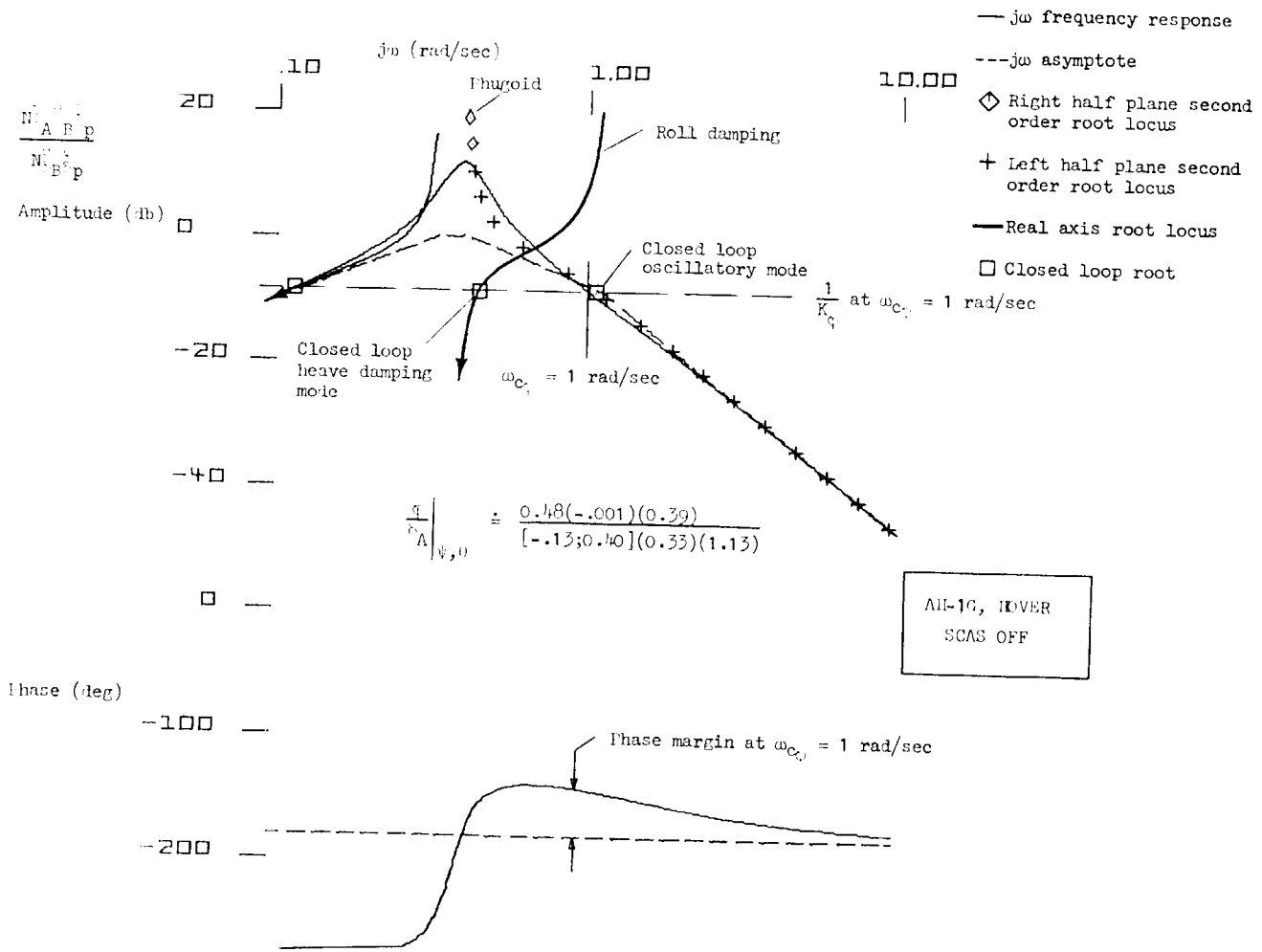

Figure VI-4. Bode Root Locus for Roll

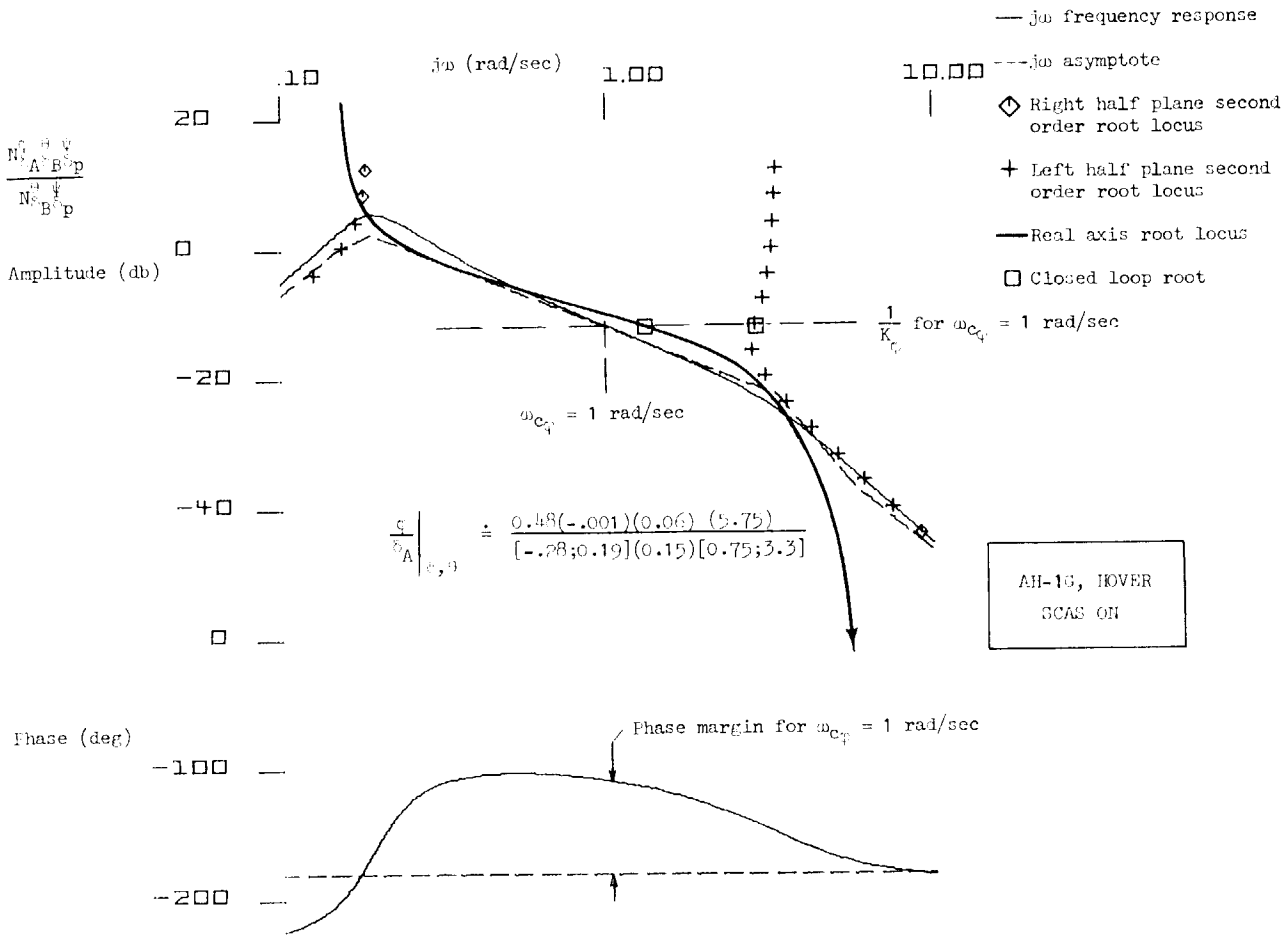

Figure VI-5. Bode Root Locus for Roll

The effect of the yaw SCAS is to augment the yaw damping from approximately 0.5 rad/sec to over 2 rad/sec. At forward velocities the yaw SCAS follows the pattern of the other two axes in that the essential features of the response remain relatively unchanged from that of the hover flight conditions.

Yaw Response in Hover:

SCAS Off:

$$\left.\frac{\psi}{\delta_p}\right|_{\varphi,\theta} \doteq \frac{-.83(0.02)(0.39)}{(0)(0.07)[0.99;0.45]} \doteq \frac{-.8}{(0)(0.5)} \qquad \text{(VI-17)}$$

SCAS On:

$$\left.\frac{\psi}{\delta_p}\right|_{\varphi,\theta} \doteq \frac{-.83(0.02)(0.08)(4)}{(0)[0.84;0.05][0.64;2.3]} \doteq \frac{-.8(4)}{(0)[0.64,2.3]} \qquad \text{(VI-18)}$$

Yaw Response at 60 kt:

SCAS On:

$$\left.\frac{\psi}{\delta_p}\right|_{\varphi,\theta} \doteq \frac{-.96(0.08)(4)}{[0.63;0.27][0.63;2.7]} \qquad \text{(VI-19)}$$

3. CH-53D SAS

The CH-53D employs a number of augmentation devices. In hover the aircraft is attitude-stabilized with velocity-command-like control in all translational axes. At forward speeds of 60 kt and above, attitude stabilization remains effective, except during lateral maneuvering, at which time roll attitude feedback is dropped and a turn coordination system is activated.

a. Pitch Axis. The pitch SAS consists of a pitch attitude feedback loop with lead compensation and a longitudinal cyclic stick feedforward loop. Pitch damping is not provided by an angular rate feedback of q; rather, an Euler angle rate, $\dot{\theta}$, is used. This otherwise avoids a pitch axis error signal in a steady turn. The net result of the θ and $\dot{\theta}$ feedback is to damp the phugoid effectively and to hold pitch attitude. Thus, the pilot is relieved of active inner loop regulation in longitudinal control of the vehicle. As we shall see shortly, the longitudinal cyclic stick with SAS on is essentially a velocity-command control.

b. Roll Axis. The roll SAS provides roll rate damping and roll attitude stabilization in hover and when the pilot's feet are off the pedals at airspeeds above 60 kt. If the pilot's feet are on the pedals above 60 kt, the roll attitude feedback is anulled, and the conventional roll rate damping remains effective.

At low speeds where roll attitude is stabilized, the lateral cyclic stick is essentially a $\dot{y}$-command control just as longitudinal cyclic is an $\dot{x}$-command control.

c. Yaw Axis. The yaw SAS contains elements to:

- Increase yaw damping
- Coordinate turns above 60 kt
- Hold heading (except when the pilot's feet are on the pedals).

The first two items are reflected in the compiled data; the third is not because the pilot's feet are assumed to be on the rudder pedals, i.e., that he is actively maneuvering laterally.

Yaw damping is provided by washed out yaw rate. Turn coordination, when active, involves roll rate and lateral specific force feedbacks. Note that the roll rate feedback, in effect, augments the derivative N'_p in such a sense as to counteract adverse yaw:

$$\Delta N'_p \doteq K_p N'_{\theta_{TR}} = -.0815 \times -3.96 = 0.32 \ (1/\text{sec})$$

The a_y feedback yaws the vehicle so as to eliminate any residual lateral specific force.

B. EFFECTS ON HANDLING

The effect of augmentation systems on the various aspects of handling qualities can be observed by applying the identical multiloop analysis procedures outlined in Sections III, IV, and V. Specifically, we can utilize the same transfer function relationships along with appropriate loop constraints in order to examine direct control response, cross-coupling effects, and gust response in both inner and outer loops. In the following pages the comparative effects on roll axis dynamics are discussed for the three augmented vehicles.

Table VI-2 lists the direct roll attitude response for the augmented helicopters in hovering flight. The responses in this table can be compared directly to corresponding unaugmented cases in Table III-6. Some of the important features shown in Table VI-2 are:

- Additional modes are evident which can be attributed to the dynamics of the augmentation systems (these are identified, where possible, by the label "A").
- Regulation of pitch and yaw axes has an effect on predominant roll modes in the case of the AH-1G and UH-1H (where attitude stabilization is not involved).
- Regulation of pitch and yaw axes does not have a significant impact on the roll response of the CH-53D.

The Bode root locus plots in Figs. VI-6 through VI-9 further illustrate roll response features and compare cases with and without augmentation devices. The following discussion considers each vehicle separately.

1. AH-1G

The SCAS shifts the phugoid to a lower frequency and increases the effective roll damping. Recall from the discussion in Section III.B.1 and III.B.2 that such features help to facilitate good attitude regulation.

TABLE VI-2. SURVEY OF APPROXIMATE* ROLL AXIS RESPONSE TRANSFER FUNCTIONS FOR AUGMENTED VEHICLES (HOVER)

(Compare with Table III-6)

	AH-1G (SCAS ON)	UH-1H (WITH STABILIZER BAR)	CH-53D (SAS ON)
Open Loop: $\frac{N^{\dot{\phi}}_{\delta_A}}{\Delta}$	$\frac{\overset{LD}{.49(.06)}\ [\overset{A}{.84,.06}][\overset{P}{-.17,.12}]\ \overset{A}{(5.75)}}{[-.51,.22](.08)(.21)[.13,.20][.72,3.4]}$ PL, A, P, R-A	$\frac{\overset{LD}{.57(.07)}\overset{A}{(.33)}\overset{YD}{(.62)}\quad\overset{P}{[.08,.19]}}{[-.2,.23]\quad(.67)[.22,2.0][.57,.22]}$ PL, YD, R-A, P	$\frac{\overset{LD}{.52(.10)}\ \overset{A}{(.30)}}{(.31)(.35)(1.1)(3.4)}$ PL, R-A
Pitch Perfectly Regulated: $\frac{N^{\dot{\phi},\theta}_{\delta_A\delta_B}}{N^{\theta}_{\delta_B}}$	$\frac{\overset{LD}{.47(-.001)}\overset{A}{(.06)[.84,.05]}\quad\overset{A}{(5.75)}}{[-.27,.20](.016)(.09)(.14)[.73,3.2]}$ PL, A, R-A	$\frac{\overset{LD}{.57(.06)}\overset{A}{(.33)}\overset{YD}{(.62)}}{[.27,.19]\quad(.68)[.22,1.9]}$ PL, YD, R-A	$\frac{\overset{LD}{.52(.10)}\ \overset{A}{(.33)}}{(.33)(.33)(1.0)(3.8)}$ PL, R-A
Pitch and Yaw Perfectly Regulated: $\frac{N^{\dot{\phi},\theta,\dot{\psi}}_{\delta_A\delta_B\delta_p}}{N^{\theta,\dot{\psi}}_{\delta_B\delta_p}}$	$\frac{\overset{LD}{.48(-.001)}\overset{A}{(.06)}\quad\overset{A}{(5.75)}}{[-.28,.19](.15)[.75,3.3]}$ PL, A, R-A	$\frac{\overset{LD}{.59(.01)}\quad\overset{A}{(.33)}}{[.27,.10][.25,1.9]}$ PL, R-A	$\frac{\overset{LD}{.54(.07)}\overset{A}{(.30)}}{[.99,.32](.96)(4.2)}$ PL, R-A
Remarks:	●$\theta \rightarrow \delta_B$ makes lateral phugoid more stable ●Lateral phugoid never stable without roll regulation ●Roll mode coupled with augmentation mode	●$\theta \rightarrow \delta_B$ stabilizes lateral phugoid ●Overall effects similar to AH-1G except roll mode less damped	●Lateral phugoid stabilized ●Bank angle commani above 0.3 rad/sec

* Approximately cancelling dipole factors are omitted from 6 DOF quasi-static transfer function expressions shown.

( ) first order factor, [ ] second order factors, $\{(\ )\ .\ .\ .\ [\ ]\}$ approximately cancelling dipole factors.

$\{(\ )_X\}$ mode label according to the following key: P - phugoid, PL - lateral phugoid, PD - pitch damping, R - roll damping, YD - yaw damping, SP - short period, D - dutch roll, S - spiral, SD - surge damping, LD - sway damping, HD - heave damping, A - augmentation mode.

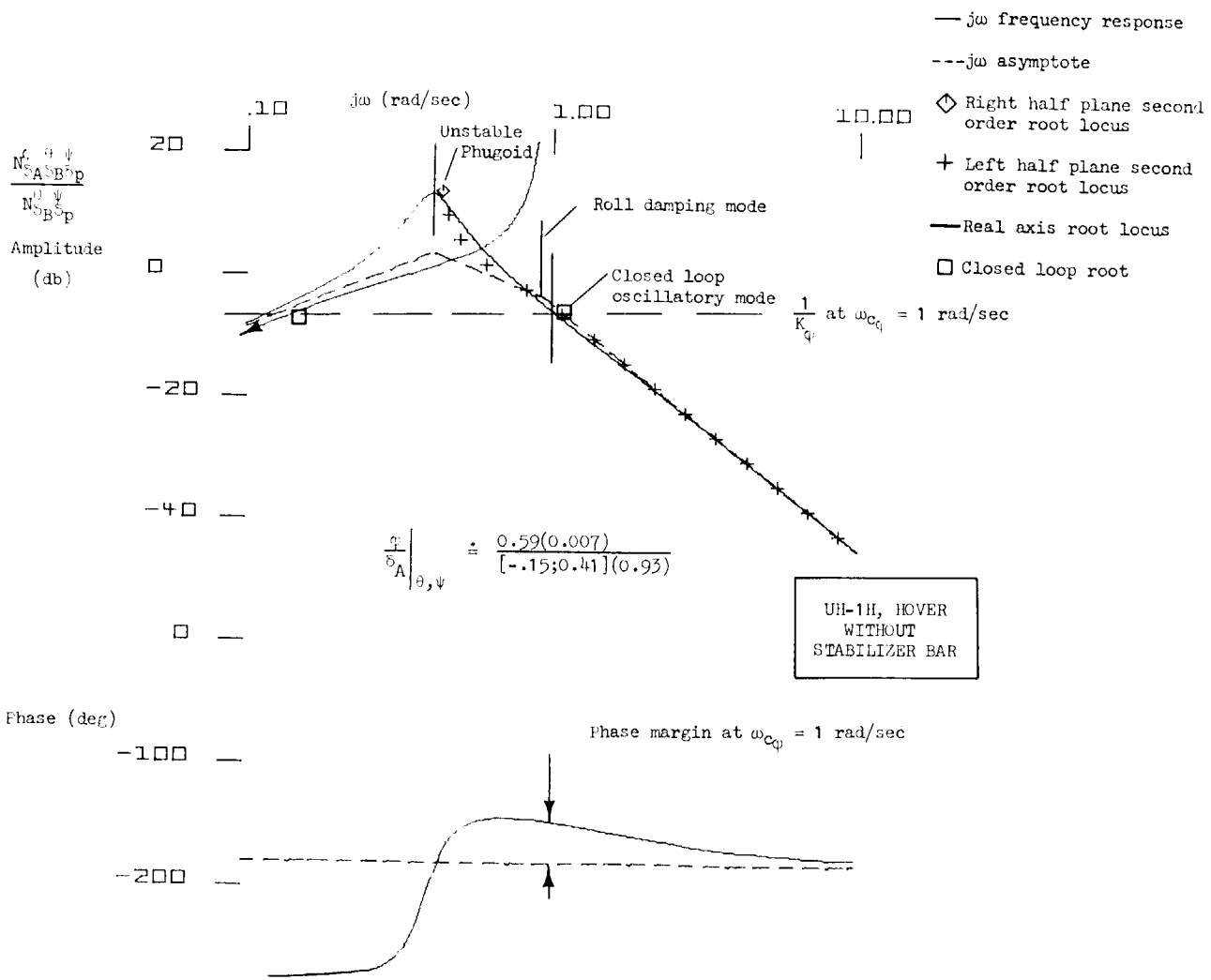

Figure VI-6. Bode Root Locus for Roll

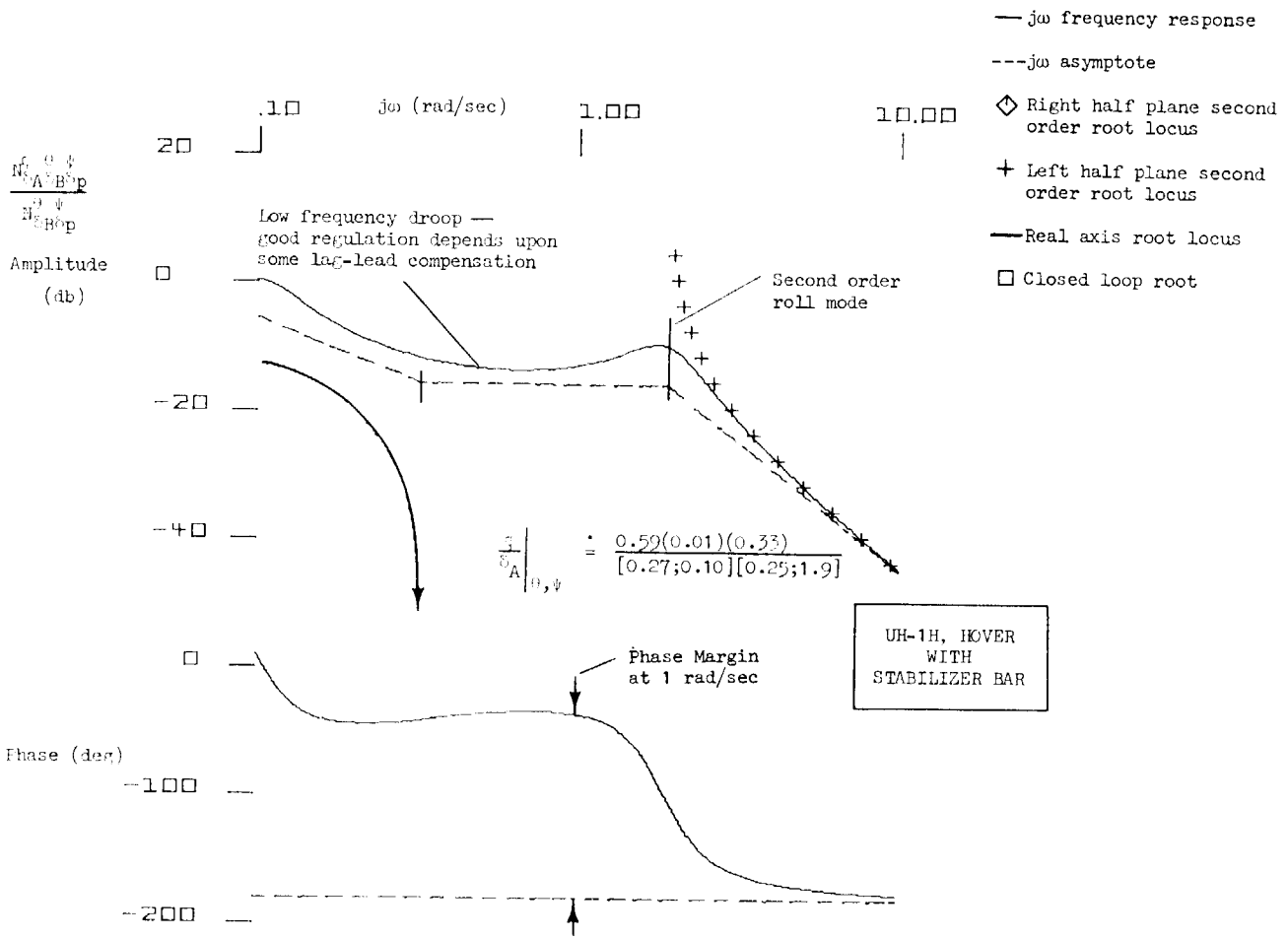

Figure VI-7. Bode Root Locus for Roll

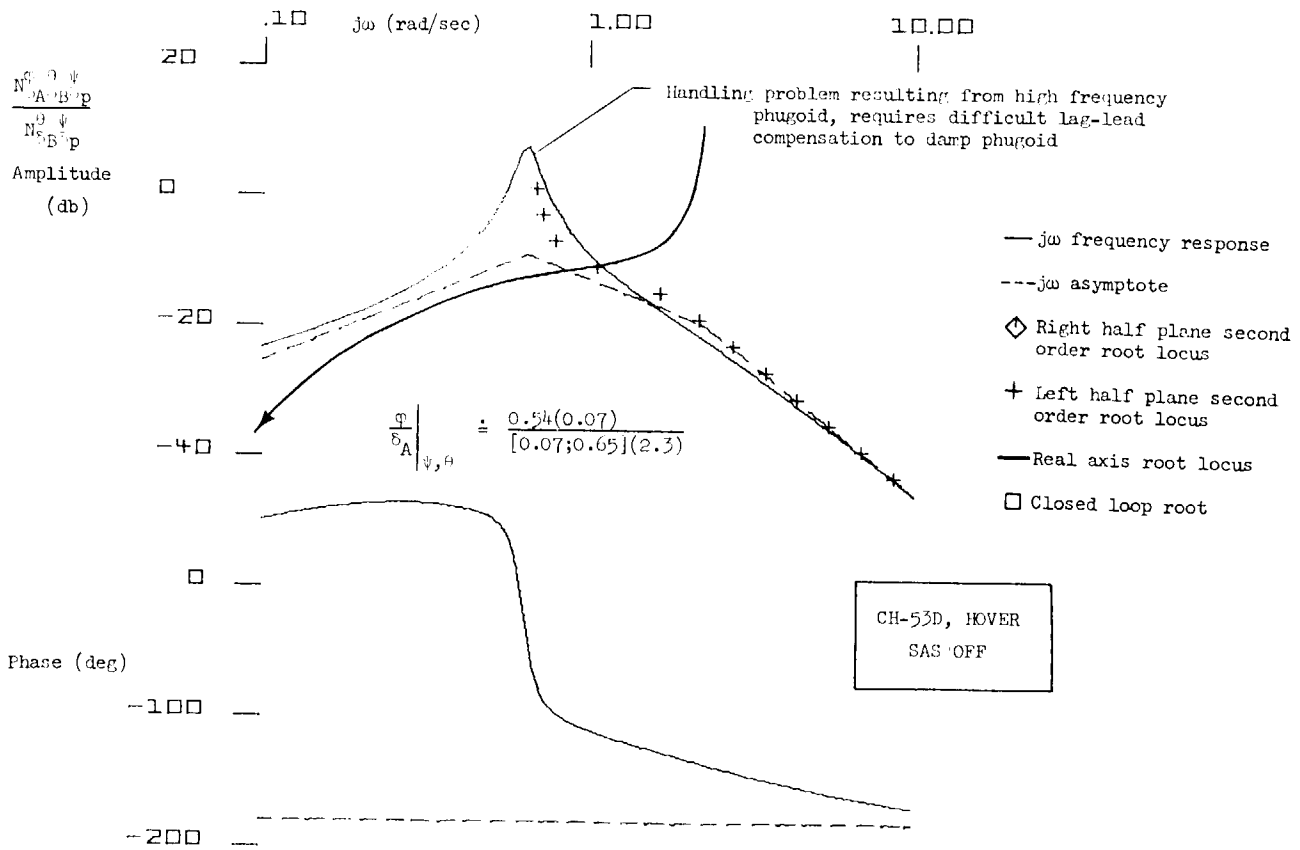

Figure VI-8. Bode Root Locus for Roll

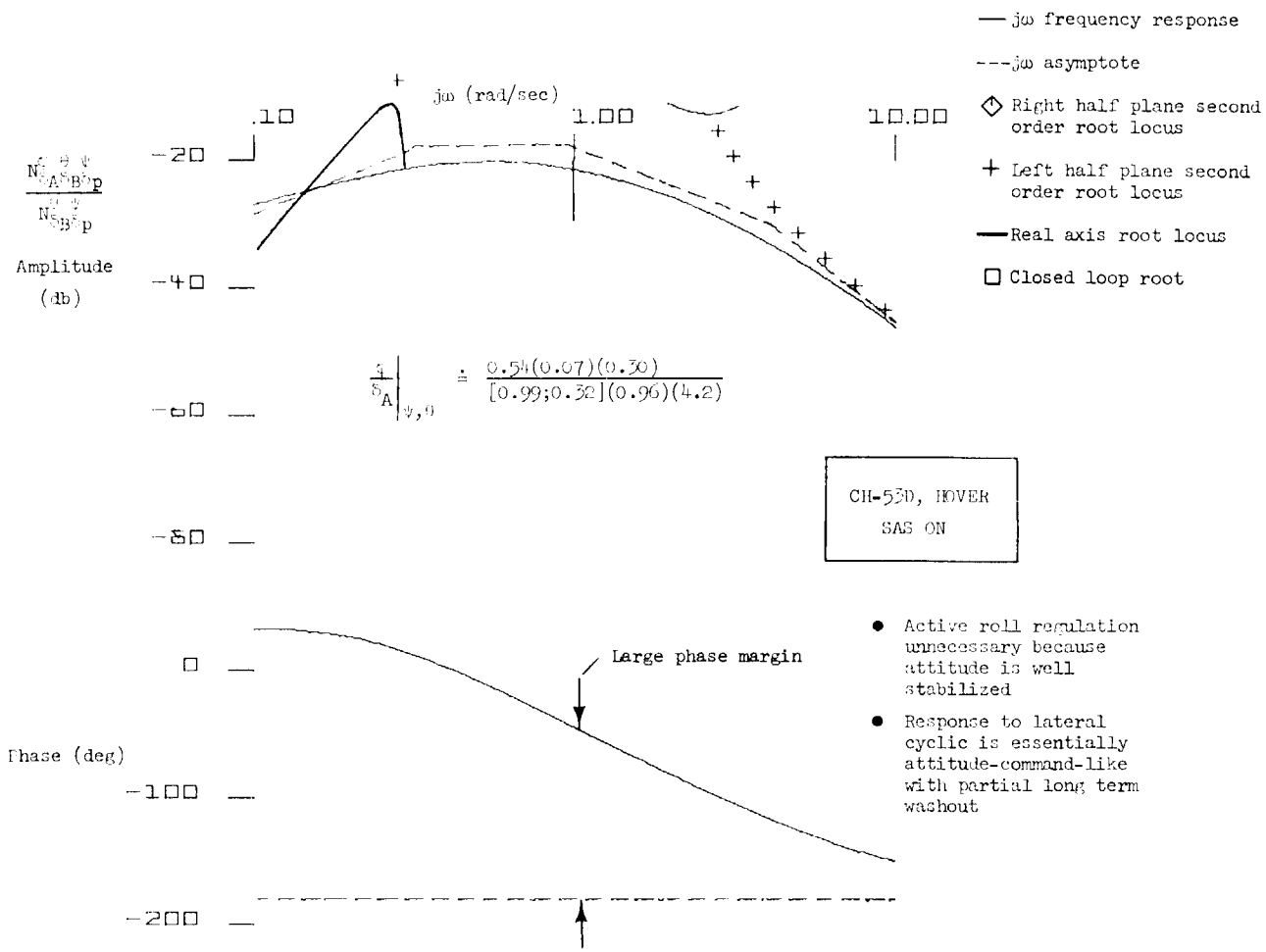

Figure VI-9. Bode Root Locus for Roll

The controllability benefits are most prominently displayed by the increase in phase margin in the vicinity of 1 rad/sec. Similar effects can be observed for other flight conditions and for pitch and yaw axes.

2. UH-1H

The stabilizer bar significantly alters roll response by (i) damping the lateral phugoid and (ii) coupling the roll damping mode with a stabilizer bar mode. The resulting Bode root locus plot shown in Fig. VI-7 depicts a low frequency drooping tendency in amplitude ratio which ordinarily would aggrevate regulation. The degree of the problem is suspected to be somewhat less in the actual vehicle than in the mathematical model, however. According to the measured vehicle characteristics reported in Ref. 29 the control derivative $L'_{A_{1_S}}$ (or L'_{δ_A}) is approximately 75% of that modeled here. Hence, the high frequency oscillatory mode would be slightly better damped ($\zeta \doteq 0.35$) and at a slightly lower natural frequency ($\omega \doteq 1.4$ rad/sec). Correspondingly less compensation would be required; therefore, the drooping tendency in amplitude ratio would be less. The same rationale would apply to the pitch axis dynamics which suffer a low frequency droop also.

Regardless of the problem cited, the stabilizer bar is beneficial in increasing the net phase margin (compare the φ_m in Figs. VI-6 and VI-7) and in stabilizing and damping the phugoid. The net result is a reduction in workload for the pitch and roll axes.

3. CH-53D

Where the AH-1G and UH-1H augmentation systems only tend to stabilize and damp the phugoid, the CH-53D augmentation system fully stabilizes roll attitude (as well as pitch attitude and heading) and provides complete hands-off stabilization capability. In effect, the roll SAS eliminates the need for active roll regulation (a difficult task with SAS off as shown in Fig. VI-8) and provides direct outer loop control of lateral position and velocity through the lateral cyclic control. We can observe this from the closed loop lateral velocity transfer function:

$$\left.\frac{\dot{y}}{\delta_A}\right|_{\text{SAS ON}} = \left.\frac{N_{\delta_A}^{\dot{y}}}{\Delta}\right|_{\text{SAS ON}} \doteq \frac{4.5(0.10)}{(0.07)(0.35)} \qquad \text{(VI-20)}$$

i.e., the lateral cyclic stick commands lateral velocity with an open loop bandwidth of 0.35 rad/sec. This is a system which permits easy and precise regulation of lateral position in the likely range of crossover frequencies.

Other outer loop controls are improved also. The surge response in hover is similar to the lateral response although with a lower bandwidth:

$$\left.\frac{\dot{x}}{\delta_B}\right|_{\text{SAS ON}} = \left.\frac{N_{\delta_B}^{\dot{x}}}{\Delta}\right|_{\text{SAS ON}} \doteq \frac{3.0}{(0.11)} \qquad \text{(VI-21)}$$

In heave, with roll and pitch SAS on, the basic heave damping prevails, and:

$$\left.\frac{\dot{z}}{\delta_c}\right|_{\text{SAS ON}} = \left.\frac{N_{\delta_c}^{\dot{z}}}{\Delta}\right|_{\text{SAS ON}} \doteq \frac{-6.4}{(0.30)} \qquad \text{(VI-22)}$$

SECTION VII

CONCLUSIONS AND RECOMMENDATIONS

In this volume we have demonstrated procedures for effectively reducing coupled longitudinal-lateral-directional equations of motion to forms which expose specific features of helicopter handling qualities in a closed-loop, pilot-vehicle context. In so doing we have utilized the compiled data from Volume One to form a realistic quantitative frame of reference. Thus beyond just a demonstration of methods, we have also a survey of several handling-qualities-related features for a variety of single rotor vehicles.

It was shown that a general compensatory manual loop structure could be applied to the coupled longitudinal-lateral-directional helicopter equations of motion with two important results:

(i) Key handling qualities features in a single loop could be examined directly with simple but appropriate constraints on other loops.

(ii) The overall mathematical complexity could be reduced from that of the basic vehicle model while retaining the significant effects of longitudinal-lateral-directional cross coupling.

The examples considered in this study demonstrated these results in the cases of basic inner loop vehicle attitude stabilization and outer loop translational control. The following is a summary of conclusions and recommendations ensuing from this work.

A. BASIC ANALYTICAL APPROACH

The analytical approach used herein to examine specific handling qualities features consisted of:

- Selecting a closed-loop transfer function relationship which addresses the handling quality feature as directly as possible (e.g., one direct measure of the quality of pitch attitude control can be taken to be the response of pitch attitude to longitudinal cyclic stick displacement with roll and yaw loops closed).

- Expressing the closed-loop transfer function in terms identifiable as (i) strictly vehicle components and (ii) combined pilot-vehicle components.

- Substituting crossover model approximations for the combined pilot-vehicle components and taking advantage of the simplification ensuing from neglecting higher order terms.

The fortuitous result which makes this procedure useful is that attitude-constrained relationships frequently predominate, reduce mathematical complexity, and enhance physical insight.

The steps outlined above were used successfully to examine:

- Direct control response for inner loop states — pitch and roll attitude and yaw.

- Inner loop cross coupling — pitch-due-to-roll, roll-due-to-pitch, and turn coordination.

- Direct control response for outer loop states — translational velocity and displacement components.

- Determination of significant inner and outer loop gust response components.

- Augmentation system effects on inner and outer loop gust response components.

- Augmentation system effects on inner and outer loop control response.

In each of these areas it was possible to determine the relative influence of various pilot-vehicle loops, determine important vehicle features, and estimate the relative success in closing the primary control loops. Summaries of some notable examples follow.

B. PRIMARY CONTROL RESPONSE IN THE INNER LOOPS

Primary inner loop control response was analyzed in the presence of appropriate off-axis regulation, and it was found that perfect regulation of off-axis states is a generally valid assumption. It results in about the same net effect on the primary inner loop control response as a moderate

degree of regulation of off-axis states. As an example, open-loop pitch response can be expressed simply in terms of ratios of coupling numerators,

$$\text{i.e.,} \qquad \frac{\theta}{\delta_B} \doteq \frac{N^{\theta}_{\delta_B} N^{\varphi}_{\delta_A} N^{\psi}_{\delta_p}}{N^{\varphi}_{\delta_A} N^{\psi}_{\delta_p}} \qquad \text{(VII-1)}$$

This formulation carries along, from the pilot's point of view, the significant cross coupling effects among roll, pitch, and yaw axes (as described by six-degrees-of-freedom equations), and it minimizes mathematical complexity (by reducing transfer function order by at least two). As an added feature, the roll and yaw pilot model elements in the above example do not appear explicitly, but their effects are appropriately imbedded in the pitch transfer function. Similar results were obtained for primary control response in roll and yaw loops.

The above analytical procedure also has implications for the formulation of handling qualities metrics and for the flight test determination of them. The key issue is how one correctly introduces the effects of pilot-furnished vehicle control when examining and measuring various stability and control features. For example, should open loop pitch response be prescribed and ultimately measured in flight with some regulation of roll and yaw? As demonstrated in Section III, such off-axis regulation can modify the handling characteristics in the axis under consideration. Further, one might claim justifiably that these modified characteristics are more relevant to the pilot. Resolution of how and to what extent control strategy should be applied in formulating handling qualities metrics and testing for them is considered to be a worthwhile task.

C. AXIS CROSS COUPLING

The six-degrees-of-freedom models used in this study offered an opportunity to explore some of the various closed-loop cross coupling effects inherent in helicopters. Roll-pitch cross coupling was one such effect considered. Two means of characterizing the closed-loop roll-pitch cross coupling effects at low forward speeds were shown to be the modal

response ratios representing roll due to a pitch command and pitch due to a roll command with yaw motion constrained via pedal control,

$$\text{i.e.,} \qquad \frac{\varphi}{\theta_c} \doteq \frac{N^{\varphi}_{\delta_B} N^{\psi}_{\delta_p}}{N^{\theta}_{\delta_B} N^{\psi}_{\delta_p}} \qquad \text{(VII-2)}$$

$$\text{and} \qquad \frac{\theta}{\varphi_c} \doteq \frac{N^{\theta}_{\delta_A} N^{\psi}_{\delta_p}}{N^{\varphi}_{\delta_A} N^{\psi}_{\delta_p}} \qquad \text{(VII-3)}$$

Analytically, these relationships were shown to be significant for either an exclusively compensatory pilot-vehicle loop structure, or one involving additional pursuit crossfeeds to off-axis controls (e.g., a precognitive application of lateral cyclic to minimize uncommanded roll response when regulating pitch). The magnitude and sense of the closed-loop cross-coupling relationships expressed above agree with what is expected in specific rotor system types — teetering, articulated, and hingeless.

Furthermore, as in the case of direct control response, implications for cross-coupling-related handling metrics and test procedures arise from the analysis applied here. These implications involve not only how and when manual control strategy should be considered, but also how cross-coupling, per se, should be classified and categorized. Pursuant to this, the matrix of cross coupling features shown in Table III-10 provides a systematic check list of characteristics which could be considered one-at-a-time in a rational closed loop context. In turn, this list suggests a form for handling qualities design specification and testing.

D. PRIMARY CONTROL RESPONSE IN THE OUTER LOOPS

Analysis of outer loop controlled elements was approached in a manner similar to that for the inner loop elements. But while the inner loops involve a variety of aerodynamic effects dependent on the specific vehicle design, the outer loop characteristics are, by contrast, rather invariant. The only outer loop control response subject to any significant variation

is heave response, which is mainly a function of disc loading and airspeed. But even this feature is remarkably similar among the vehicles studied.

In view of the inherent restriction on outer-loop response properties it is somewhat understandable that specific flying qualities requirements have not been well established. At the same time it is conceivable that a severe NOE operating environment could demand a level of outer loop response superior to that occurring naturally in the basic helicopter vehicle. This would, in turn, necessitate the use of additional force generation and would require prescribing levels and forms of surge, sway, or heave response.

E. GUST RESPONSE

The important atmospheric gust induced response components for a helicopter model including longitudinal-lateral-directional cross coupling were examined. Closed-loop analysis was applied but was shown to give about the same results as simply considering the relative magnitudes of appropriate aerodynamic stability derivatives.

The sensitivity of helicopters to spatially dependent wind shear was illustrated by considering the closed-loop interactions among the pilot, vehicle, and terrain. Based on the predominant gust derivative, Z_u, the peak gust sensitivity was found likely to occur at forward velocities of approximately 20 kt. This could be critical in an NOE environment if a significant headwind component were to exist above tree level and decay nearly linearly between the tree tops and ground level (as compared to a natural planetary boundary layer logarithmic decay). Velocity profile data from wind tunnel tests suggest that just such a low level wind shear condition is possible. It is recommended that not only the hazard potential be further studied, but that the necessity for including such effects in manned simulation be considered.

F. EFFECTS OF VEHICLE AUGMENTATION

For vehicles having the added complexity of stability and control augmentation systems, the same procedures described previously were applied. Even with the appearance of additional response modes, the resulting dynamics were expressed with about the same degree of simplicity as for the unaugmented vehicle. This is a significant result and leads to the following notion.

G. APPLICATION TO MORE COMPLEX MATHEMATICAL MODELS

In this study the unaugmented vehicle equations of motion were limited to six-degrees-of-freedom, quasi-static. The complexity of any vehicle augmentation was commensurate with the vehicle complexity. It is important to recognize, however, that the analysis procedures applied in this study lend themselves to system models involving the addition of rotor system and structural degrees of freedom just as they lent themselves to the additional complexity of control augmentation. Therefore, it is recommended that these procedures be considered as aids to reducing higher order rotorcraft systems to their essential properties within a pilot-vehicle context.

REFERENCES

1. McRuer, Duane, Irving Ashkenas, and Dunstan Graham, Aircraft Dynamics and Automatic Control, Princeton University Press, Princeton, N.J., 1973.

2. McRuer, D. T., and E. S. Krendel, Mathematical Models of Human Pilot Behavior, AGARD AG-188, Jan. 1974.

3. "Effect of Nap-of-the-Earth Requirements on Aircrew Performance During Night Attack Helicopter Operations," The Guidance and Control of V/STOL Aircraft and Helicopters at Night and in Poor Visibility, AGARD CP-148, Paper No. 4, May 1975, pp. 4-1 to 4-10.

4. Dooley, Larry W., "Handling Qualities Considerations for NOE Flight," J. of the American Helicopter Society, Vol. 22, No. 4, Oct. 1977, pp. 20-27.

5. McRuer, D. T., and D. Graham, "Pilot-Vehicle Control System Analysis," Guidance and Control —, Eds. R. C. Langford and C. J. Mundo, (Progress in Astronautics and Aeronautics, Vol. 13), Academic Press, N.Y., June 1964.

6. Teper, Gary L., An Assessment of the "Paper Pilot" — An Analytical Approach to the Specification and Evaluation of Flying Qualities, AFFDL-TR-71-174, June 1972.

7. Ringland, R. F., R. L. Stapleford, and R. E. Magdaleno, Motion Effects on an IFR Hovering Task — Analytical Predictions and Experimental Results, NASA CR-1933, Nov. 1971.

8. Allen, R. W., W. F. Clement, and H. R. Jex, Research on Display Scanning, Sampling, and Reconstruction Using Separate Main and Secondary Tracking Tasks, NASA CR-1569, July 1970.

9. Clement, Warren F., R. Wade Allen, and Dunstan Graham, Pilot Experiments for a Theory of Integrated Display Format, JANAIR Report 711107, Oct. 1971

10. Stapleford, Robert L., Samuel J. Craig, and Jean A. Tennant, Measurement of Pilot Describing Functions in Single-Controller Multiloop Tasks, NASA CR-1238, Jan. 1969.

11. McRuer, Duane, and Dunstan Graham, Human Pilot Dynamics in Compensatory Systems, AFFDL-TR-65-15, July 1965.

12. Clement, Warren F., and Lee Gregor Hofmann, A Systems Analysis of Manual Control Techniques and Display Arrangements for Instrument Landing Approaches in Helicopters, Volume I: Speed and Height Regulation, JANAIR Report 690717, July 1969.

13. Hunsaker, J. C., and E. B. Wilson, Report on Behavior of Aeroplanes in Gusts. Part I — Experimental Analysis of Inherent Longitudinal Stability for a Typical Biplane. Part II — Theory of an Aeroplane Encountering Gusts, NACA Report No. 1, 1915.

14. Wilson, Edwin B., Theory of an Airplane Encountering Gusts, II, NACA Report No. 21, 1916.

15. Wolkovitch, Julian, and Richard P. Walton, VTOL and Helicopter Approximate Transfer Functions and Closed-Loop Handling Qualities, Systems Technology, Inc., TR-128-1, June 1965.

16. Craig, Samuel J., and Anthony Campbell, Analysis of VTOL Handling Qualities Requirements, Part I: Longitudinal Hover and Transition, AFFDL-TR-67-179, Pt. I, Oct. 1968; and Craig, Samuel J. and Anthony Campbell, Analysis of VTOL Handling Qualities Requirements, Part II: Lateral-Directional Hover and Transition, AFFDL-67-179, Pt. II, Feb. 1970.

17. Bramwell, A. R. S., Helicopter Dynamics, John Wiley and Sons, N.Y., 1976.

18. Seckel, Edward, Stability and Control of Airplanes and Helicopters, Academic Press, N.Y., 1964.

19. Walton, R. P., and I. L. Ashkenas, Analytical Review of Military Helicopter Flying Qualities, Systems Technology, Inc., TR-143-1, Aug. 1967.

20. Military Specification; Helicopter Flying and Ground Handling Qualities; General Requirements for, MIL-H-8501A, Amendment 1, 3 Apr. 1962.

21. Edenborough, H. K., and K. G. Wernicke, Control and Maneuver Requirements for Armed Helicopters, American Helicopter Society Twentieth Annual National Forum, Washington, D. C., May 13-15, 1964.

22. Chen, Robert T. N., and Peter D. Talbot, An Exploratory Investigation of the Effects of Large Variations in Rotor System Dynamics Design Parameters on Helicopter Handling Characteristics in Nap-of-the-Earth Flight, American Helicopter Society 33rd Annual National Forum, Washingtion, D.C., May 1977.

23. Rade, M., "Requirements for Operation of Light Helicopters at Night and in Poor Visibility," The Guidance and Control of V/STOL Aircraft and Helicopters at Night and in Poor Visibility, AGARD CP-148, Paper No. 7, May 1975, pp. 7-1 to 7-12.

24. Hohenemser, K. H., Hingeless Rotorcraft Flight Dynamics, AGARD AG-197, Sept. 1974.

25. Kelley, Henry L., Robert J. Pegg, and Robert A. Champine, Flying Quality Factors Currently Limiting Helicopter Nap-of-the-Earth Maneuverability as Identified by Flight Investigation, NASA TN D-4931, Dec. 1968.

26. Finnestead, Rodger L., Ralph J. Pelikan, Donald P. Wray, and Marvin W. Buss, Engineering Flight Test, AH-1G Helicopter (Hueycobra), Phase D, Part 1, Handling Qualities, USAASTA Project No. 66-06, Dec. 1970.

27. Chalk, C. R., T. P. Neal, T. M. Harris, F. E. Pritchard, and R. J. Woodcock, Background Information and User Guide for MIL-F-8785B(ASG), "Military Specification — Flying Qualities of Piloted Airplanes," AFFDL-TR-69-72, Aug. 1969.

28. Chalk, Charles R., Dante A. DiFranco, J. Victor Lebacqz, and T. Peter Neal, Revisions to MIL-F-8785B(ASG) Proposed by Cornell Aeronautical Laboratory Under Contract F33615-71-C-1254, AFFDL-TR-72-41, Apr. 1973.

29. Lehman, John M., Robert K. Heffley, and Warren F. Clement, Simulation and Analysis of Wind Shear Hazard, Systems Technology, Inc., TR-1063-3, Dec. 1977.

30. Maynard, Harry W., Wind Tunnel Modeling of Velocity Profiles of the Atmospheric Surface Layer, ECOM-6019, Apr. 1966.

APPENDIX

SUMMARY OF CLOSED-LOOP HELICOPTER TRANSFER FUNCTIONS

The following tables are presented as a guide to computing various pilot-vehicle response quantities using the data compiled in Volume One. The relationships listed contain primarily first-order effects. Where significant second-order effects are suspected a more thorough derivation should be made in the manner illustrated in the foregoing sections of this report.

TABLE A-1

INNER LOOP PRIMARY CONTROL RESPONSE

	TRANSFER FUNCTION	APPROPRIATE CLOSED LOOP NUMERATOR RATIO	PREDOMINANT GENERIC FORM	REMARKS
Hover or Very Low Speed Flight				
Pitch	$\frac{\theta}{\delta_B}$	$\frac{N^{\theta}_{\delta_B} N^{\varphi}_{\delta_A} N^{\psi}_{\delta_p}}{N^{\varphi}_{\delta_A} N^{\psi}_{\delta_p}}$	$\frac{A_{\theta}\left(\frac{1}{T_{\theta_1}}\right)^{SD}}{[\zeta_p, \omega_p]\left(\frac{1}{T_{sp_2}}\right)}$ (P, PD)	$\theta \rightarrow \delta_B$ should damp phugoid without hindrance of low pitch damping.
Roll	$\frac{\varphi}{\delta_A}$	$\frac{N^{\varphi}_{\delta_A} N^{\theta}_{\delta_B} N^{\psi}_{\delta_p}}{N^{\theta}_{\delta_B} N^{\psi}_{\delta_p}}$	$\frac{A_{\varphi}\left(\frac{1}{T_{\theta_1}}\right)^{LD}}{[\zeta_{pl}, \omega_{pl}]\left(\frac{1}{T_R}\right)}$ (PL, R)	$\varphi \rightarrow \delta_A$ should damp lateral phugoid without hindrance of low roll damping
Yaw	$\frac{\psi}{\delta_p}$	$\frac{N^{\psi}_{\delta_p} N^{\theta}_{\delta_B} N^{\varphi}_{\delta_A}}{N^{\theta}_{\delta_B} N^{\varphi}_{\delta_A}}$	$\frac{A_{\psi}}{(0)\left(\frac{1}{T_{yd}}\right)}$ (YD)	$\psi \rightarrow \delta_p$ required for direct regulation of yaw

TABLE A-1 (Concluded)

	TRANSFER FUNCTION	APPROPRIATE CLOSED LOOP NUMERATOR RATIO	PREDOMINANT GENERIC FORM	REMARKS
Forward Flight (Adequate Directional Stiffness)				
Pitch	$\frac{\theta}{\delta_B}$	$\frac{N^{\theta}_{\delta_B} N^{\varphi}_{\delta_A}}{N^{\varphi}_{\delta_A}}$	$\frac{A_\theta \left(\frac{1}{T_{\theta_1}}\right)_{SD} \left(\frac{1}{T_{\theta_2}}\right)_{HD}}{[\zeta_p, \omega_p]_P [\zeta_{sp}, \omega_{sp}]_{SP}}$	$\theta \rightarrow \delta_B$ should damp phugoid without hindrance from short period
Roll	$\frac{\varphi}{\delta_A}$	$\frac{N^{\varphi}_{\delta_A} N^{\theta}_{\delta_B}}{N^{\theta}_{\delta_B}}$	$\frac{A_\varphi}{\left(\frac{1}{T_s}\right)_S \left(\frac{1}{T_R}\right)_R}$	$\varphi \rightarrow \delta_A$ should damp spiral without hindrance of low roll damping
Yaw	$\frac{\psi}{\delta_p}$	$\frac{N^{\psi}_{\delta_p} N^{\varphi}_{\delta_A} N^{\theta}_{\delta_B}}{N^{\varphi}_{\delta_A} N^{\theta}_{\delta_B}}$	$\frac{A_\psi \quad [\zeta_\varphi, \omega_\psi]}{(0)\left(\frac{1}{T_s}\right)_S [\zeta_d, \omega_d]_D}$	$\psi \rightarrow \delta_p$ primarily to aid in turn coordination

TABLE A-2

INNER LOOP CROSS COUPLING

	TRANSFER FUNCTION	APPROPRIATE CLOSED LOOP NUMERATOR RATIO	REMARKS
Pitch Due to Roll	$\frac{\theta}{\varphi_c}$	$\left.\begin{array}{c\|c} N^{\theta}_{\delta_A} & N^{\psi}_{\delta_p} \\ \hline N^{\varphi}_{\delta_A} & N^{\psi}_{\delta_p} \end{array}\right.$ *	Source is inertial cross coupling. Normally greater for hover than for forward flight.
Pitch Due to Yaw	$\frac{\theta}{\psi_c}$	$\frac{N^{\theta}_{\delta_p} N^{\varphi}_{\delta_A}}{N^{\psi}_{\delta_p} N^{\varphi}_{\delta_A}}$	
Pitch Due to Collective	$\frac{\theta}{\delta_c}$	$\left.\begin{array}{c\|c} N^{\theta}_{\delta_c} N^{\varphi}_{\delta_A} & N^{\psi}_{\delta_p} \\ \hline N^{\varphi}_{\delta_A} & N^{\psi}_{\delta_p} \end{array}\right.$	Could be serious when decreased collective produces excessive pitch down.

* $\left.\begin{array}{c\|c} N^{\theta}_{\delta_A} & N^{\psi}_{\delta_p} \\ \hline N^{\varphi}_{\delta_A} & N^{\psi}_{\delta_p} \end{array}\right.$ implies $\frac{N^{\theta}_{\delta_A}}{N^{\varphi}_{\delta_A}}$ for forward flight and $\frac{N^{\theta}_{\delta_A} N^{\psi}_{\delta_p}}{N^{\varphi}_{\delta_A} N^{\psi}_{\delta_p}}$ for hover (where yaw regulation is involved).

TABLE A-2 (Continued)

	TRANSFER FUNCTION	APPROPRIATE CLOSED LOOP NUMERATOR RATIO	REMARKS
Roll Due to Pitch	$\frac{\varphi}{\theta_c}$	$\frac{N^{\varphi}_{\delta_B} \mid N^{\psi}_{\delta_p}}{N^{\theta}_{\delta_B} \mid N^{\psi}_{\delta_p}}$	Source is inertial cross coupling. Normally greater in forward flight than in hover
Roll Due to Yaw	$\frac{\varphi}{\psi_c}$	$\frac{N^{\varphi}_{\delta_p} N^{\theta}_{\delta_B}}{N^{\psi}_{\delta_p} N^{\theta}_{\delta_B}}$	
Roll Due to Collective	$\frac{\varphi}{\delta_c}$	$\frac{N^{\varphi}_{\delta_c} N^{\theta}_{\delta_B} \mid N^{\psi}_{\delta_p}}{N^{\theta}_{\delta_B} \mid N^{\psi}_{\delta_p}}$	
Yaw Due to Pitch	$\frac{\psi}{\theta_c}$	$\frac{N^{\psi}_{\delta_B} N^{\varphi}_{\delta_A}}{N^{\theta}_{\delta_B} N^{\varphi}_{\delta_A}}$	

TABLE A-2 (Concluded)

	TRANSFER FUNCTION	APPROPRIATE CLOSED LOOP NUMERATOR RATIO	REMARKS
Yaw Due to Roll	$\frac{\dot{\psi}}{\varphi_c}$	$\frac{N^{\dot{\psi}\ \theta}_{\delta_A \delta_B}}{N^{\varphi\ \theta}_{\delta_A \delta_B}}$	Basic turn coordination relationship in forward flight. $\dot{\psi}$ should equal $g/V \cdot \varphi$ in short term. N'_p in main source of incorrect turn coordination.
Yaw Due to Collective	$\frac{\dot{\psi}}{\delta_c}$	$\frac{N^{\dot{\psi}\ \theta\ \varphi}_{\delta_c \delta_B \delta_A}}{N^{\theta\ \varphi}_{\delta_B \delta_A}}$	Normally the predominant form of cross coupling in helicopters.

TABLE A-3

OUTER LOOP PRIMARY CONTROL RESPONSE

	TRANSFER FUNCTION	APPROPRIATE CLOSED LOOP NUMERATOR RATIO	PREDOMINANT GENERIC FORM	REMARKS
Surge (or Forward Velocity)	$\frac{\dot{x}}{\theta_c}$	$\frac{N^{\dot{x}\ \varphi}_{\delta_B \delta_A} \mid {}^{\psi}_{\delta_p}}{N^{\theta\ \varphi}_{B\ A} \mid {}^{\psi}_{\delta_p}}$	$\frac{-g}{\left(\frac{1}{T_{\theta_1}}\right)}$ SD	Where ψ is regulated, $\dot{y}/\varphi_c \doteq \frac{g}{\left(\frac{1}{T_{\theta_1}}\right)}$ LD
Sway (or Lateral Velocity)	$\frac{\dot{y}}{\varphi_c}$	$\frac{N^{\dot{y}\ \theta}_{\delta_A \delta_B} \mid {}^{\psi}_{\delta_p}}{N^{\varphi\ \theta}_{\delta_A \delta_B} \mid {}^{\psi}_{\delta_p}}$	$\frac{g}{(0)}$	
Heave	$\frac{\dot{z}}{\delta_c}$	$\frac{N^{\dot{z}\ \theta\ \varphi}_{\delta_c \delta_B \delta_A} \mid {}^{\psi}_{\delta_p}}{N^{\theta\ \varphi}_{\delta_B \delta_A} \mid {}^{\psi}_{\delta_p}}$	$\frac{Z_{\delta_c}}{\left(\frac{1}{T_{\theta_2}}\right)}$ HD	

TABLE A-4

INNER LOOP GUST RESPONSE

	TRANSFER FUNCTION	APPROPRIATE CLOSED LOOP NUMERATOR RATIO	REMARKS
Pitch	$\frac{\theta}{u_g}$ (similarly for w_g, q_g)	$\dfrac{N^{\theta}_{u_g} N^{\varphi}_{\delta_A} \mid N^{\psi}_{\delta_p}}{N^{\varphi}_{\delta_A} \mid N^{\psi}_{\delta_p}}$	
Roll	$\frac{\varphi}{v_g}$ (similarly for p_g, r_g)	$\dfrac{N^{\varphi}_{\delta_g} N^{\theta}_{\delta_B} \mid N^{\psi}_{\delta_p}}{N^{\theta}_{\delta_B} \mid N^{\psi}_{\delta_p}}$	
Yaw	$\frac{\psi}{v_g}$ (similarly for p_g, r_g)	$\dfrac{N^{\psi}_{v_g} N^{\theta}_{\delta_B} N^{\varphi}_{\delta_A}}{N^{\theta}_{\delta_B} N^{\varphi}_{\delta_A}}$	Can be a significant effect from u_g: $\frac{\psi}{u_g} \doteq \dfrac{N^{\psi}_{u_g} N^{\theta}_{\delta_B} N^{\varphi}_{\delta_A}}{N^{\theta}_{\delta_B} N^{\varphi}_{\delta_A}}$

TABLE A-5

OUTER LOOP GUST RESPONSE

	TRANSFER FUNCTION	APPROPRIATE CLOSED LOOP NUMERATOR RATIO	PREDOMINANT GENERIC FORM	REMARKS
Surge	$\frac{\dot{x}}{u_g}$	$\frac{N^{\dot{x}\ \theta\ \varphi}_{u_g \delta_B \delta_A} \mid \delta^{\psi}_p}{N^{\theta\ \varphi}_{\delta_B \delta_A} \mid \delta^{\psi}_p}$	$\doteq 0$	Small effect because X_u is low
	$\frac{\dot{x}}{w_g}$	$\frac{N^{\dot{x}\ \theta\ \varphi}_{u_g \delta_B \delta_A} \mid \delta^{\psi}_p}{N^{\theta\ \varphi}_{\delta_B \delta_A} \mid \delta^{\psi}_p}$	$\doteq 0$	Small effect because X_w is low
Sway	$\frac{\dot{y}}{v_g}$	$\frac{N^{\dot{y}\ \theta\ \varphi}_{u_g \delta_B \delta_A} \mid \delta^{\psi}_p}{N^{\theta\ \varphi}_{\delta_B \delta_A} \mid \delta^{\psi}_p}$	$\doteq 0$	Small effect because Y_v is low

TABLE A-5 (Concluded)

	TRANSFER FUNCTION	APPROPRIATE CLOSED LOOP NUMERATOR RATIO	PREDOMINANT GENERIC FORM	REMARKS
Heave	$\frac{\dot{z}}{u_g}$	$\frac{N_{u_g}^{\dot{z}\ \theta\ \varphi}\delta_B\delta_A \mid \delta_p^{\psi}}{N_{\delta_B\delta_A}^{\theta\ \varphi} \mid \delta_p^{\psi}}$	$\frac{Z_u(0)}{\left(\frac{1}{T_{\theta_1}}\right)\left(\frac{1}{T_{\theta_2}}\right)}$ SD HD	Most sensitive Z_u is in low speed forward flight (approximately 20 kt)
	$\frac{\dot{z}}{w_g}$	$\frac{N_{w_g}^{\dot{z}\ \theta\ \varphi}\delta_B\delta_A \mid \delta_p^{\psi}}{N_{\delta_B\delta_A}^{\theta\ \varphi} \mid \delta_p^{\psi}}$	$\frac{Z_w}{\left(\frac{1}{T_{\theta_2}}\right)}$ HD	Most direct form of outer loop gust sensitivity

1. Report No.	2. Government Accession No.	3. Recipient's Catalog No.
NASA CR-3145		

4. Title and Subtitle	5. Report Date
A COMPILATION AND ANALYSIS OF HELICOPTER HANDLING QUALITIES DATA. Volume Two: Data Analysis	August 1979
	6. Performing Organization Code
7. Author(s)	8. Performing Organization Report No.
Robert K. Heffley	TR 1087-2
	10. Work Unit No.
9. Performing Organization Name and Address	11. Contract or Grant No.
Systems Technology, Inc. 2672 Bayshore-Frontage Rd., Suite 505 Mountain View, CA 94043	NAS2-9344
	13. Type of Report and Period Covered
12. Sponsoring Agency Name and Address	Contractor Report
National Aeronautics and Space Administration Ames Research Center Moffett Field, CA 94035	14. Sponsoring Agency Code

15. Supplementary Notes

16. Abstract

A compilation and an analysis of helicopter handling qualities data are presented. Volume One contains a collection of basic descriptive data, stability derivatives, and transfer functions for a six-degrees-of-freedom, quasi-static model. This, the second volume, analyzes those data using multi-loop manual control methods. A general compensatory loop structure is applied to coupled longitudinal-lateral-directional equations in such a way that key handling qualities features can be examined directly. But the overall mathematical complexity is reduced from that of the basic vehicle model. Extensive use is made of constrained state variable relationships and approximate factors in order to gain physical insight.

17. Key Words (Suggested by Author(s))		18. Distribution Statement
Helicopters	OH-6A	UNCLASSIFIED - UNLIMITED
Handling Qualities	BO-105	
Gust and Wind Shear Response	AH-1G	Star Category - 08
Manual Control	UH-1H	
Pilot-Vehicle Analysis	CH-53D	

19. Security Classif. (of this report)	20. Security Classif. (of this page)	21. No. of Pages	22. Price*
Unclassified	Unclassified	176	$9.00

*For sale by the National Technical Information Service, Springfield, Virginia 22161

NASA-Langley, 1979